ABSTRACT

GORE, MATTHEW ROYCE. Experimental Development of a High Power Density Generator Utilizing Renewable Fuel. (Under the direction of Dr. Tiegang Fang).

The increasing pressure from worldwide political influences is motivating a global transition from conventional petroleum-fueled internal combustion engines to alternative energy sources, such as hybrid powertrains and battery electric powertrains in pursuit of reducing anthropogenic carbon emissions. Recently, the transition to electric vehicles (EVs) has been accelerating, motivated by governments who continue to pass legislation strongly partial to both EVs and manufacturers who continue to introduce more EVs each year. Although EV adoption has increased over recent years, there remains a confluence of barriers that dissuade many consumers from considering EVs. Among these, range anxiety, or the driver's apprehension that an electric vehicle lacks sufficient battery capacity and has limited charging opportunities to cover the required distance to reach their destination is predominant.

This work investigated the state of the art in high power density electric generators for hybrid powertrains suitable for use in a plurality of on and off-highway applications as well as in combination with EVs as range extenders. In addition, this work investigated the viability of alternative fuels in small engines for power generation applications. Finally, this work includes the experimental development of a novel high power-density range extender prototype which can be operable on synthetic fuel to provide reduced emissions.

First, the adaptability of a current gasoline electric generator to be readily modified to function on E-fuels was investigated. In this work, a commercially available electric generator was modified to operate on a synthetic byproduct gaseous fuel mixture derived from an industrial chemical reaction. Specifically, the synthetic gaseous fuel mixture comprised Methane, Ethane, and Carbon Dioxide. It was found that through moderate modifications, commercially available

spark ignition engines can operate on E-fuel and provide similar power output compared to gasoline while providing a reduction in certain emissions. The methods and techniques acquired during these experiments were incorporated into the next phase of this work.

Secondly, a parametric study into the state of the art of electric generators, range extenders, electric dynamos, and small internal combustion engines was performed to identify design criteria and performance benchmarks for a prototype high power electric generator. Design targets including low cost, high specific power, high portability, and high adaptability were identified. From there, the systematic selection of components in view of the criteria was completed in parallel with the iterative engineering design of the prototype. Once the final design was identified, a prototype high power density range extender was constructed and optimized for experimental investigation.

After the prototype was constructed, a series of experiments were conducted utilizing gasoline to explore the performance and emissions of the prototype. The experiments simulated a variety of operating scenarios to thoroughly assess the performance of the prototype. It was found that the prototype generator provided a higher specific power than any known commercially available or theoretically proposed electric generator. What's more, is that the generator produced sufficient power to rapidly charge an EV and function as a hybrid powertrain in certain applications.

Next, the prototype was modified to operate on a net carbon zero E-fuel to understand the potential for emissions reduction in the prototype through alternative fuels. The previous experiments using gasoline fuel were repeated with E-fuel. It was found that, in addition to increased performance, the prototype exhibited a substantial reduction in specific engine emissions. The results show that the prototype, through minor modifications, can operate on E-

fuel and meet and exceed performance and design criteria. A comparative analysis between gasoline performance and E-fuel performance is also included. Finally, a commercially viable design of the range extender is presented.

Experimental Development of a High Power Density Generator Utilizing Renewable Fuel.

by
Matthew R. Gore

A dissertation submitted to the Graduate Faculty of
North Carolina State University
in partial fulfillment of the
requirements for the degree of
Doctor of Philosophy

Mechanical Engineering

Raleigh, North Carolina
2024

APPROVED BY:

_____	_____
Dr. Tiegang Fang Committee Chair	Dr. Tarek Echekki
_____	_____
Dr. Alexei Saveliev	Dr. Fanxing Li

DEDICATION

To my family, especially my grandmother.

BIOGRAPHY

Matthew Gore was born in Tabor City, N.C., which is a small town close to Myrtle Beach. Matthew grew up in a loving home with his sister Alex Gore, his mother Suzanne Gore who was a schoolteacher, and his father Al Gore who owned a carpet retail store. At a young age, Matthew was inquisitive young man who, throughout his childhood, had a noticeable fascination with all things fast and loud. This captivation continued as he grew up; building chainsaw-powered bikes, riding dirt bikes, BB guns, and building tree forts on any summer afternoon was commonplace. Matthew spent most of his high school afternoons working in his garage and at machine shops, where he gained skills as a mechanic, welder, and machinist. Matthew graduated from Loris High School in 2013.

Matthew obtained a bachelor's in mechanical engineering from The University of North Carolina at Charlotte in 2018 with a concentration in motorsports engineering. After completing his undergraduate degree, Matthew joined Dr. Tiegang Fang's group as a Ph.D. student where he investigated advanced topics in internal combustion engines, combustion, and machine design. After graduation, Matthew plans to continue his research on internal combustion engines and teach as a lecturer. In addition, Matthew is a registered patent agent and plans to continue his career in patent law.

ACKNOWLEDGMENTS

First, I would like to give my advisor, Dr. Tiegang Fang, my most sincere and utmost thanks and appreciation. I have said many times throughout my Ph.D. and continue to maintain that I could not have done this without him. I hold the professor in the highest esteem and am humbled to have spent these years working in his lab and to be his student. Dr. Fang's kind patience and incredible wisdom have guided me through the completion of this Ph.D. and have influenced my life in a substantial way. I am thankful for his willingness to pass on his great wisdom and knowledge and for his encouragement which inspired me during the most trying moments of my Ph.D. I have learned so much under his instruction and will continue to rely on his influence and teaching for the rest of my life.

Next, I would like to give my deepest thanks to my Committee: Dr. Tarek Echekki, Dr. Alexei Saveliev, and Dr. Fanxing Li. I am very thankful for the knowledge and skills I learned through their instruction. The knowledge I gained through Dr. Echekki's combustion classes and Dr. Saveliev's heat transfer and thermodynamic classes helped set the foundation for my research and I continue to rely on their teaching every day. I am also thankful for Dr. Li's willingness to sacrifice his valuable time to serve as the GSP during the preliminary and final defense. I have great respect for each of these professors, their knowledge, and guidance.

I would also like to thank my lab mates for all the help they have given me during my Ph.D. I appreciate all the helping hands they gave me during the experimental phase of my Ph.D. In particular, I would like to thank my cohort, Kaushik Vinod. We have worked together on many projects and have shared many victories. His skills and willingness to share them helped me through many challenges during my Ph.D. I consider Kaushik to be one of my dearest friends.

I want to thank Kermit Buller of Buller Built Karting for providing the components to assemble portions of the apparatus of this work. I would also like to thank Todd's Welding and Machining for their willingness to share their shop and tools. In particular, I would like to thank Ryan Todd and Timmy Todd for their willingness to share their skills and expertise which helped me through this work.

Without the love and support of my family, I would never have experienced this success. My mother and her beautiful faith, my father and his hard work and wisdom, my grandfather and his strong leadership, and my grandmother and her encouragement and passion are the reason I am where I am today.

The work presented in Chapter 3 was supported in part by the US Department of Energy (RAPID Sub-award DE-EE0007888-05-6). Any opinions, findings, conclusions, or recommendations expressed in this material are those of the author(s) and do not necessarily reflect the views of the funding agencies.

TABLE OF CONTENTS

LIST OF TABLES viii
LIST OF FIGURES ix

Chapter 1: Introduction 1
1.1 Motivation and Background 1
1.2 Research Objectives 20
1.3 Outline 21

Chapter 2: Experimental Investigation of Engine Adaptability on Alternative Fuels for Power Generation
2.1 Introduction 23
2.1.1 Motivation 23
2.1.2 The CL-ODH Process 24
2.2 Materials and Methods 28
2.2.1 Test Stand Setup 28
2.2.2 Experimental Parameters 36
2.3 Engine Performance Evaluation 38
2.3.1 In-Cylinder Combustion Comparison 38
2.3.2 Fuel Efficiency Analysis 46
2.4 Exhaust Gas Analysis 49
2.4.1 Exhaust Gas Temperature 49
2.4.2 Unburned Hydrocarbons 51
2.4.3 Carbon Monoxide 52
2.4.4 Carbon Dioxide 53
2.4.5 Oxides of Nitrogen 54
2.5 Engine Mechanical Health Analysis 55
2.6 Conclusions 59

Chapter 3: Design & Development of the Prototype High Power Density Generator
3.1 Introduction 60
3.1.1 Dynamo 61
3.1.2 Two-Stroke Engines & The Yamaha KT-100 65
3.2 Test Stand Design & Construction 72
3.3 Instrumentation & Data Collection 90
3.4 Preliminary Testing 95

Chapter 4: Experimental Validation: GASOLINE
4.1 Introduction 101
4.2 Experimental Procedure 103
4.3 Results and Discussion 105
4.3.1 Brake Power & Torque Analysis 105
4.3.2 In-Cylinder Pressure 109
4.3.3 Efficiency Analysis 117
4.3.4 Emissions Analysis 124
4.4 Conclusions 131

Chapter 5: Experimental Validation: METHANOL
5.1 Introduction 132
5.2 Methanol 134
5.2.1 Methanol as a Fuel 134
5.2.2 Methanol Conversion 137
5.3 Experimental Procedure 141
5.4 Results and Discussion 143
5.4.1 Brake Power & Torque Analysis 143
5.4.2 In-Cylinder Pressure 147
5.4.3 Efficiency Analysis 156
5.4.4 Emissions Analysis 166
5.5 Conclusions 176

Chapter 6: FUTURE WORK & CONCLUSIONS
6.1 Conclusions 178
6.2 Future Work 181

REFERENCES 191

APPENDICES 212

LIST OF TABLES

Table 2.1 *Specification of Engine Test Stand* 29

Table 2.2 *Fuel Mixture Ratio Used in the Experiments in Weight %* 37

Table 2.3 *Operating Air Fuel Ratios* 37

Table 2.4 *Lower Heating Values of the Fuel Mixtures Tested* 38

Table 2.5 *Calculated Indicated Power with Altering Fuel & Loading* 42

Table 3.1 *Motor Unit Specifications* 65

Table 3.2 *Yamaha KT-100 Specifications* 70

Table 3.3 *ATO Digital Rotary Torque Sensor Specifications* 73

Table 4.1 *Description of Loading Conditions* 105

Table 4.2 *Calculated Indicated Thermal Efficiency* 117

Table 4.3 *Calculated Mechanical Efficiency in Percent (%)* 121

Table 4.4 *Electrical Efficiency at Discrete Loading and Engine Speeds* 123

Table 4.5 *Generator Performance at 9100 RPM* 123

Table 5.1 *Description of Loading Conditions* 143

Table 5.2 *Calculated Indicated Thermal Efficiency* 156

Table 5.3 *Calculated Mechanical Efficiency in Percent (%)* 161

Table 5.4 *Electrical Efficiency at Discrete Loading and Engine Speeds* 164

Table 5.5 *Generator Performance at 9100 RPM* 164

LIST OF FIGURES

Figure 1.1 *Comparison of the Drivable Range of EVs and ICE vehicles* 3

Figure 1.2 *Illustration of Range Extender Design* 6

Figure 1.3 *Common Charging Strategy for Range Extenders* 7

Figure 1.4 *Common Range Extender Charging Strategy* 7

Figure 1.5 *Schematic of a Series Hybrid Range Extender* 8

Figure 1.6 *MAHLE Prototype Range Extender* 10

Figure 1.7 *ROTAX Prototype Range Extender* 11

Figure 1.8 *LOTUS Range Extender* 12

Figure 1.9 *CNR Prototype Range Extender* 13

Figure 1.10 *Example of Portable Commercially Available Range Extender* 14

Figure 1.11 *HYBRiX UAV Range Extender* 15

Figure 1.12 *Hirth UAV Range Extender Prototype* 16

Figure 1.13 *Schematic of a Proposed Hybrid Electric ATV* 19

Figure 2.1 *Illustration of the CL-ODH Process* 25

Figure 2.2 *Sportsman Gas Generator* 29

Figure 2.3 *Schematic of Intake Runner* 30

Figure 2.4 *PVC Accumulation Chaber* 31

Figure 2.5 *3-D Printed Intake Runner* 32

Figure 2.6 *Machining the In-cylinder Pressure Sensor* 33

Figure 2.7 *In-cylinder Pressure Sensor Installed in the Cylinder Head* 33

Figure 2.8 *Shaft Encoder & Hall Effect Sensor* 34

Figure 2.9 *Schematic of the Control Scheme and Experimental Setup* 35

Figure 2.10 *In-cylinder Pressure Comparison; A. Low load, B. Part Load, C. Full Load* 40

Figure 2.11 *Heat Release Rate Comparison Between Fuel Mixtures* 44

Figure 2.12 *Peak Heat Release Rate Comparison Between Fuel Mixtures* 45

Figure 2.13 *Indicated Fuel Consumption Comparison for all the Fuels and Loads* 47

Figure 2.14 *Fuel Efficiency Comparison Between Fuels and Loading* 48

Figure 2.15 *Exhaust Gas Temperature Comparison* 51

Figure 2.16 *Unburned Hydrocarbon Analysis* 52

Figure 2.17 *Carbon Monoxide Analysis* 53

Figure 2.18 *Carbon Dioxide Analysis* 54

Figure 2.19 *Oxides of Nitrogen Analysis* 55

Figure 2.20 *Image of Cylinder Head After Experiments* 57

Figure 2.21 *Image of Pison and Cylinder After Experiments* 57

Figure 2.22 *Image of Carburetor Bowl After Experiments* 58

Figure 3.1 *Honda IMA Powertrain* 63

Figure 3.2 *Honda IMA Motor Unit* 63

Figure 3.3 *Expanded View of the IMA Motor Unit* 64

Figure 3.4 *Two-Stroke vs Four-Stroke* 67

Figure 3.5 *Operation of a Two-Stroke Engine* 68

Figure 3.6 *Yamaha KT-100* 69

Figure 3.7 *Schematic View of the KT-100* 70

Figure 3.8 *Alternative View of the Yamaha KT-100* 71

Figure 3.9 *Image of ATO Digital Rotary Torque Sensor* 73

Figure 3.10 *Example of a Lovejoy Connection* 74

Figure 3.11 *Schematic of Test Stand Layout* 75

Figure 3.12 *Measured Drawing of Test Stand Layout* 76

Figure 3.13 *Pulley and Bearing Block Assembly* 77

Figure 3.14 *Engine Side Plate Machining Collage* 78

Figure 3.15 *Spacer Machining Collage* 79

Figure 3.16 *Engine Side Driveline Schematic* 80

Figure 3.17 *Shaft Adapter Collage* 81

Figure 3.18 *Engine Side Final Assembly* 82

Figure 3.19 *Housing Construction Collage* 84

Figure 3.20 *Armature Construction Collage* 85

Figure 3.21 *Final Dynamo Assembly Collage* 86

Figure 3.22 *Miscellaneous Component Collage* 88

Figure 3.23 *Final Test Stand I* 89

Figure 3.24 *Final Test Stand II* 89

Figure 3.25 *Final Test Stand III* 89

Figure 3.26 *In-Cylinder Pressure Sensor Installation Collage* 92

Figure 3.27 *Image of Exhaust Gas Analyzer* 94

Figure 3.28 *Tuning of Ignition & Fuel Collage* 97

Figure 3.29 *KT-100 Dyno Results* 98

Figure 3.30 *Motoring In-cylinder Pressure Curve* 99

Figure 3.31 *Preliminary Calibration Test Results* 100

Figure 4.1 *Brake Power at Varying Loads and Engine Speeds* 106

Figure 4.2 *Brake Torque at varying Loads and Engine Speeds* 108

Figure 4.3 *In-cylinder Pressure Comparison* 111

Figure 4.4 *Heat Release Rate Comparison* 114

Figure 4.5 *Cumulative Heat Release Rate Comparison* 116

Figure 4.6 *Brake Thermal Efficiency Comparison* 119

Figure 4.7 *Calculated Dynamo Efficiency* 122

Figure 4.8 *Unburnt Hydrocarbon Emissions* 125

Figure 4.9 *Carbon Monoxide Emissions* 128

Figure 4.10 *Carbon Dioxide Emissions* 129

Figure 4.11 *Oxides of Nitrogen Emissions* 130

Figure 5.1 *Image of Buller Atomizer Methanol Carburetor* 139

Figure 5.2 *Methanol Conversion Collage* 141

Figure 5.3 *Brake Power at Varying Loads and Engine Speeds* 144

Figure 5.4 *Brake Torque at varying Loads and Engine Speeds* 146

Figure 5.5 *In-cylinder Pressure Comparison* 149

Figure 5.6 *Heat Release Rate Comparison* 152

Figure 5.7 *Cumulative Heat Release Rate Comparison* 155

Figure 5.8 *Brake Thermal Efficiency Comparison* 159

Figure 5.9 *Calculated Dynamo Efficiency* 163

Figure 5.10 *Unburnt Hydrocarbon Emissions* 167

Figure 5.11 *Carbon Monoxide Emissions* 171

Figure 5.12 *Carbon Dioxide Emissions* 172

Figure 5.13 *Oxides of Nitrogen Emissions* 173

Figure 6.1 *CAD Model of Final Design* 182

Figure 6.2 *Two-Stroke Expansion Chamber Schematic* 185

Figure 6.3 *Yz250 Expansion Chamber Example* 186

Figure 6.4 *Example of a Tuned Pipe* 186

Figure 6.5 *Schematic of Two-Stroke Power Valve* 187

Figure 6.6 *Schematic of KTM Transfer Port Fuel Injection* 188

Figure 6.7 *Schematic of Direct Injected Two-Stroke* 189

Figure 6.8 *Image of BRP E-TEC Engine* 190

CHAPTER 1: Introduction

1.1 Motivation and Background.

Internal combustion engines have been incorporated in virtually every industry since their introduction in the late 1800s. By any standard, they have influenced everyone's life in some measurable way. Transportation, power generation, industry, agriculture, recreation, aviation, shipping, marine, and countless other industries rely on their ability to produce useful work from a readily available fuel source. The development of internal combustion engines through the decades can be benchmarked by a variety of technological innovations and has brought forth increasingly more powerful and advanced engines that emit fewer pollutants than ever before. However, there exists a threat to internal combustion engines; the continued tightening of emissions and environmental regulation challenges their existence and disrupts the security of their future. There are many who insist that the shortcomings of internal combustion engines can only be ameliorated by full electrification. However, the complete replacement of one technology with another will only introduce new shortcomings associated with an all-electric fleet. It is clear that an eclectic approach is required to meet the upcoming environmental targets.

Recently, the introduction of electrified powertrains, or the combination of internal combustion engines with electrical assistance, has gained significant attention. In many aspects, such hybrid powertrain architecture retains the benefits of both internal combustion engines and electrified power with few compromises. Moreover, hybridized powertrains can be operable to provide electrical power for use in, for example, electric motors or batteries while retaining the ability to utilize conventional and synthetic liquid fuels. However, many such powertrains continue to rely on fossil fuels and are otherwise responsible for some emissions. What's more,

the state of the art only includes large, complicated, and low power density units that are not suitable for certain applications that would benefit from hybridization.

One increasingly popular approach to lower carbon emissions is to encourage consumers to transition to electric vehicles. These electric vehicles (EVs) are being introduced as a solution to the problems associated with the dependency on fossil fuels, increasing carbon emissions, and other environmental issues [1]. Importantly, EVs alone do not solve the problem of global fossil fuel dependency and are not able to entirely replace internal combustion engines; they are merely one of many solutions included in an eclectic approach to reducing carbon emissions [2]. However, EVs have been shown in certain scenarios to provide some relief to the reliance on carbon-based fuels and as a result, their adoption should be encouraged.

Although EV adoption has increased over recent years, there remains a confluence of barriers that dissuade many consumers from considering EVs. Some of the common barriers include limited range, lack of charging infrastructure, high initial cost, high charging downtime, limited model choices, battery degradation, and poor resale value. Amongst these, range anxiety, or the driver's fear that an EV contains insufficient energy/battery capacity to drive the distance needed and that charging infrastructure will be unavailable to reach a destination is predominant [3]. What's more, EVs have a significantly lower drivable range when compared to their gasoline. In 2022, the average internal engine vehicle provided a drivable range of 413 miles while the average EV provided a drivable range of only 217 miles. Range becomes a more pertinent issue given the expense and limitations of lithium-ion batteries. While there are some EVs that have ranges in excess of 400 miles, the large battery pack and associated costs make these cars prohibitively expensive. New battery chemistries will likely not be able to substantially increase the energy density of lithium-ion batteries [3]. In addition, the cost of

lithium-ion batteries is expected to increase [4]. It should also be noted that high load conditions, such as towing and driving up gradients, as well as colder weather can further decrease the drivable range of EVs [2]. Figure 1.1 illustrates the average drivable range of a conventional internal combustion engine vehicle compared to an EV [4].

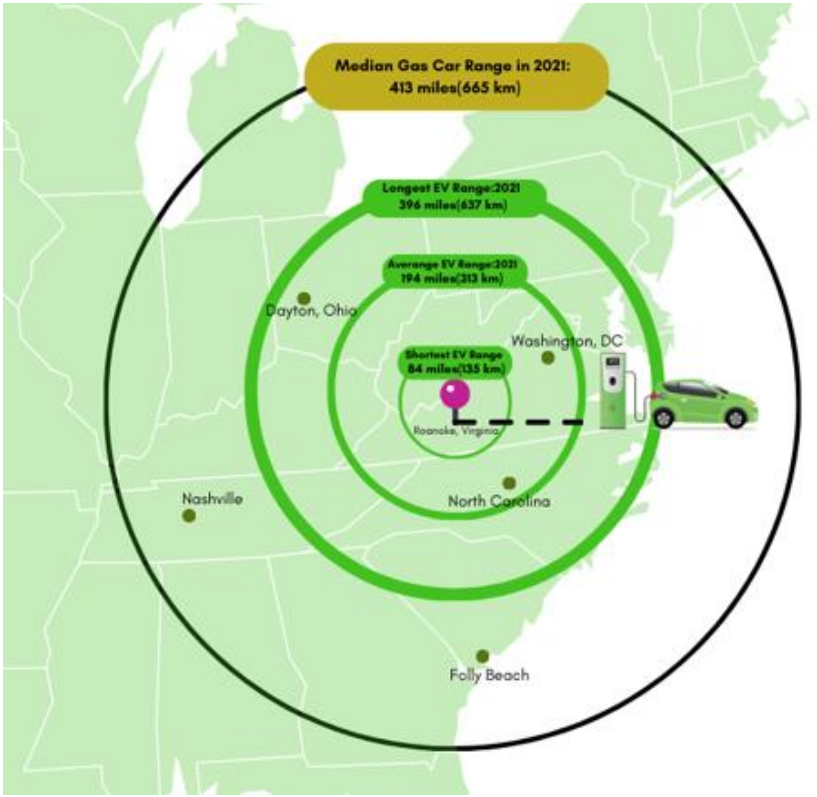

Figure 1.1: *Comparison of the Drivable Range of EVs and ICE vehicles* [5]

In addition, EVs are hindered by relatively large charging times when compared to internal combustion engine liquid fuel refill times. Many new EVs can take up to 12 hours to charge using household plug-in chargers. The conventional approach to ameliorate range anxiety can include deploying more robust charging infrastructure, developing higher battery capacity EVs, battery swapping technology, and free loan vehicles for long trips [6-7]. However, these approaches remain either long-term, impractical, or costly. Such practical issues and prices play a large role in car purchase decisions and negative sentiment toward electric vehicle technology

[8-9]. It is clear that a more viable solution to improving the drivable range of electric vehicles is necessary.

A range extender is a fuel-based auxiliary power source that is configured to add additional drivable range to the battery of an EV independent from grid charging [10]. So far as the discussion for range extenders is concerned, it is important to distinguish between range extenders and hybrid electric vehicles; hybrid EVs utilize the energy from both an electric motor and an IC engine to propel the vehicle while range extenders only add energy to the battery of EVs [11]. Importantly, range extenders do not include the added weight and complexity of gearboxes, transmissions, etc. that burden conventional hybrid electric vehicles. In addition, range extenders generally operate at a single RPM and can be tuned for superior efficiency when compared to traditional IC propulsion [8]. The most common types of range extenders are powered by conventional IC engines, but many configurations have been considered including fuel cells, free-piston generators, and micro gas turbines [12-13]. In most cases, these range extenders are adapted to use a liquid hydrocarbon fuel, such as gasoline [14]. Thus, an EV equipped with a range extender (REEV) can conveniently utilize the existing network of refueling stations. Further, range REEVs can avoid long charging times because of the utilization of internal combustion engines and existing fueling stations [15].

Unfortunately, the state-of-the-art range extenders only include small low-power units (<5kW) that are unfit for rapid charging and offer only small boosts in EV range and large permanently affixed range extenders that optionally accompany vehicles such as the Chevrolet Volt, Cadillac ELR, and BMW i3 [16-17]. In many cases, permanently attached range extenders are prohibitively expensive, often adding up to $6,300 to the purchase price of an EV, which already exceeds the price of similar IC vehicles [17]. Thus, there exists a need for a lightweight,

portable, and inexpensive range extender that has suitable power density to rapidly charge an EV**.** Further, in view of tightening emission regulations such as those set forth by the United States EPA, there exists a need for IC-powered range extenders that are adapted to operate on alternative fuels such as E-fuels and net zero carbon fuels.

When compared to the current lithium-based batteries common in EVs, gasoline has roughly 50 to 100 times higher power density in terms of energy per unit volume or weight. It is therefore difficult to configure an EV to have a similar drivable range when compared to IC-powered vehicles. Most consumers are unable to or unwilling to consider a vehicle that is unable to provide sufficient drivable range [18]. What's more, certain operating conditions exacerbate the low drivable range of EVs; people who live in rural areas, long commutes, utility tasks such as pulling a trailer or hauling, cold weather operation, etc. all further diminish the drivable range of EVs. Andwari et. al. analyzed the barriers to market penetration of EVs and the technological readiness of different components of battery electric vehicles (BEVs) [13]. Amongst increasing battery capacity, developing a more robust charging infrastructure, introducing swappable battery technology, and other similar approaches, the authors considered range extenders as the solution to free battery EVs from the 'range anxiety' issue and lower the vehicle weight and capital costs by downsizing the battery.

A range extender is a device that is configured to add drivable range to the battery of an EV by converting conventional fuel into electricity. This arrangement of range extenders is known as a series hybrid drivetrain. Range extenders are most commonly powered by internal combustion engines that are operable on traditional fuels such as gasoline or diesel [19]. According to *A Review of Range Extender Technologies in Electric Vehicles*., A range extender should be configured to comply with the following criteria [20]:

- The vehicle must have a rated all-electric range of at least 120 km.
- The range extender must provide a range less than or equal to the main battery range.
- The range extender must not be switched on until the main battery charge has been depleted.
- The vehicle must meet the super low emissions vehicle (SULEV) requirements.

Importantly, a range extender is distinguishable from a hybrid powertrain in that it must not be part of the drivetrain; a range extender may only provide power to the battery and not mechanically linked to the wheels of a vehicle. Range extenders occupy a category of powertrains between pure internal combustion engine power and pure battery power. Figure 1.2 illustrates a simple schematic of a series hybrid powertrain with a range extender adapted from Tran et. al. [6].

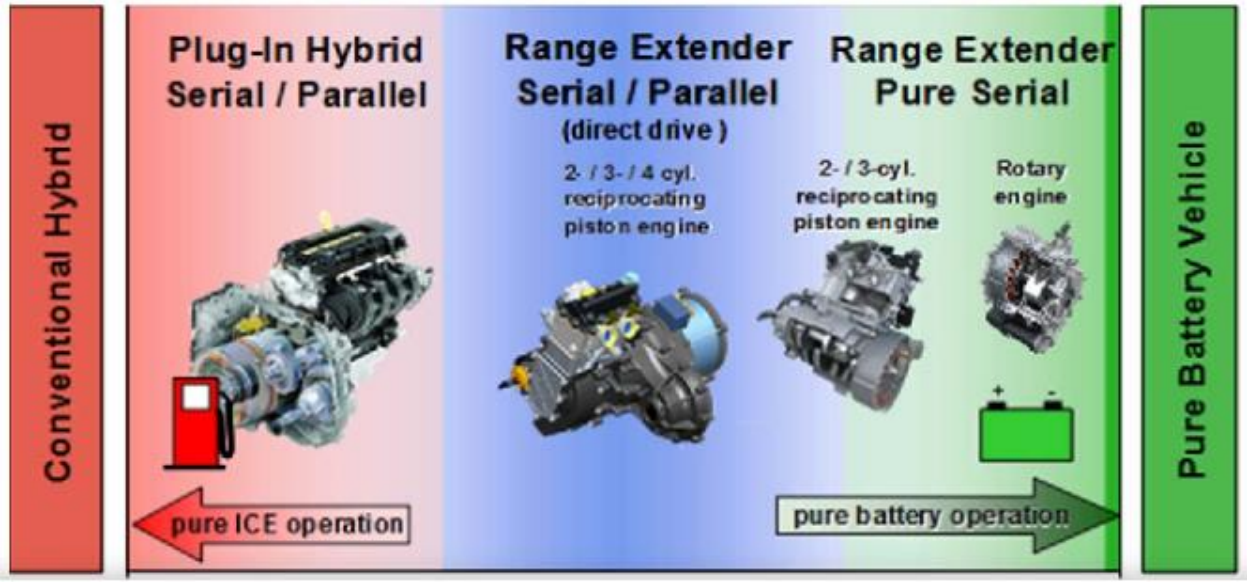

Figure 1.2: *Illustration of Range Extender Design* [14]

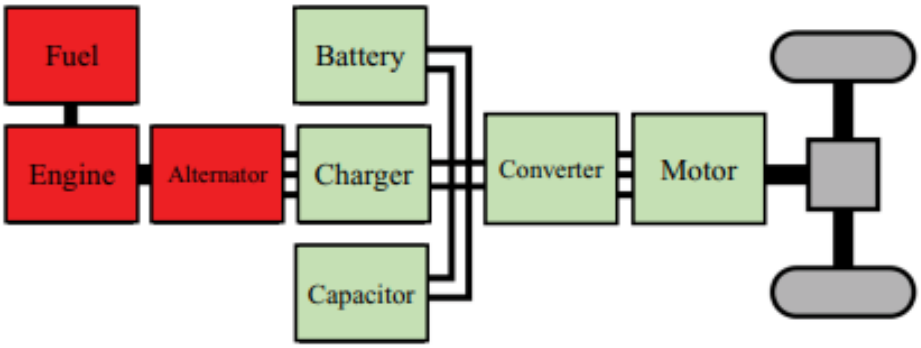

***Figure 1.3**: Schematic of a Series Hybrid Powertrain Incorporating a Range Extender* [6].

Further, range extenders can be activated whenever the drivable range of a battery is low to avoid irreversible cell damage. The battery should always be charged externally via a standard charger whenever possible. In some aspects, a range extender could have a positive impact on battery life as it can prevent deep cycle degradation of the battery [14]. In certain aspects, range extenders can be configured to provide electrical power when the battery on an electric car falls below a certain threshold and increase the state of charge of the battery. Range extenders are not often used to completely charge the battery of an EV, but to provide a slight increase in the level of charge of the battery. Figure 1.4 illustrates common range extender charging schemes.

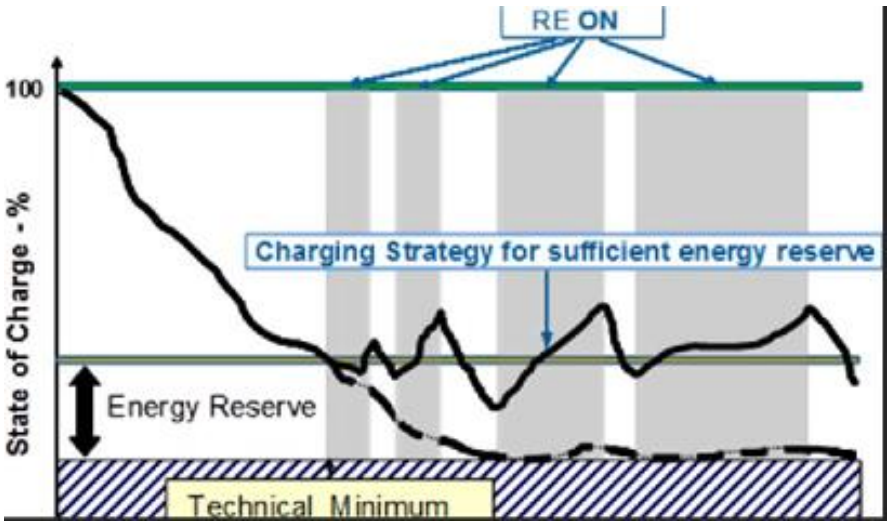

***Figure 1.4:** Common Charging Strategy for Range Extenders* [16]

Internal combustion engines are often used as the power source for range extenders. Advantageously, because range extenders require constant RPM operation, these engines can be tuned to always operate at peak efficiency. The integration of internal combustion engines with range extenders is simple and straightforward; internal combustion engines are well understood, simplifying their integration into range extender technology. Most importantly, a range extender equipped with an internal combustion engine will be able to utilize the highly robust existing fueling infrastructure. Many configurations of both two-stroke and four-stroke internal combustion engines have been contemplated for use in conjunction with range extenders, including single-cylinder, multi-cylinder engines, rotary engines, free piston engines, and micro gas turbines. From there, the engines are connected to a rotary dynamo that can produce electrical power. Figure 1.5 illustrates an example of internal combustion engine-based range extender architecture.

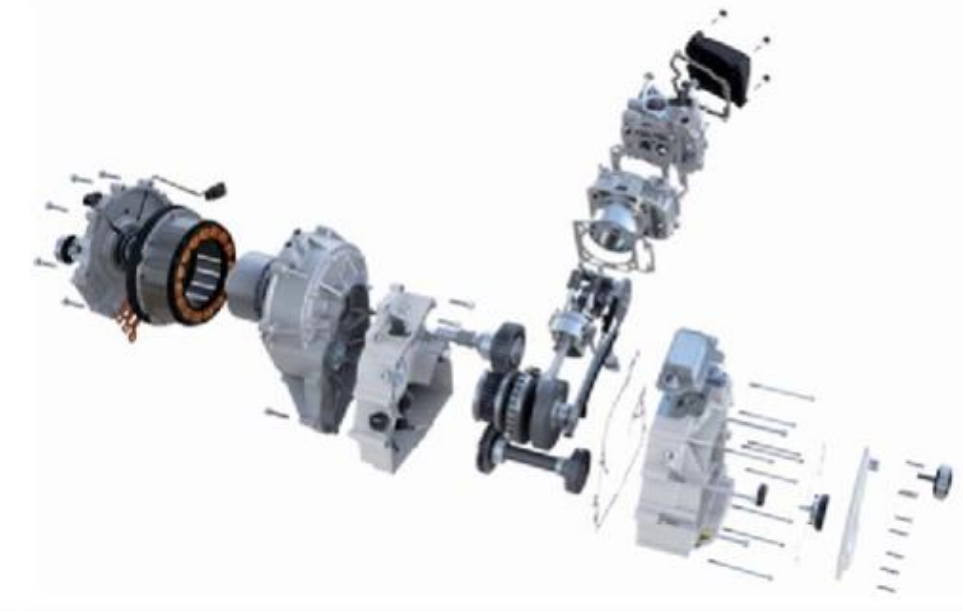

Figure 1.5: *Schematic of a Series Hybrid Range Extender* [15]

A plurality of research and development groups in academic and commercial settings have proposed, constructed, and brought to market range extenders. Borghi et. al. considered the design and conducted the experimental development of a range extender powered by a two-stroke, single-cylinder engine [15]. The engine was rated at 30 kW and had a maximum engine speed of 4500 rpm. The proposed range extender had a theoretical weight of 105 kg, resulting in a power density of .29 kW/kg. The engine was also compared to existing four-stroke engines and found that the two-stroke engine provided significantly higher power density and that the range extender addressed many of the issues associated with EVs. However, it was found that the new engine could not meet the compliance requirements of the very low NO_x limit of standard EVs.

MALHE Powertrains presented a prototype range extender in 2022 that is adapted to be integrated into the structure of an EV [21]. The prototype utilized a twin-cylinder 900cc internal combustion engine coupled to a dynamo. Further, the prototype produced 30 kW of electrical power and weighed approximately 200 kg. It was found that the range extender was operable to increase the drivable range of the EV it was coupled with to 500. The range extender was able to meet Euro 6 emissions standards. In this configuration, the range extender provided a power density of .15 kW/kg. Importantly, range extenders of this type are fixedly attached to the vehicle and cannot be shared with different vehicles. Figure 1.6 is an image of the MAHLE Range extender.

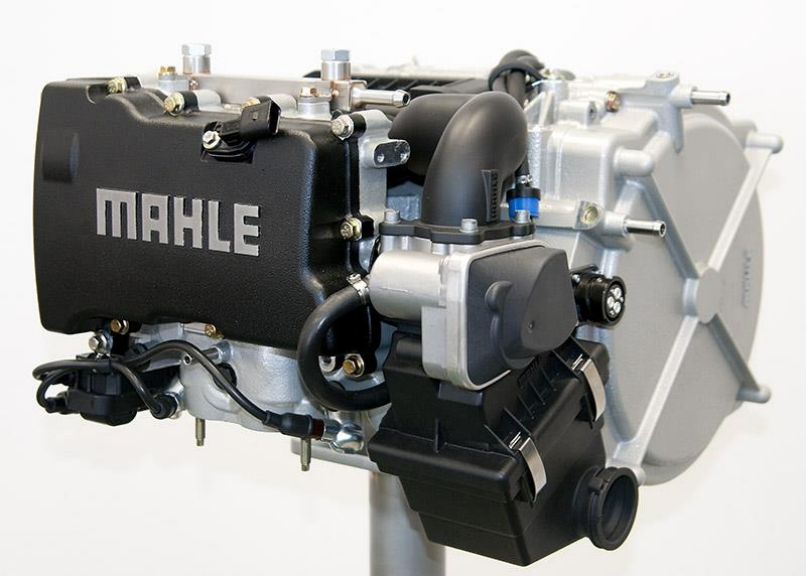

***Figure 1.6**: MAHLE Prototype Range Extender* [21]

In 2014, BRP-Powertrain and AVL Powertrain systems developed a range extender package for electrified vehicles [22]. The range extender could be mounted onto an electrified vehicle and was configured to provide additional charge to the battery. The range extender comprised a single-cylinder ROTAX 1000cc engine and was able to produce 25 kW of electrical power while weighing 120 kg, giving a power density of .21 kW/kg. Unlike the MAHLE range extender, this model can be incorporated into an existing EV but is not portable or moveable between different EVs. Figure 1.7 provides an image of the ROTAX-based range extender prototype.

Figure 1.7*: ROTAX Prototype Range Extender* [22].

LOTUS Engineering designed and developed an internal combustion engine range extender that was configured for use with passenger cars of approximately 1650 kg. In addition, this range extender could be used in conjunction with a series hybrid powertrain to power the electric motors [23]. A bespoke internal combustion engine was designed and constructed in view of target specifications established from order of importance. The LOTUS range extender comprised a three-cylinder, four-stroke 1.2l fuel-injected gasoline engine. The engine produced a maximum of 37 kW of electrical power and a combined weight between the engine and generator of 101 kg, yielding a power density of .366 kW/kg. The engine was able to produce a continuous 15 kW of electrical power for use in hybrid and range-extending applications while maintaining a low fuel consumption of .245 g/kWh. Future developments of the LOTUS range extender include modifying the engine to achieve Tier-1 emissions standards and potentially converting the range extender to operate on renewable fuels, such as alcohol-based fuels. In addition, LOTUS posits the potential to increase power by incorporating forced induction techniques, such as turbocharging. Figure 1.8 is an image of the LOTUS range extender [23].

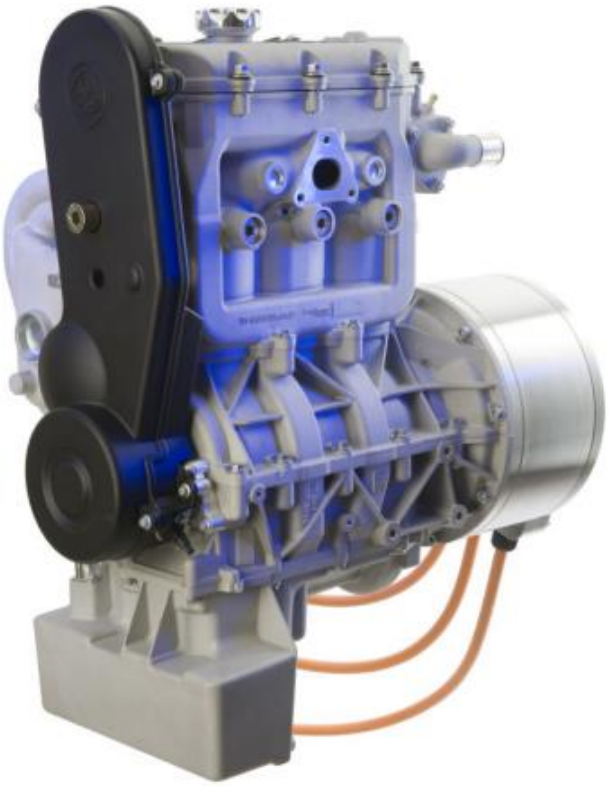

Figure 1.8: *Image of LOTUS Range Extender* [23]

CNR Istituto Motori proposed a prototype for a compact 10 kW engine-based range extender which was suitable for plug-in hybrids and series hybrid vehicles [24]. The product of their work could be used as a range extender or a component in lightweight series hybrid powertrains. The device comprised a modified four-stroke, 250cc scooter engine connected to a bespoke three-phase dynamometer. The unit demonstrated 10 kW of electrical power and an overall weight of 23 kg, yielding a power density of .41 kW/kg [24]. The range extender concept of this work was a theoretical model and was not produced as a result of a custom engine and bespoke dynamo. The author proposed that the prototype could be further improved by incorporating a more efficient intake design and a high-inertia flywheel. The author also concluded that the power density of this model led to decreased fuel efficiency. Figure 1.9 is an image of the CNR range extender prototype.

Figure 1.9: *CNR Prototype Range Extender* [24]

There exists a variety of small range extenders that comprise single-cylinder air-cooled engines commonly utilized in power equipment connected to small Dynamos. These range extenders are available from suppliers such as eBay. Typically, these range extenders comprise a 212 cc single-cylinder 4 stroke engine connected to an electric motor. They are operable to produce a maximum of 3 kW while generally weighing 25 kg. Thus, these range extenders provide a power density of .12 kW/kg. Advantageously, these range extenders are substantially portable and can be used amongst a variety of vehicles. However, they provide are unable to provide enough power to rapidly charge an EV. Figure 1.10 is an example of an embodiment of these range extenders.

***Figure 1.10**: Example of Portable Commercially Available Range Extender*

It is clear that there exists a gap in the state of the art of range extender technology. Range extenders that are sufficiently powerful to rapidly charge an EV are not portable and are otherwise inconvenient to use. They are also expensive and may not be compatible with certain vehicles. Range extenders that are lightweight and portable do not provide sufficient power to quickly charge an EV with substantial useful range. Thus, there exists a need for a range extender that has a high power density, is lightweight, portable, and can provide enough power to rapidly charge an EV.

In addition to EV applications, range extenders are particularly useful for unmanned aerial vehicle (UAV) aircraft, drones, and other experimental aircraft that operate with electric motors. UAVs require power sources that have a small form factor and high power density. Typically, drones are equipped with one or more electric motors that receive power from a battery or capacitor [25]. As a result of the relatively low power density of batteries, flight time can be limited. In many applications, such as long flight times, heavy payloads, or military applications, the flight range of drones is insufficient. In an attempt to lengthen the flight time,

drones can be equipped with small range extenders that are configured to increase the state of charge to a drone battery [25-26]. Obviously, weight is a critical factor in UAV range extenders because it directly impacts the payload of the drone. Thus, a generator with a high power density is required [27]. The future of UAV propulsion relies on high density generator design; designs with high power densities are favorable because they increase the payload capacity of the UAV.

There exists a small and limited selection of gasoline-powered range extenders that are suitable for use in UAV applications. Quaternium technology offers a range extender for hybrid drones that is commercially available [28]. The range extender comprises a 32cc two-stroke internal combustion engine coupled to an electric generator. The generator produces 2600 Watts and provides a continuous 48 Volts. In its configuration, the HYBRiX 2.1 can provide up to 4 hours of additional operation flight time with to existing drones. Figure 1.11 shows an embodiment of the HYBRiX UAV range extender [29].

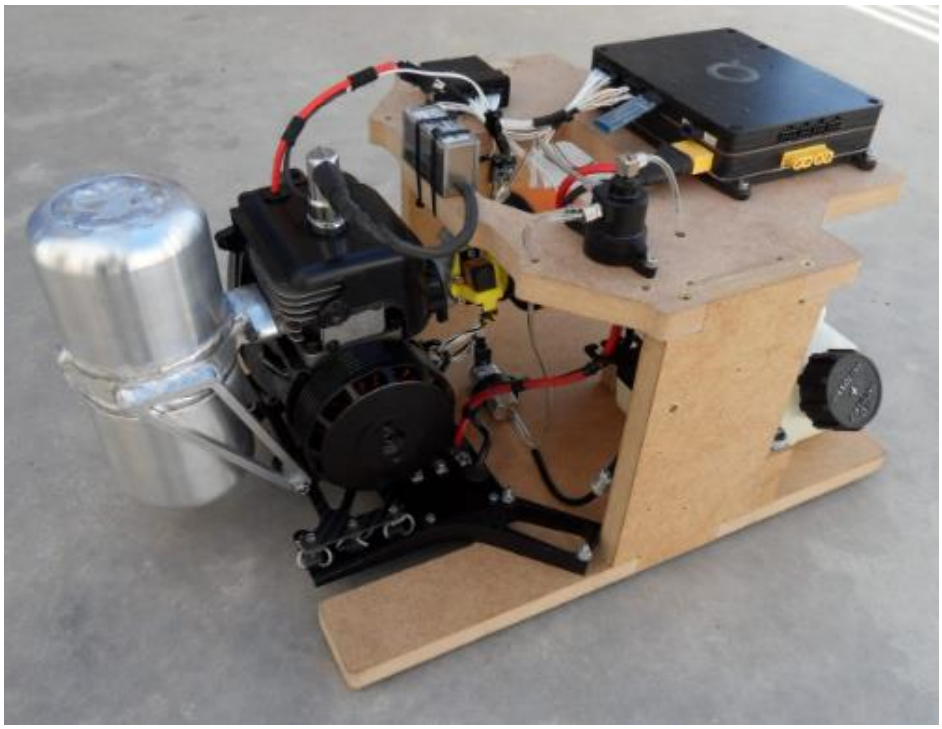

Figure 1.11: *HYBRiX UAV Range Extender* [29].

There are several other manufacturers that offer similarly sized range extenders for UAVs that provide similar power output. Unfortunately, such range extenders are only able to provide useful power to drones that have a maximum take-off weight (MTOW) of up to 25 kg [29]. Accordingly, there exists a gap in the state of the art for larger drones that require a higher power range extender.

Hirth engines have investigated the viability of a liquid-cooled hybrid UAV range extender [30]. The range extender concept comprised a parallel twin two-stroke engine. The engine half was used only to generate power for the system. The electric-driven half was configured to provide low-noise operation. The theoretically proposed model would include a 625cc fuel-injected, two-stroke engine and a small compact dynamo. Figure 1.12 is an image of the Hirth series hybrid UAV powertrain.

Figure 1.12: *Hirth UAV Range Extender Prototype* [30]

Hybrid vehicle propulsion systems are becoming increasingly popular as they in many aspects combine the advantages of internal combustion engine propulsion and electric powertrain propulsion [31]. Additionally, the flexibility and configurability of hybrid powertrains is even more interesting. By definition, hybrid powertrains selectively combine more than one motive architecture [31]. For example, a hybrid powertrain could comprise the unity of an internal combustion engine and an electric powertrain to provide a motive force to a vehicle. Among the existing hybrid powertrain architecture, the series hybrid, also referred to as range-extended electric vehicles, are of particular interest [31-32]. In the case of the series hybrid, the engine is simply used to recharge the battery bank or provide electrical power directly to the motor. The engine can be substantially smaller because in many cases they operate at a steady state and can be allowed to recharge the batteries over a longer period of time. [33]. Moreover, electric motors are more efficient than internal combustion engines and do not require gear changes while internal combustion engines are more efficient when operating at a steady state [33]. From a practical standpoint, the series hybrid arrangement is a desirable combination of technologies. Moreover, the series hybrid offers flexibility that pure internal combustion engine and battery EVs cannot. It has been shown that series hybrid powertrains can offer approximately 90% of the capacity of an electric vehicle [30]. If the driver is in a situation where they cannot charge their vehicle (e.g., unavailable charging stations, power outages, etc.) the user can simply engage the engine to recharge. Some series hybrid arrangements do not require a battery at all and can rely on the current directly from the generator to power the motor. The vast majority of series hybrid powertrains are in the order of 100 horsepower or more [32]. These powertrains are complex, expensive, and have relatively lower power densities [32]. Further, there is a need for more compact and cheaper series hybrid powertrains that can power smaller vehicles. There exists a

vacancy in the state of the art of hybrid propulsion for small, compact power generation that is structured for use with a series hybrid. Small engines are responsible for 242 million tons of Carbon emissions each year [32]. Because of the cost, size, and practical limitations, it is difficult to incorporate advanced emissions reduction strategies. Moreover, because of the current limitations of hybrid powertrains, it is difficult to incorporate hybrid power. In many examples, the engine configurations that are adapted for use with series hybrid powertrains are large, heavy, and low-powered. The advent of such lightweight, high power density generators could address the vacancy in the state of the art and provide useful electrical power for hybrid powertrains for use in, for example, powersports, recreational vehicles, small off-road vehicles, power equipment, or other similarly sized applications [34]. Simic et. al. simulated the use of a hybrid powertrain in an ATV and proposed and suggested that an optimized hybrid electric powertrain configured for use in such applications could lower fuel consumption and certain emissions species [34]. Further, *Simic* proposed a theoretical model for a hybrid powertrain to be used in an exemplary embodiment of a hybrid electric ATV. It is envisioned that a similar model could be adapted for a variety of applications where small, lightweight, high specific powertrains are required. Figure 1.13 is a schematic for a proposed hybrid electric ATV proposed by *Simic* [34].

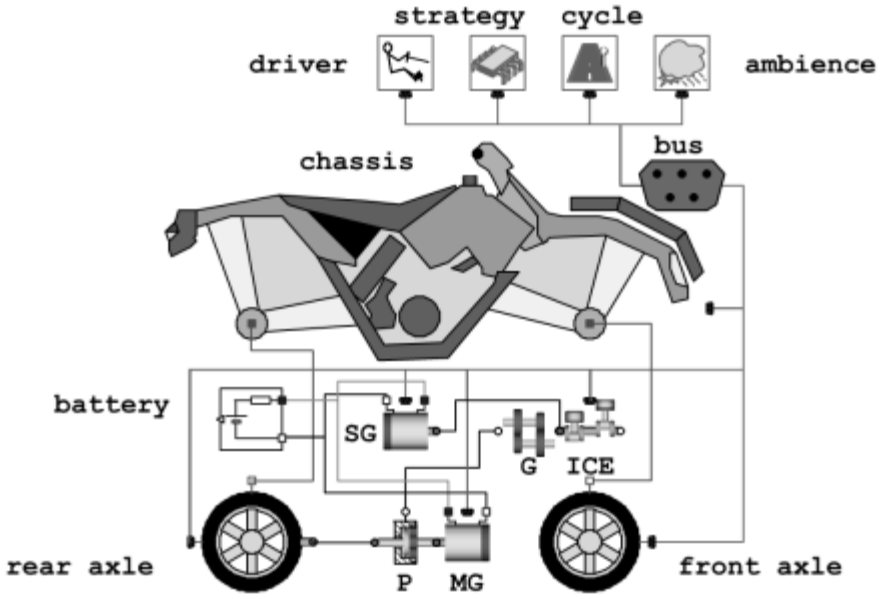

Figure 1.13: *Schematic of a Proposed Hybrid Electric ATV* [34]

In modern internal combustion engines, a plurality of emissions control methods exists with the intent to reduce harmful exhaust emissions. Some examples of such emissions control methods include catalytic converters, exhaust gas recirculation (EGR), selective catalytic reduction (SCR), particulate filters, lean-burn schemes, air injection, and closed-loop fuel injection systems [35-36]. Each of these approaches requires complex engine architecture, adds weight, and complexity, and decreases reliability and thus are not suitable for small engine applications [37-38]. One promising technique is the use of synthetic fuels or "E-fuels." E-fuels are fuels for use in an internal combustion engine that is produced through a process that involves the use of a renewable energy source to convert carbon dioxide and water into hydrocarbons, alcohols, or other combustible liquid fuels [39]. These fuels are considered synthetic because they are not naturally occurring and are produced through artificial processes. Importantly, these fuels can be net carbon zero and do not increase the free carbon dioxide in the atmosphere and produce no net greenhouse gas emissions [40]. Many such fuels can be readily

adaptable to existing internal combustion engines and are well suited for the reduction of certain emissions species and lower or eliminate the carbon footprint of internal combustion engines.

In practice, E-fuels are usually made from carbon dioxide that is hydrogenated. The carbon dioxide used to make E-fuels may be directly captured from the air, derived from seawater, or captured from industrial processes [41]. Common examples of E-fuels used to replace gasoline or diesel fuel in existing engines include ammonia and methane. In addition to being carbon neutral, such E-fuels can alleviate the dependency and costs associated with drilling and importing fossil fuels [40]. The energy used to generate E-fuels can be provided from a renewable source, for example, nuclear power, wind power, solar, and geothermal. E-fuels or other carbon-neutral fuels can potentially reduce the need for fossil fuels entirely assuming that enough renewable energy could be produced [41].

1.2 Research Objectives

The objective of this dissertation is mainly focused on the experimental development of a high-power-density electric generator as well as the experimental investigation of small internal combustion engines that are adapted to operate on E-fuels. It is contemplated that the objects of this work can be incorporated into, for example, hybrid powertrain and range extender design and development. Further, techniques and emissions reduction potential of using E-fuels are also investigated. The major objectives are as follows:

I. Modify an existing commercially available spark ignition generator to operate on E-fuel mixtures; Study the effects on emissions and performance with the E-fuel and compare to gasoline.

II. Design and construct a prototype electric generator having at least a high power density that comports with identified design constraints.
III. Investigate the performance of the prototype electric generator through operation on gasoline fuel; explore the performance and emissions of the generator and compare to commercially available units.
IV. Modify the prototype to operate on E-fuel and repeat the experiments; study the effects of E-fuel on performance and emissions.
V. Propose a final design of a commercially viable product; explore options to increase performance while decreasing emissions.

1.3 Outline

Chapter 2 focuses on the viability and performance of byproduct exhaust gases from industrial processes for use in internal combustion engines for power generation. The fuel of concern comprises varying mixtures of methane and ethane in high dilutions of carbon dioxide which can simulate high EGR operating conditions. A small commercially available 13 hp internal combustion engine generator was modified and instrumented to operate on the synthetic fuel. Various fuel mixtures and loading conditions were tested and compared to gasoline. Further, the adaptability and reliability of the engine operable on such fuels was investigated.

Chapter 3 focuses on the design process and construction of a prototype high power density range extender. A variety of performance goals were set in view of the limitations of currently available generators and performance benchmarks were identified. Chapter 3 details the design and construction process used in developing the prototype high power density generator. The design iterations and modifications were also described to better identify the design process.

Further, Chapter 3 presents the optimization and tuning process to provide the highest performance from the prototype.

Chapter 4 presents the first series of experiments and validation of the high power density generator prototype when operated on gasoline. The prototype was connected to a series of load elements and instrumented to understand the performance limitations and establish baseline data on gasoline fuel. Further, the emissions species were evaluated to understand the carbon footprint of the prototype. The experiments were repeated to understand the reliability and performance of the prototype.

Chapter 5 presents the modification and reevaluation of the prototype on E-fuels. More specifically, the engine was modified to operate on methanol with the intent to reduce certain emissions species. The performance was evaluated against baseline data collected from gasoline experiments. Further, the emissions reductions and potential for the prototype to be a carbon-neutral generator were evaluated.

Chapter 6 discusses future evolutions of the high power density generator as well as proposes a final design for commercial utilization. In addition, techniques and technologies that could be used to improve the design are also discussed. Moreover, chapter 6 summarizes the important conclusions and all the studies discussed in the previous section. In addition, future work is also presented at the end.

CHAPTER 2: Experimental Investigation of Engine Adaptability on Alternative Fuels for Power Generation

2.1 Introduction

2.1.1. Motivation

The first step in developing a generator that is operable on non-conventional fuels is to investigate the ease at which existing engines can be adapted for such use. In addition, it is important to evaluate the performance of the engine and the effects the alternative fuels may have on the engine. In this chapter, a commercially available internal combustion engine generator was selected for testing. A gasoline generator was selected as it closely mimics the conditions that the prototype high power density generator would be subjected to, such as varying loading at constant throttle conditions and, in some aspects, steady state loading. Importantly, a commercially available model was chosen as part of this work to investigate how readily adaptable existing engines are for use in the development of the high power density electric generator. A 13 horsepower, single-cylinder gasoline generator was selected and repurposed for this work as a test stand by incorporating a modified fuel induction system and the engine was instrumented for data collection.

A synthetic gaseous fuel was chosen for use in the experiments of this chapter. In particular, the synthetic gaseous fuel, or SIM fuel, comprises a mixture of approximately 40% methane, 5% ethane, and a 41% diluent component along with other minor compounds. The flammable methane and ethane components in combination with the non-flammable carbon dioxide component can closely simulate an engine operating under high exhaust gas circulating conditions. Exhaust Gas Recirculation, or EGR, is a common technique used in modern internal

combustion engine emissions control schemes wherein the products of combustion collected from the exhaust system are redirected into the combustion chamber to dilute the fuel charge. In practice, EGR systems can reduce oxides of nitrogen emissions (NO_x) and certain carbon emissions. The fuel for these experiments was sourced from an industrial process where it is a common waste product. In addition to investigating the adaptability and performance of an engine with alternative fuel, an aspect of this work pertains to the potential of increasing the industrial process efficiency.

2.1.2. The CL-ODH Process

Ethylene is an important and necessary industrial organic chemical that has many uses in manufacturing and industry. However, the production of ethylene for such uses is one of the largest producers of anthropogenic CO_2 today. Greenhouse gas emissions from similar industrial processes surpass that of the transportation industry by almost 50% [43]. Therefore, it is envisioned that large reductions in such anthropogenic carbon dioxide emissions from these industrial processes will be required to stabilize the atmospheric concentration of greenhouse gases [44]. Concordantly, substantial efforts have been made to find a suitable alternative method of production for ethylene. Ethylene is conventionally produced by steam cracking or heating natural gas containing ethane and propane to 800 – 900 Celsius which yields a mixture of gases from which ethylene is separated.

Significant attention has been paid to carbon-capturing techniques used to control the CO_2 emitted during power generation, commercial and residential heating, and manufacturing. Chemical-looping-based oxidative dehydrogenation (CL-ODH) is a process that can be used to produce ethylene from ethane vastly more efficiently & safely than the traditional steam cracking

processes [39]. Following the CL-ODH process, the resulting ethylene can be readily converted into liquid fuels via an oligomerization step. Figure 2.1 illustrates the CL-ODH process used for ethylene production.

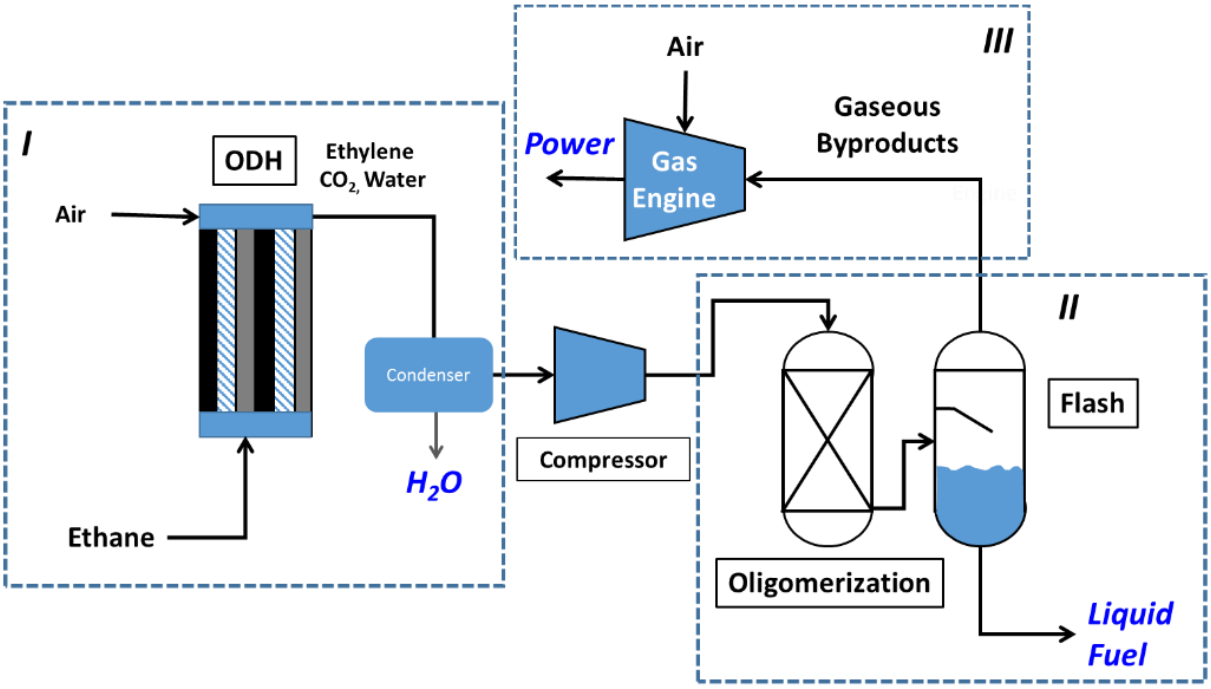

Figure 2.1: *Illustration of the CL-ODH Process* [45].

This novel gas-to-liquids process has several gaseous by-products; one of which is a mixture of gasses comprising different species including carbon dioxide, ethane, methane, carbon monoxide, water, ethylene, etc. [46]. As a result of these mixtures containing hydrocarbons, these by-product gasses have a considerable amount of energy that can be extracted and utilized to improve the overall efficiency of the CL-ODH process by converting the chemical energy in the fuel to electrical energy to power the plant and conversion process. Even though the CL-ODH process is a modern approach to clean production of ethylene that boasts thermal efficiencies of up to 96%, there is room for improvement so far as incorporating techniques to utilize the byproduct gases [47]. The byproduct gas of concern has a concentration

of 41% CO_2, 40% ethane, and 5% methane by weight with other minor compounds, which is represented in this work as a simulated (SIM) gas.

One of the least involved methods to convert the chemical energy from the SIM gas to mechanical energy would be to combust the gases in an internal-combustion-engine based stationary generator due to the presence of hydrocarbons and the fuel pre-existing in a gaseous state. Since this fuel contains large amounts of methane, the major species in natural gas fuel, performance and viability are expected to be similar to natural gas. In recent decades, natural gas combustion has been used as an alternative fuel in internal combustion engines to reduce the carbon footprint in transportation, power generation, and other related industries [48].

Methane as a fuel has a high research octane and a wide flammability range thus allowing operation in high compression engines. Further, lean mixtures, such as those promulgated by methane provide enhanced knock resistance [49]. Therefore, in many ways using this fuel in an internal combustion engine can provide measurable advantages so far as thermal efficiency resulting from increased specific heat ratio, lower temperature of combustion, higher compression ratio, and decreased throttling losses. Spark ignition engines in use throughout the world, when operated on such natural gas fuels, often emit up to 50% fewer unburnt hydrocarbon emissions at WOT [50]. The biggest problem in using the fuel of concern would be the presence of up to 45% CO_2 by weight in the gas byproduct. High concentrations of non-combustible CO_2 in the fuel mixture led to a delay in the ignition and heat release, which is attributed to the increased heat capacity of CO_2 [51-52]. In other words, the high concentration of carbon dioxide acts as a diluent of the fuel species which removes energy from the combustion event. In many ways, this fuel is likened to a fuel charge subjected to high exhaust gas recirculation or EGR. Conventional EGR comprises a system to reintroduce inert products of combustion at a

concentration of about 10% - 20% back into the intake to manipulate combustion and alter the products of combustion [53, 54].

Some of the issues of having a high concentration of CO_2 can be overcome by the mixture having high concentrations of ethane. Studies show that with increasing concentration of ethane in a fuel mixture there can be a reduction in the ignition delay of the mixture [55]. The reduction in ignition delay is also dependent on the equivalence ratio of the fuel mixture [56-58]. The gas mixture also has a major portion of methane, which will also help in energy production. With a complex gas mixture like this, there are much more complex mechanisms involved in the combustion process [59-60]. Molecular ethane species in the mixture are very reactive and readily degrade into a more complex species in the chamber reducing the concentration of the primary fuel element. This degradation also affects the ability of methane to combust even more thus increasing the complexity of ignition [63-64]. Previous studies have been performed on the same fuel mixture in a constant volume combustion chamber environment and the results concluded that while the mixture is harder to ignite, the performance of the fuel in an engine combustion scenario is viable with relative performance [65]. To better understand the effects of the fuel composition on the effectiveness of the fuel the emissions of the engine were recorded. In general, the addition of natural gas or methane to the fuel mixture shows a reduction in the overall concentrations of carbon monoxide and nitrous oxides [66-67]. The addition of CO_2 while simulating EGR also reduces the flame temperature inside the combustion chamber helping with the control of emissions by the engine [68-69].

This study explores the efficacy of utilizing synthetic fuel, such as the byproduct gas resulting from the CL-ODH process, in an internal combustion engine for power generation. Further, the emissions characteristics of the fuel are also studied and compared against

conventional fuels to identify the effectiveness of this fuel as a replacement or supplement to gasoline for power generation in internal combustion engines. Finally, the ability to modify and adapt existing internal combustion engines to use this fuel, as well as to cycle operation between conventional and SIM fuels is considered. The techniques and lessons from this chapter will be applied to the development and experimentation of the high power density electric generator.

2.2 Materials and Methods

2.2.1 Test Stand Setup

A commercially available gasoline generator was instrumented and modified to conduct the experiments. Such a generator was chosen for these experiments primarily in order to simulate real world conditions more closely, as these fuels are being investigated for use in power generation in similar conventions. The engine used is an air-cooled, single-cylinder, four-stroke spark-ignition engine with a displacement of 420 cc. It has a compression ratio of 8.5:1 and a bore and stroke of 90 mm x 66 mm. The engine has a push rod style single overhead cam valve arrangement and is fed via a single fuel circuit carburetor. When run on 87 octane or higher gasoline, the engine is capable of producing 10 kW and 25 N-m of torque at 3600 rpm. These engines are common in the art and are utilized in a variety of applications. Table 2.1 lists the specifications of the engine. Figure 2.2 illustrates the generator in its commercially available configuration.

TABLE 2.1: *Specifications of the Engine Generator Test Stand*

Specification	Value
Engine displacement	420 CC
Compression ratio	8.5:1
Bore x Stroke	90 mm x 66 mm
Cooling type	Forced Air Cooling
Rated RPM	3600
Rated Power	10 kW

Figure 2.2: *Sportsman Gasoline Generator*

A generator head comprising a series of heating elements, who's current and voltage could be measured, was configured to provide constant load to the engine. To simulate this operational load, these electric heating elements were connected to the generator whereupon large iron castings were placed on the heaters to absorb the heat produced to ensure they could continuously provide load to the engine.

Several modifications were made to the engine intake to enhance its ability to operate with the gas supply. The most significant of these included a custom intake runner that was

optimized, and 3-D printed to adapt the gas mixing chamber to the carburetor. Constraints on this intake runner included retaining variability between mixed gas induction and regular air induction to the carburetor for conventional gas operation. Figure 2.3 provides a schematic view of the 3-D printed intake runner for the engine.

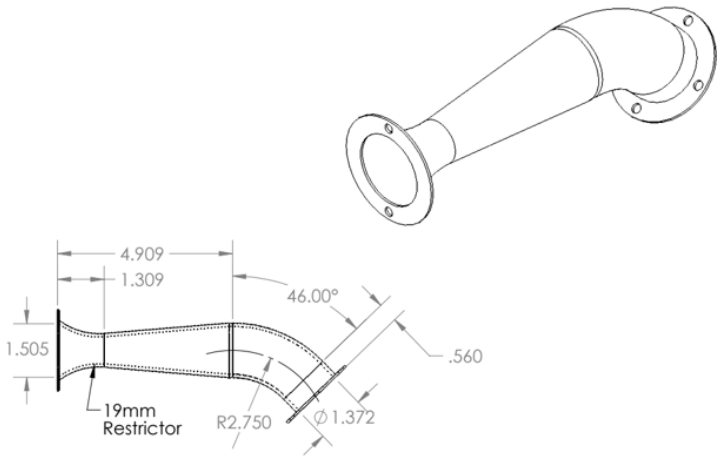

Figure 2.3: *Schematic of Intake Runner*

A PVC accumulation chamber was installed above the engine and connected to the intake runner via a hose and a small port on the side of the chamber to properly mix the fuels. This chamber was used to create a homogeneous and thorough mixture of methane, ethane, and CO_2 prior to induction into the engine. For the experiments with mixed gas, the carburetor was decommissioned, and the fuel lines were bypassed by the intake manifold so that no gasoline was introduced into the engine. Gasoline supplies were restricted as well to prevent interference from the fuel tank. Figure 2.4 is an image of the PVC accumulation chamber used during testing. The accumulation chamber includes a gas line that was directly connected to the intake runner and configured to provide a homogeneous mixture of gas to the engine.

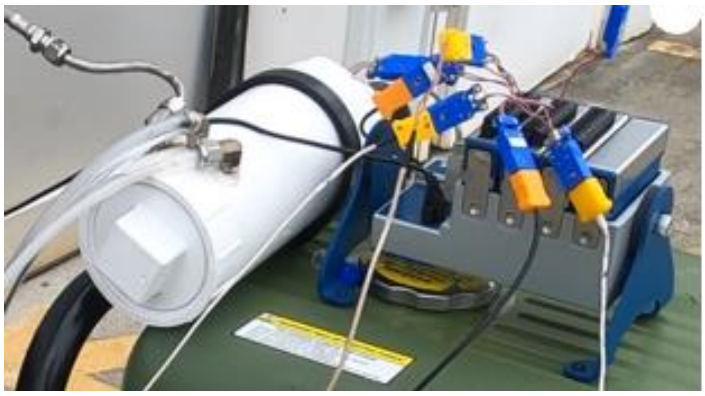

Figure 2.4: *PVC Accumulation Chaber*

Most generators are equipped with governor systems to ensure the engine operates as close to 3600 rpm as possible to provide a constant 60 Hz. The governor works by limiting the ignition if the engine RPM varies too much. The governor was deactivated when testing the gas mixtures so the engine speed could be manually controlled by controlling the mass flow of mixed gases.

The generator system was Instrumented to record the parameters of the engine during operation. K-Type thermocouples were installed in a plurality of locations on the engine, including the cylinder head, exhaust, cylinder, crankcase, ambient, intake charge (premixed), and oil reservoir. A Bosch mass airflow (MAF) sensor was used to measure the quantity of air induced into the engine continuously. The 3D-printed intake runner was modified to adapt the MAP sensor to monitor intake manifold pressure. Figure 2.5 is an image of the 3-D printed intake runner. The port on the left side is the fitting to receive the fuel mixture from the PVC accumulator.

Figure 2.5: *3-D Printed Intake Runner*

A Kistler model 6052A piezoelectric pressure transducer was installed into the cylinder head to measure in-cylinder pressure. To install the in-cylinder pressure sensor, the cylinder head was removed and machined to accept the transducer. The locations for the thermocouples were also machined. Figure 2.6 is an image taken during the machining of the cylinder head to accept the in-cylinder pressure sensor. A small section of the cooling fins was machined to make room for the sensor. The sensor was located in an area between the valve landings and the cylinder wall. Figure 2.7 is an image of the in-cylinder pressure sensor once installed in the cylinder head.

Figure 2.6: *Machining the In-Cylinder Pressure Sensor*

Figure 2.7: *In-cylinder Pressure Sensor Installed*

To measure the exhaust emissions, an Infrared Industries FGA 4000XDS exhaust gas analyzer was used in the exhaust stream. The exhaust analyzer used NDIR (non-dispersive infrared) to measure HC, CO, and CO_2 species. The analyzer also used an electrochemical cell to measure the NO_x emissions with a 1% full-scale accuracy. On the end of the engine, a gearbox assembly was mounted to the crankshaft which contained a Hengstler 0521097 shaft encoder that

was used in combination with an MP1007 Hall effect sensor to accurately determine crank angle position, top dead center, and RPM of the engine. Figure 2.8 is an image of the aluminum housing used to contain the hall effect sensor and shaft encoder.

Figure 2.8: *Shaft Encoder & Hall Effect Sensor*

Finally, a Bosch intake manifold pressure sensor was installed on the intake track to monitor the pressure drop of the fuel charge as it entered the engine. Data from each sensor was collected with a bespoke LabVIEW program; the program was used to record the data and synchronize the signals. Further, the LabVIEW program was also used to control the flow of the gases. From there, the data was analyzed with MATLAB. The systems deliver reliable measurement results with an accuracy of 5% based on the least accurate instrument. To supply the fuel, bottles of each gas were connected to the accumulator and controlled with Brookfield electronic mass flow controllers. Once the gas was mixed via the accumulator, it was throttled

into the intake via the carburetor. On this engine, the throttling was accomplished automatically via the centrifugal governor on the engine connected to the carburetor. During gasoline operation, the carburetor assumed standard function. For mixed gas operation, gasoline flow was blocked off and residual gasoline was drained. Further, the orifices were blocked such that the carburetor only functioned as a throttling apparatus. Apart from these modifications, all other engine parameters such as timing, A/F ratio, etc. were held constant. Figure 2.9 is a schematic of the control scheme and experimental setup.

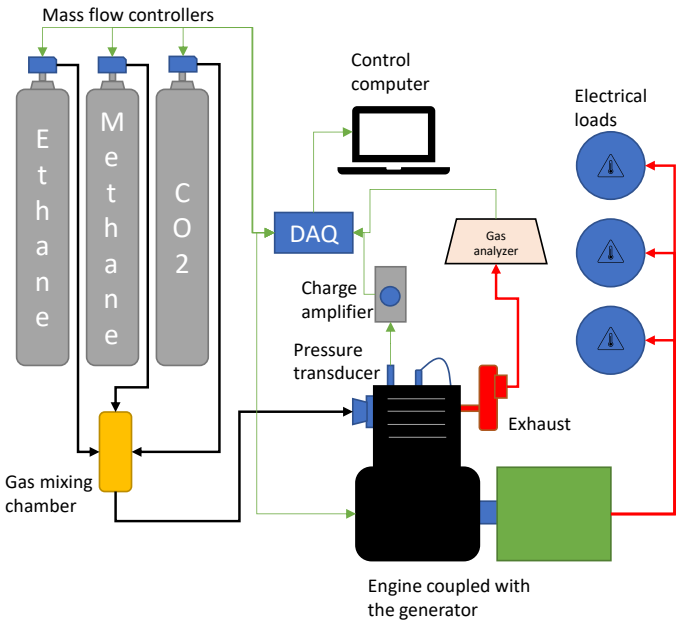

Figure 2.9: *Schematic of the Control Scheme and Experimental Setup*

Several modifications were necessary to measure the amount of fuel used for each of the fuel types. For gasoline, the gas tank was bypassed with a fuel inlet line to the carburetor fed by a graduated container. The engine was first run with no gasoline in the container to dry out the carburetor bowl and make sure that there was no fuel in the lines. Once the engine stalled, the container was filled to a specific level and the flow valves were opened. Then the engine was started, and the test case was run while time was recorded to exhaust the supply of fuel. Because

the gaseous fuel mixtures were controlled by calibrated mass flow controllers, the outputs of the controllers were taken as the fuel consumption over time.

2.2.2 Experimental Parameters

For this study, different load conditions were tested to understand the performance of the fuels. The test stand was operated with the generator disabled for no-load operation. For full load, a series of electrical heaters with 5.5 kW of power output was used to electrically load the generator to its rated continuous power output. Part load was tested without any external electrical load attached to the generator and only energizing the coils of the generator and the internal control circuitry. Due to uncertainties in the performance of the connected generator, the indicated power was calculated from the measured indicated mean effective pressure (IMEP). Prior to testing the gas mixtures, a series of experiments were conducted with gasoline to establish a baseline with which to compare the gas mixture performance. The gasoline was obtained from a local gas station and was 90-octane non-ethanol. The efficiency and emissions of the pure gasoline case were measured and tabulated to establish baseline results. The tests performed were repeated 15 times with the same setup to test repeatability and eliminate errors, and the data was taken as an average of 10 continuous minutes of running at a fixed load and RPM for each test. The variation bars in the graphs show the standard deviation for the data presented. After the gasoline cases were conducted, varying mixtures of methane, ethane, and CO_2 were used as fuel based on the outputs of the CL-ODH process.

Three different were chosen based on their resemblance to the original byproduct gas from the CL-ODH process as they closely resemble the variety of the byproduct mixture

identified as Mix-1, Mix-2, and Mix-3. The ratios of methane, ethane, and CO_2 tested are shown in Table 2.2.

Table 2.2: *Fuel Mixture Ratios Used in the Experiments in Weight %*

Mix	Wt. % Ethane	Wt. % Methane	Wt. % CO_2
Mix-1	46	12	42
Mix-2	46	10	44
Mix-3	47	7	46

The operating air-fuel ratio was kept constant during operation and was measured with the exhaust gas analyzer. Table 2.3 shows the operating air-fuel ratio of each mixture. In addition, Table 2.3 shows the gasoline operating air-fuel ratio. It should be noted that the carburetor was set to provide a slightly fuel-rich A/F ratio for gasoline to prevent overheating. This setting could not be adjusted.

Table 2.3: *Operating Air Fuel Ratios*

Fuel	A/F Ratio
Mix-1	19.2
Mix-2	19.6
Mix-3	19.8
Gasoline	13.2

Due to the complex nature of the original byproduct gas, a simulation gas with the major components was employed based on the study in a constant volume combustion chamber to identify the mixtures with the highest likelihood of being viable for use in an engine application [19]. This simulation was set up in Converge-CFD™ and included modified solvers with detailed chemistry to model the combustion of the byproduct gasses. The initial cases were used to simplify the fuel mixture to reduce the complexity of the SIM gases prior to testing. It is

important to consider carbon dioxide does not contribute to the lower heating value calculation. This is because carbon dioxide does not contribute to the lower heating value of the fuel. Based on the simulation, ethane and methane were identified to have the largest influence on the heat release of the fuel. Table 2.4 shows the lower heating values of the fuel mixtures measured.

Table 2.4: *Lower Heating Values of the Fuel Mixtures Tested*

Fuel	LHV (MJ/kg) excluding CO_2	LHV (MJ/kg)
Mix-1	47.6	27.7
Mix-2	47.5	26.7
Mix-3	47.4	25.7
Gasoline	-	43.4

As a result of the experiments, it was possible to eliminate the minor species and develop simulated gas mixtures consisting essentially of methane, ethane, and CO_2. By eliminating the minor species, it is possible to dramatically increase the ease of experimentation while maintaining a good match to the actual fuel.

2.3 Engine Performance Evaluation

2.3.1 In-Cylinder Combustion Comparison

The pressure transducer installed on the cylinder head provided the transient combustion pressure inside the combustion chamber. The data collection was synced to the rotation of the engine to obtain the pressure data as a function of crank angle. This pressure data was then used to calculate the indicated mean effective pressure (IMEP). Indicated mean effective pressure is a quantity that relates the internal combustion engine to its capacity to do work. Significantly, this measurement quantifies engine performance independent of engine displacement.

Figure 2.10 shows a plot containing the in-cylinder combustion pressure vs. crank angle degree at varying loads. From Figure 2.10, it is observed that the peak pressure for Mix-2 and gasoline are very close and almost overlap. It was also shown that the Mix-1 shows a substantially higher peak, because of the highest concentration of fuel components and lowest concentration of diluent CO_2. The increased ratio of methane in the fuel mixture coupled with the lowest ratio of CO_2 is responsible for this high peak pressure resulting from gaseous fuels having a higher heating value. Lower concentrations of CO_2 also reduce the energy removed by the diluent species. Conversely, with Mix-3 having the most CO_2 in the fuel, the mixture shows the lowest peak pressure. Similar trends are seen with all the loads tested with the fuels.

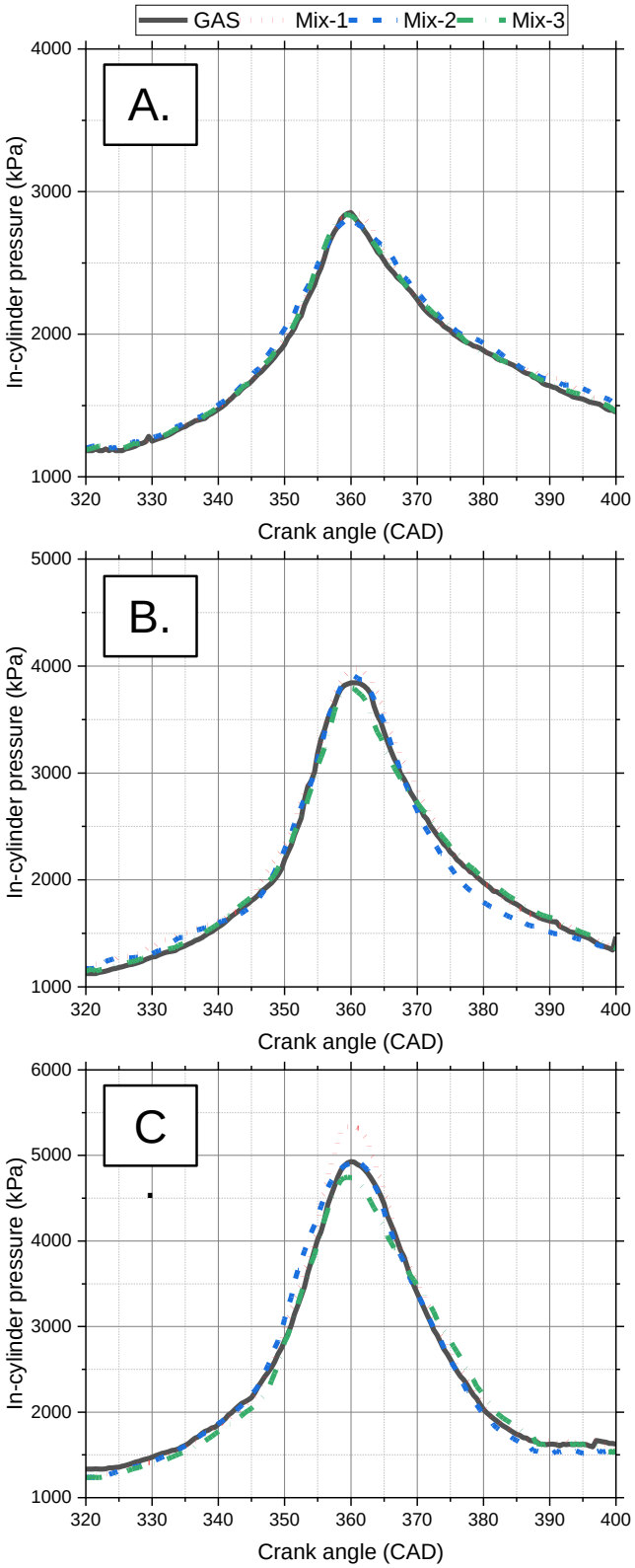

Figure 2.10: *In-cylinder Pressure Comparison; A. Low load, B. Part Load, C. Full Load*

When comparing part load to full load, it is observed that the differences between each of the fuels are much less significant. It is important to note that the peaks' location relative to diluent content is consistent throughout loading conditions; increasing amounts of diluent leads to a lower in-cylinder pressure. Mix-1, having the greatest energy content, continues to demonstrate the highest peak pressure, and Mix-3, having the lowest energy content, shows the lowest peak pressure. Mix-1 shows the greatest decrease in-cylinder pressure when engine operation is reduced to part load. Continuing to comport with the trends from full to part load, the discriminable differences between each fuel diminish further when considering low load, and the relationship between diluent and in-cylinder pressure continues to be maintained. It is important to consider that each of the fuels exhibits similar performance to gasoline at low load situations, which is most likely due to heavy throttling at low load.

Using the IMEP results, the indicated power produced by the engine at the various loading conditions can be calculated using the following equation [70]:

$$P_i\ (kW) = \frac{IMEP * Vd * N}{2 * 10^3} \qquad (2.1)$$

where P_i is the indicated power, V_d is the displaced volume, and N is the rotational speed of the engine in revolutions per second. Table 2.5 shows the calculated indicated power for different load conditions. Note that the achieved max loading on the engine is lower than the rated power of the engine. While the engine is rated for 10 kW, the generator is only able to supply 75% of the rated load during continuous load operation, reserving full power for surge operation. This safety feature is incorporated to prevent overloading of the generator.

Using the in-cylinder pressure data, the heat release rate (HRR) of the combustion cycles was also calculated and analyzed. The heat release rate is critical in understanding the combustion characteristics of the fuel because it can describe the fuel burning rate. The heat

release rate was calculated using the first law heat release model as shown in Equation 2.2, with γ =1.325 being the specific heat ratio [61]. Table 2.5 shows the calculated indicated power with different fuels and operating conditions.

$$\frac{dQ}{d\theta} = \frac{\gamma}{\gamma-1} P \frac{dV}{d\theta} + \frac{1}{\gamma-1} V \frac{dP}{d\theta} \qquad (2.2)$$

Table 2.5: *Calculated Indicated Power with Altering Fuel & Loading*

Indicated power kW	Gasoline	Mix-1	Mix-2	Mix-3
No-load	1.07	1.16	1.12	1.08
Part-load	5.70	6.01	5.83	4.95
Full-load	7.98	8.81	7.99	7.22

In a similar way to in-cylinder pressure, the heat release rate between the fuels was compared. Comparing the heat release rate to the crank angle further develops an understanding of fuel-burning behavior and fuel viability as a replacement for gasoline. Figure 3 shows the comparison between heat release rates at varying load conditions.

When comparing heat release rates, slightly different trends are observed between loading conditions. As load increases, the differences between the mixtures increase. Conversely to in-cylinder pressure trends, however, it was observed that Mix-1, whose energy content is the greatest among the three mixtures, shows the lowest heat release at low loads. As loading increases, the heat release rate increases more rapidly than any other mixture. At high load operation, Mix-1 demonstrates a heat release rate that is higher than any mixture.

Mix-2 demonstrates a heat release rate closest to that of gasoline in terms of peak heat release rate under all loading conditions, further suggesting that it may operate as a viable

replacement for gasoline. Despite this close match in absolute heat release, the heat release event extends over a slightly longer duration. Mix-3 exhibits the lowest heat release rate. This low heat release rate, as is the case with low in-cylinder pressure, is a result of containing the greatest concentration of CO_2 diluents which absorb heat from combustion. The heat release rate of Mix-3 continues to diminish relatively lower when compared to other mixes and gasoline as the load increases. Another discrepancy between the fuels that should be noted is the peak of the heat release rate curve compared between the mixes. When compared to Gasoline, Mix-1 is most closely aligned, indicating that peak heat release occurs at similar CAD. Mix-2 has the broadest curve indicating that the heat release rate is sustained over a greater duration. Figure 2.11 shows the heat release rate comparisons between fuel mixtures at altering loading conditions.

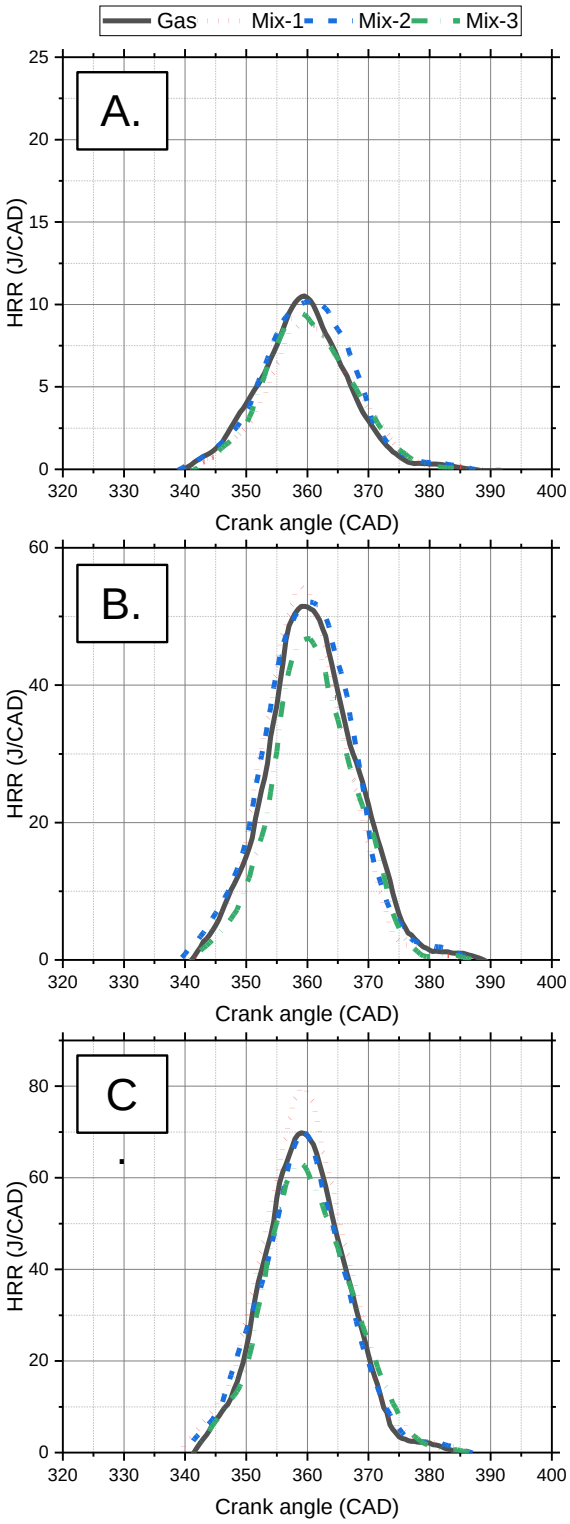

Figure 2.11: *Heat Release Rate Comparison Between Fuel Mixtures*

Figure 2.12 shows the peak heat release rate results for different engine loads and fuel mixtures. From Figure 4, the gas mixtures show a difference based on the mixture condition being tested. At the low load condition, all the fuels tested show similar peak HRR. But Mix-1 shows a marginally higher heat release rate compared to others. A similar trend is observed with the other loading cases as well, where Mix-1 has the highest HRR. As the load increased to full load, it was noticed that the difference increased between each fuel mixture tested. Mix-2 is quite close to the performance of gasoline. Mix-3 proves to be the slowest burning among all the fuels due to its highest CO_2 concentration. The heat release from the gas mixtures is a consistent match to gasoline. Even in light of the varying heat release rates demonstrated by these fuels, it can be argued that the heat release rate of the fuels is sufficient for the fuel to be utilized in an internal combustion engine.

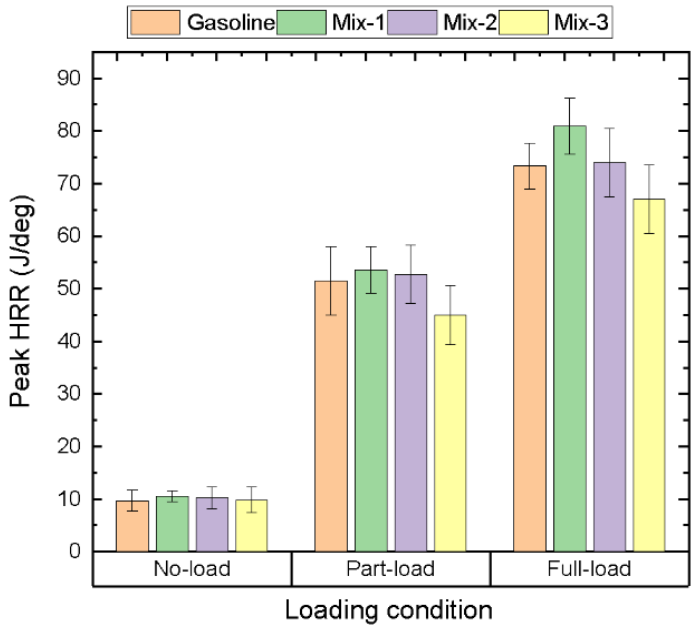

Figure 2.12: *Peak Heat Release Rate Comparison Between Fuel Mixtures*

2.3.2 Fuel Efficiency Analysis

With the power measured, the indicated efficiency can be calculated. Indicated efficiency is defined as the ratio between indicated power and the chemical energy provided by the fuel, also known as indicated fuel conversion efficiency. The formula below was used to calculate fuel conversion efficiency [70].

$$\varepsilon = \frac{P_i}{Q_{hv} * \dot{m}_{fuel}} \qquad (2.3)$$

Where Q_{hv} are the lower heating values of the fuel and $\dot{m}_{fuel}$ is the mass flow rate of the fuel. Figure 2.13 shows the energy equivalent mass of gasoline consumed per kilowatt hour generated for the various fuel mixtures and loads tested. The calculation and conversion of fuel consumption values shown in Figure 4 includes only the combustible gases in the gas mixtures tested. The mass of CO_2 has not been accounted for here as it does not contribute to releasing any energy through combustion. The fuel consumption calculations are also based on the indicated power calculated from IMEP measurements. Figure 2.13, which demonstrates indicated fuel conversion efficiency, shows at lower loads gasoline fuel tests show reduced fuel consumption compared to gas mix cases even though the gases have higher chemical energy in the fuel. Gas Mix-3 also shows the highest specific fuel consumption per cycle of all the gaseous mix fuels tested, which is expected as it contains the lowest number of hydrocarbons and the greatest concentration of carbon dioxide. With an increase in loading, the fuel consumption for gaseous mixture fuels reduces and then increases slightly. Overall, Mix-1 with its increased methane concentration shows a good reduction in fuel consumption at mid to high loading conditions compared to all the fuels tested. It should be noted that the carbon dioxide content is excluded in these calculations.

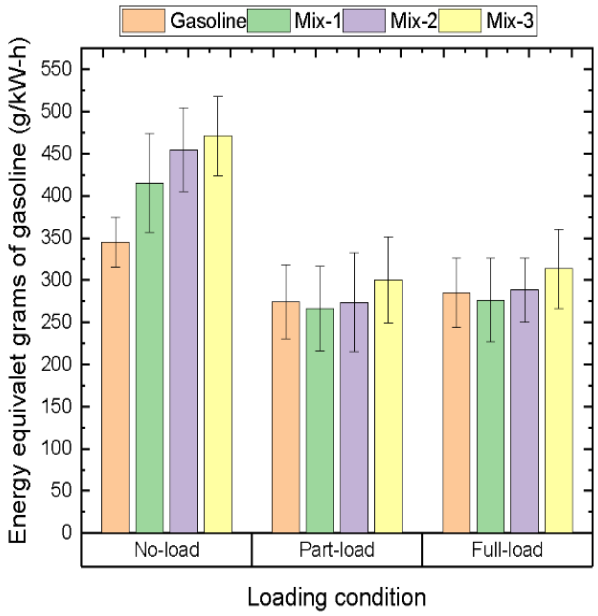

Figure 2.13: *Indicated Fuel Consumption Comparison for all the Fuel and Loads*

Figure 2.13 illustrates the indicated fuel conversion efficiency for all the conditions. From Figure 2.14, it can be seen that the indicated efficiency of the engine does not follow the same trend for all the loads. The no-load condition shows that the gasoline engine has a relatively higher indicated efficiency as compared to the gas mixtures. This effect can be attributed to the system used to induce the gas mixture into the engine. For gasoline, the carburetor was unmodified, and the throttle was adjusted and fixed to run the engine at 3600 rpm based on the load applied. But for the gas mixtures, the overall control of the fuel mass entering the chamber was accomplished by strictly controlling the flow rate of individual gases being fed into the mixing chamber, which empties into the intake of the engine. As a result of intake and induction inefficiencies, the engine required a considerable influx of gas to keep it running at idle or with low loads, most of which were ultimately lost to the atmosphere and never entered the engine. The overall trend of the reduction in efficiency with the changing mixture properties

remains the same between the gas mixtures. It should be noted that improvements to the gas induction system and throttling mechanism would decrease the fuel consumption of the mixed gases.

The data suggests the highest indicated efficiency is from using gasoline rather than from using the mixed gasses. Although EGR systems and fuels of the like are appealing for their ability to reduce emissions, they have detrimental effects on fuel efficiency [71]. These facts are evident in light of comparing gasoline to the SIM fuels which mimic EGR behavior.

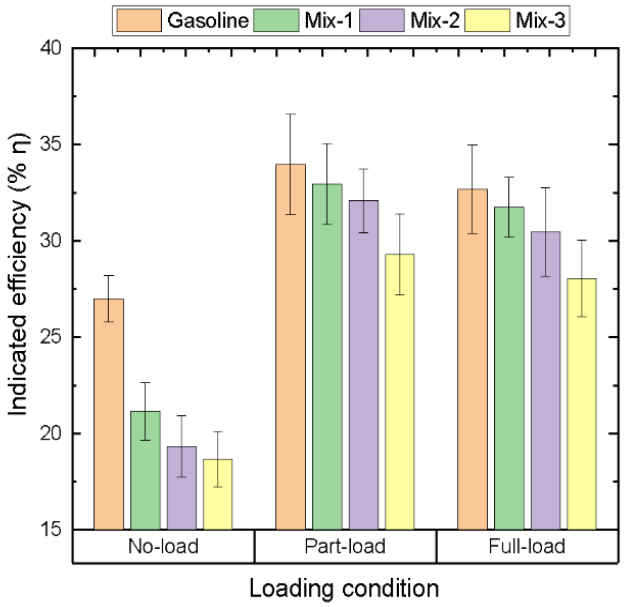

Figure 2.14: *Fuel Efficiency Comparison Between Fuels and Loading*

Mix-1 shows a better indicated efficiency compared to the mixed gases across the board as it has the least amount of CO_2 dilution compared to the three mixtures. Similarly, Mix-3 suffers from the lowest indicated efficiency of all as it has a higher CO_2 dilution. As the CO_2 dilution increases, the indicated efficiency decreases. This is a result of the CO_2 absorbing energy from the combustion process. More fuel is then required to replace the lost heat. Further, the reduction in indicated fuel conversion efficiency for the gas mixtures is also because of

increased CO_2 concentration leading to slow combustion and lower combustion temperature. At part load there is only a 3% difference between gasoline and the Mix-1 gas, 6% between gasoline and Mix-2, and 14% between gasoline and Mix-3. The difference reduces further with increasing loads. It is likely this difference decreases as load increases because of the increased turbulence and decreased throttling losses experienced during lower load operation. The efficiency of the gas-fed systems can possibly be further improved by the modification of the fuel induction system and improving the mixture homogeneity of the gases being fed into the engine.

2.4. Exhaust Gas Analysis

In this study, the exhaust temperature and gases from the engine were sampled and tested to analyze the emissions and understand combustion characteristics for each of the SIM gases using a calibrated exhaust analyzer. First, the exhaust gas temperature was sampled. Next, the exhaust was sampled to measure quantities of unburnt hydrocarbons (HC), carbon monoxide (CO), carbon dioxide (CO_2), and oxides of nitrogen (NO_x). All the emissions data shown are in units of grams per indicated kilowatt hour (g/kW-h) for accurate comparison.

The exhaust gas analyzer in this study was configured to measure the concentration of specific emissions species. More particularly, the EGA measured species in either parts per million (ppm) or by mass percentage. For comparative analysis, the concentrations have been converted to g/kW-h, which reports the emissions species per unit of energy produced.

2.4.1 Exhaust Gas Temperature

Exhaust gas temperature (EGT) is critical in understanding the combustion event; in many cases, EGT can indicate a rich or lean condition. Further, monitoring EGT is important to

ensure that the mixed gases are not exceeding the safe limits of engine design. Catastrophic engine failure often results from exhaust gas temperatures exceeding these designed limits. Thus, it is critical to understand exhaust gas temperature when evaluating the compatibility of this fuel in an engine.

Although EGT can be influenced by a variety of engine parameters such as ignition timing and engine tuning, these are neglected for this study because they are all held constant; consider that exhaust gas temperature is primarily influenced by the combustion behavior and stoichiometry of the fuel charge [72-73]. Figure 2.15 shows the variation in exhaust gas temperature for the different fuels tested under different loads. It can be seen that the exhaust temperature for the fuel Mix-3 is the lowest. Lower EGTs can be the result of variation in the A/F ratio and less energetic combustion [73]. In this case, it could be caused by the increased CO_2 absorbing more heat inside the chamber and in the exhaust of the engine. Mixtures with lower exhaust gas temperatures indicate the combustion event corresponds to fuel that has a lower adiabatic flame temperature. As load increases, the exhaust gas temperature increases as a result of more fuel being consumed and higher cylinder combustion temperature.

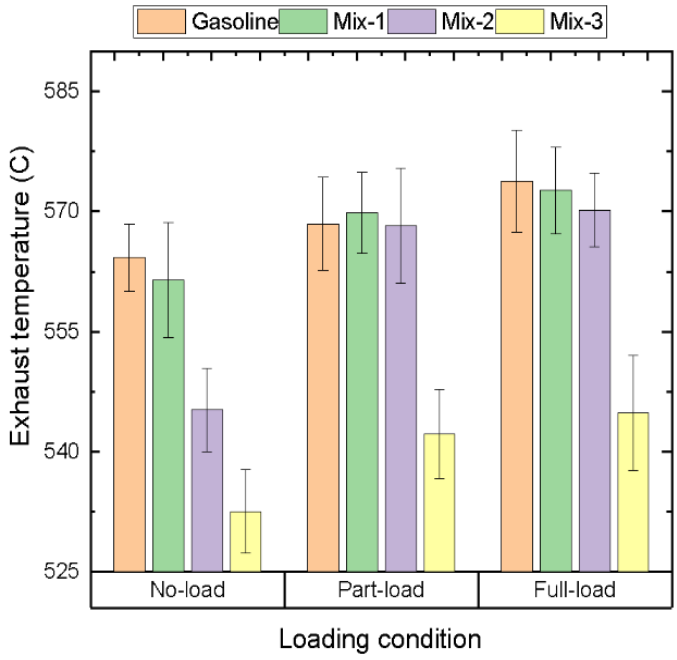

Figure 2.15: *Exhaust Gas Temperature Comparison*

2.4.2 Unburned Hydrocarbons (HC)

Figure 2.16 shows the HC emissions for different fuel mixtures and loads tested. Results show that the HC emissions for gasoline are considerably lower than that of any gas mixtures tested. This could be due to the relatively slower combustion of the gas mixtures as identified in tests of said mixtures in a constant volume combustion chamber [75]. This slower combustion can cause some of the induced gases to not completely combust and exit out through the exhaust causing an increase in the overall HC levels. Another reason could be that there is a possibility of the induced gas mix being locally richer inside the combustion chamber causing some unburnt gases to be exhausted out and increase the overall HC levels. A better control of the induced gas mixture may help reduce the overall HC emissions when using the gas mixtures as fuel.

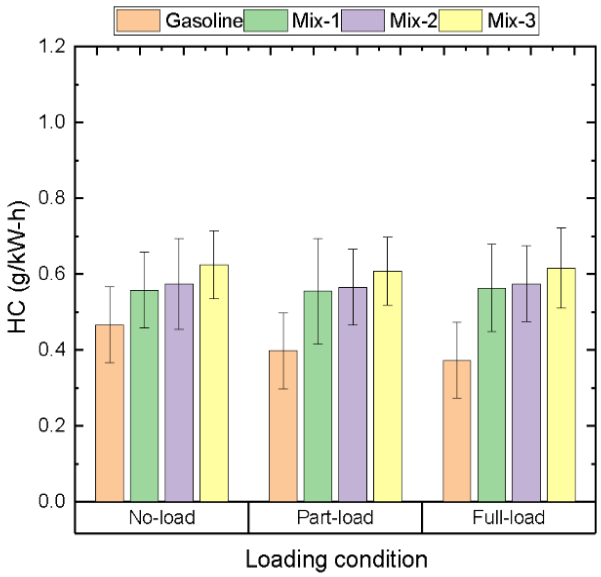

Figure 2.16: *Unburned Hydrocarbon Analysis*

2.4.3 Carbon Monoxide (CO)

Figure 2.17 shows the CO emissions for different fuels and loads. For CO emissions, a trend that is essentially opposite to the HC emissions can be observed, where the gasoline system emits approximately twice the amount of CO at higher loads compared to the gas mixtures. This is likely the result of the fuel/air mixture becoming richer as load increases. The relatively high flame temperature of the induced gas mixtures could also help in burning the CO species, leading to a reduction in the overall CO levels [75].

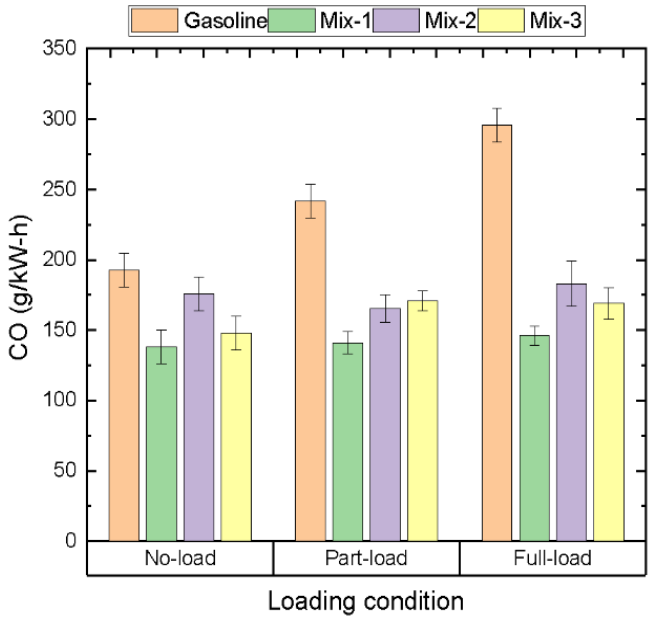

Figure 2.17: *Carbon Monoxide Analysis*

2.4.4 Carbon Dioxide (CO_2)

Figure 2.18 shows the relative amount of CO_2 emissions produced by each fuel. CO_2 production for all the fuels remains close to each other; there is an increase in CO_2 emissions with increasing loads for all the fuels. But at all loads, the gas mixture fuels exhaust more CO_2 compared to gasoline. Mix-3 consistently has the highest CO_2 as it has the highest CO_2 in the mixture. The CO_2 emissions produced by the fuels are directly proportional to the amount of CO_2 in the fuel. When compared to gasoline, the SIM fuels have substantially more carbon dioxide. This increase in CO_2 is a result of the introduced carbon dioxide as part of the fuel that ends up as emissions from the engine, which increases the overall CO_2 levels in the exhaust. An argument could be made that the CO_2 emitted is a combination of products of combustion and fuel constituents, where the CO_2 introduced as fuel should be represented with a different weight than that of a product of combustion. It is likely that the CO_2 emissions that are products of

combustion from the SIM gas are of substantially less quantity than that produced from gasoline [76].

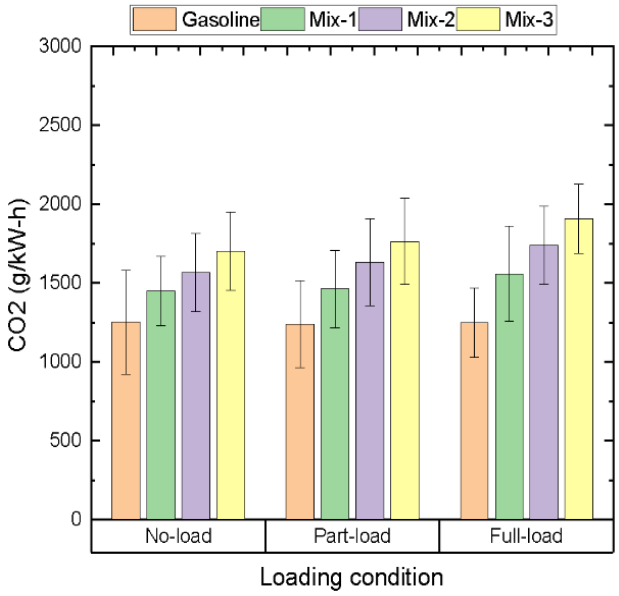

Figure 2.18: *Carbon Dioxide Analysis*

2.4.5 Oxides of Nitrogen (NO_x)

NO_x emissions in internal combustion engines are mainly influenced by the temperature of combustion inside the chamber [77]. On its face, it is expected that these gas mixtures would emit lower NO_x emissions resulting from the lower temperatures within the cylinder from the heat removed by the CO_2. These presumptions are somewhat consistent with the measurements taken, but more analysis is required. Figure 2.19 shows the NO_x levels for different fuels and the loading conditions tested. From Figure 2.19, it can be seen that the NO_x emissions for the gasoline cases generally increase with the increase in the load applied to the engine. This is due to the increase in the combustion temperature under higher loads coupled with a warmer engine. The increasing temperature of combustion also indirectly heats the engine to a higher

temperature at higher loads causing the inlet charge to be hotter. This phenomenon can also increase the overall NO_x production in the exhaust. But with the gas mixtures the NO_x initially increases and then almost stagnates. Since the gasses that are used are in a mixing chamber and forced into the inlet of the engine, the mixture stays relatively cooler. This reduces the amount of NO_x produced. Reiterating, the increased CO_2 in the fuel mixture helps in absorbing some of the energy that leads to a lower flame temperature with less thermal NO_x formation.

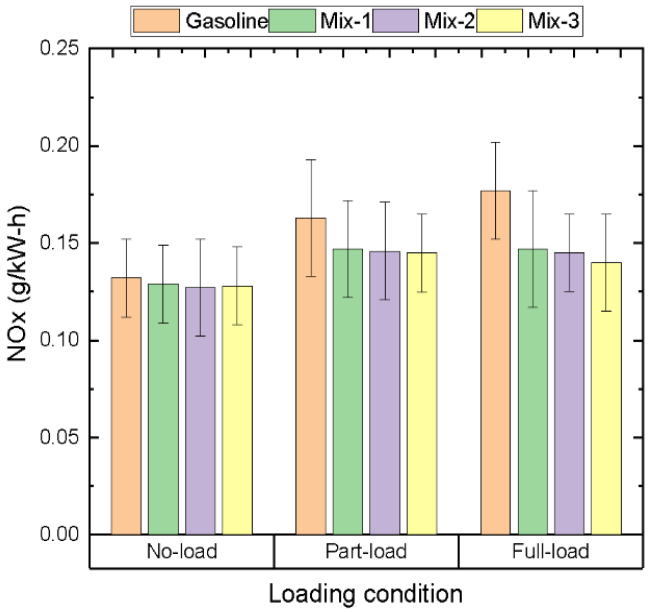

Figure 2.19: *Oxides of Nitrogen Analysis*

2.5 Engine Mechanical Health Analysis

It is common when investigating alternative fuels to consider the effects these unconventional fuels exert on an engine. Several parameters, such as corrosivity and heat quenching should be considered when evaluating whether an alternative fuel is suitable for use in an engine designed for conventional gasoline or diesel operation. For this study, the mechanical health of the engine was evaluated prior to and after operation of the gas mixtures.

A compression test is normally performed to quantify the mechanical integrity of a cylinder & combustion chamber on an internal combustion engine whereby it measures the static pressure developed during compression. Low compression is indicative of poor mechanical health resulting from wear [70,78]. A compression test was performed on the engine when it was new and after extensive operation on the fuels and on gasoline. The initial compression test indicated 118 psi and the subsequent test indicated 116 psi. This loss of 2 psi is negligible and can be attributed to normal “break-in” or wear from extended operation. In other words, there was no accelerated decline in compression experienced by the engine resulting from SIM gas operation. If there were a negative phenomenon, such as auto-ignition, detonation, flame quenching, overheating, etc. it would have damaged the cylinder, head, and valvetrain and caused a detectable loss of compression.

A series of qualitative engine assessments were performed to further strengthen the assessment of minimal impact from these fuels. When an engine experiences detonation, or unfavorable combustion conditions, localized pitting and distortion occur on the cylinder head and piston. The boundary layer is disrupted by the shockwave which decreases the quenching distance between the flame and cylinder wall resulting in oversaturation of heat and melting. Melting may also occur by relatively slow combustion events which increase the effective time of the flame. Figure 2.19 shows an image of the cylinder head after experimentation. Note that the larger, more centered hole is configured to receive the sparkplug and the second hole above the exhaust valve is the hole prepared to receive the in-cylinder pressure sensor. Figure 2.20 is an image of the piston with the cylinder head removed after the experiments.

Figure 2.20: *Image of Cylinder Head After Testing*

Figure 2.21: *Image of Piston and Cylinder After Experiments*

From the image in Figures 2.20 & 2.21, it can be assumed that no such damage occurred from inconsistent or unfavorable combustion. Further, the discoloration from products of combustion is quite similar to that experienced by an engine operated on conventional gasoline. It is also common with the introduction of certain unconventional fuels for chemical reactions to occur resulting in the corrosion of internal parts. Exemplary interactions include ammonia-brass reactions when ammonia is used as a fuel, and it reacts with the brass items in the fuel intake.

The carburetor was disassembled and inspected for such interactions. Figure 2.21 contains an image of the carburetor after the experiments were performed. From the image in Figure 2.22, it is evident that no such corrosion exists from adverse reactions from the fuels or any of their products. Further testing is required to understand the complete effects of these fuels on existing internal combustion engines.

Figure 2.22: *Image of Carburetor Bowl After Experiments*

Overall, the experiments and results in this work suggest the gas mixtures show improvement in CO and NO_x emissions when compared to gasoline. It was also shown that the fuel can be operated in existing spark ignition internal combustion engines without substantial internal modifications. Consider that an intake system similar to the one used in this work could be improved upon to provide finer control over the mixtures to reduce slight variations and be commercialized and mass-produced. Further, after mixed gas operation, it was concluded that there were no adverse effects on engine health because of operating on mixed gas. It should be noted, however, that long-term studies on engine health should be conducted. It is also

hypothesized that these alternative fuels would show even greater performance if used in a compression ignition engine.

2.6 Conclusions

Simulated gas mixtures, which modeled the byproducts of the CL-ODH processes, were tested in a spark ignition engine to evaluate the combustion, performance, and emissions, and to understand its compatibility in existing internal combustion engine-based power generation units with little modifications. It was concluded that the gas mixture can be used in spark-ignition engines with slight modifications to the intake system and produce little to no side effects. Further, the engine can be cycled between mixed gas mode and conventional gasoline operation with no adverse effects. It was found that at higher loads, the simulated gas mixture shows between 6% to 16% lower thermal efficiency than gasoline. It is likely that this is the result of a higher concentration of diluents in the fuel. When compared to gasoline, the byproduct gas mixtures yield lower CO and NO_x emissions; at higher loads, the byproduct gas mixtures demonstrated up to 41% reduction in CO and up to 21% reduction in NO_x. This substantial improvement in harmful emissions increases the attractiveness of the use of the fuel in stationary power generation settings. For steady load applications, it is seen that the byproduct gas mixtures can be successfully used in an engine with similar performance. Further improvements in the overall performance may be done with modifications and optimization to the intake system to decrease the amount of fuel lost and the consistency of fuel delivery.

CHAPTER 3: Design & Development of the Prototype High Power Density Generator

3.1 Introduction

The work in this chapter outlines the design, development, construction, testing, and optimization process of the high-power density generator of this work. All of the machining, welding, fabricating, and engine tuning was performed by Matthew Gore by way of a lifetime's worth of experience in machining, welding, and mechanical arts.

The design and development of the high power density generator of this chapter were heavily influenced by the techniques and lessons learned from the previous work. Specifically, the methods used to conduct experiments and gather data, as well as instrument and modify engines were incorporated into the work of this chapter and future chapters. Further, schemes to operate engines on alternative fuel were incorporated into future chapters [62].

To begin the development of the prototype, the current limitations and needs not yet met must be identified and the problem to be solved must be identified. From a survey of the literature, there exists a need for a high-power density electric generator that can be used as, for example, a range extender for EVs, a hybrid powertrain for small vehicles, UAV powertrains or range extenders, or the like. In addition, the prototype should be able to provide reduced emissions and reliably function [79]. The options that are available now do not provide the necessary power for the previously identified applications, are too heavy or have insufficient power, are too expensive, or a combination of the same. Therefore, the object of this chapter is to design and develop a high power density generator [80].

A series of design criteria based on the identified problem can be set based on the problem. The generator must be substantially lightweight, relatively cheap, simple in design, and

portable. Importantly, the primary design consideration for the prototype is power density. In this context, power density is the ratio of total electrical power to weight. The power density should surpass that of available models. Based on the literature cited in this work, currently available models comprise an average power density of .247 kW/kg, and theoretically proposed models comprise an average power density of .348 kW/kg [30]. Secondary considerations for the prototype include cost-effectiveness; the prototype generator needs to be a cost-effective alternative to current range-extending and hybrid generator/powertrain methods and designs, such as long-range battery upgrades and software that can range from $2,000-$10,000 [28] and smaller less powerful onboard generators for UAVs. Third, the generator must be substantially portable and configured to provide power to a variety of applications, such as varying EV modes. The generator must also be operable to provide sufficient electrical power for the above-mentioned applications. Finally, the prototype should be adapted to show a reduction in emissions and potentially meet emissions targets. It is envisioned that the prototype can be formed into a commercially available unit.

The prototype will share a similar architecture to currently available models and will comprise an engine, dynamo, and apparatus that can couple the two. For this work, an engine and dynamo were selected based on the criteria provided. Below is a discussion of the specific components and their specifications.

3.1.1 Dynamo

The dynamo is the component of the generator that receives rotational power from the engine and converts the rotational power to electrical power. In some aspects, the dynamo can function similarly to a conventional generator. For this work, it is important to select a dynamo

that is lightweight, compact, has an operable RPM range similar to an internal combustion engine, and can produce sufficient power. Further, it is important to source a dynamo that is cost-effective.

One important consideration for the dynamo is the voltage output. The voltage output of the dynamo must be sufficient to function as, for example, a range extender or component in a series hybrid powertrain [82]. It was decided that the chosen nominal voltage for this application is at least 200 VDC (Voltage in Direct Current). This value is the same standard chosen by the US Department of Energy (DOE) for electric cars [83-84]. There exists a variety of choices for dynamos, each of them capable of producing the required power around the above-seen voltage interval and compatible speeds for internal combustion engines. After an analysis of commercially available units, it was clear that the required performances could only be met by a three-phase permanent magnet unit, because of their high specific power and efficiency [85].

For the development of the prototype, the motor assist mechanism from the Honda Integrated Motor Assist system was selected. The Honda Integrated Motor Assist (IMA) is a powertrain technology incorporated into many hybrid models for the purpose of increasing overall vehicle efficiency and reducing emissions [86]. Although the IMA is configured to function as a motor, it, like many electric motors can operate as a generator when provided with input mechanical energy. The system comprises an electric motor-assisted parallel powertrain which combines a highly efficient electric motor with a small displacement VTEC engine [87]. The motor from the system was chosen as the dynamo for this work as it is powerful, lightweight, relatively cost-effective, and substantially compact. Figure 3.1 is an image of the Honda IMA connected to a four-cylinder 2.5l V4 engine. Figure 3.2 is an image of the IMA.

Figure 3.1: *Honda IMA Powertrain* [86].

Figure 3.2: *Honda IMA Motor Unit* [86]

The IMA motor unit is a high-efficiency, compact, and lightweight permanent magnet-type three-phase synchronous electric motor that has a maximum output of 10 kW. The motor is configured to be substantially thin and thus would have as little impact on the profile of the prototype as possible. The rotor of the motor unit is formed from a lost wax precision casting process to ensure that the rotor is high-strength and lightweight. The motor utilizes neodymium-sintered magnets to increase the torque density of the motor. Importantly this motor design does not require a cooling system [89]. Figure 3.3 is an expanded view of the motor unit.

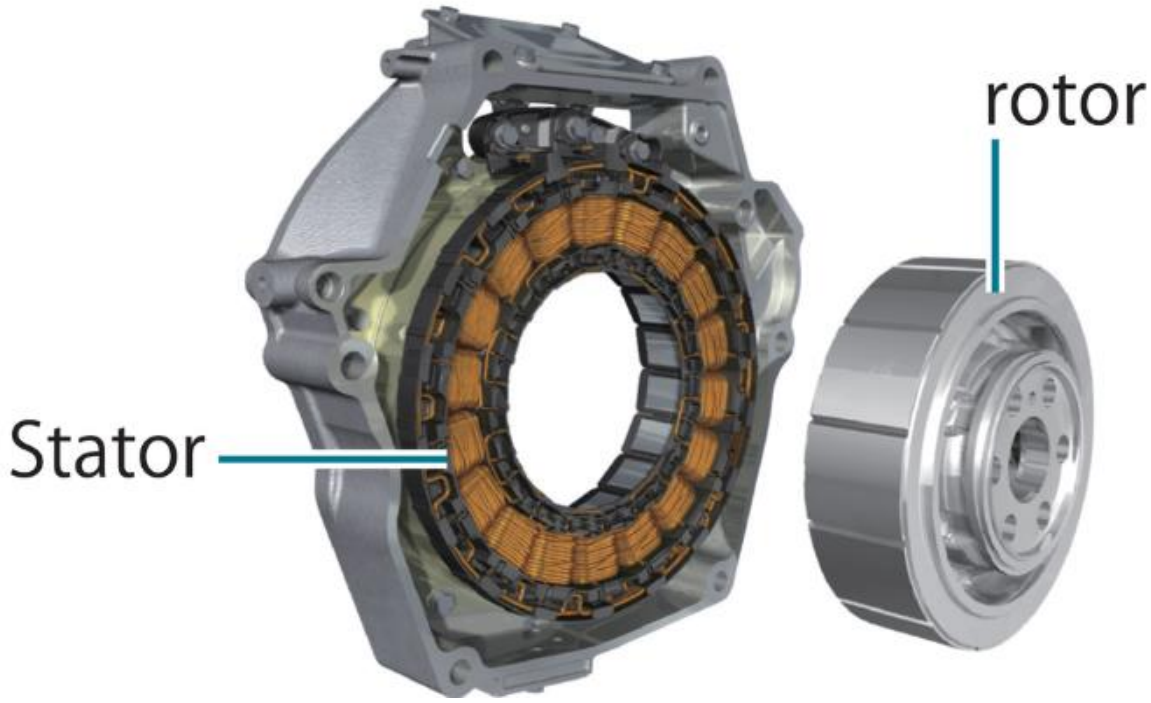

Figure 3.3: *Expanded View of the IMA Motor Unit* [88]

The IMA motor unit utilizes a split stator structure with salient pole centralized winding. In addition, the motor includes centralized distribution bus rings that are formed from copper sheets to energize the coils. It is through these features that the motor unit maintains a small, lightweight profile. Table 3.1 lists the specifications of the motor unit [86].

Table 3.1: *Motor Unit Specifications* [91]

Specification	Value
Type	Permanent Magnet BLDC
Weight	22 kg
L x W x H	16 in x 3 in x 16 in
Rated Power	10 kW, 79 Nm @ 1000 RP

The motor unit possesses several attributes that make it desirable for this application. The operating RPM range of the motor units is within the operating range of most small engines. The motor unit is self-energizing and does not require complex motor control schemes to operate. The output voltage of the motor is proportional to the rotor speed which allows for simple voltage regulation and variable voltage supply for different applications. More specifically, the output voltage of the dynamo can be controlled based on the driven rotor speed. For higher voltage applications, the rotor speed can simply be increased. The motor unit can act as a starter motor when energized, which can provide dual function. In essence, the prototype could use the IMA as both a dynamo and a starter [92]. Finally, the motor unit is a mass-produced item and is relatively available and cost-effective. For at least these reasons, the IMA was chosen as the dynamo for the prototype.

3.1.2 Two-Stroke Engines & The Yamaha KT-100

Internal combustion engines have been used to power vehicles and machines for more than a century; they are the most widely used power-producing device in the world. As a result of their proliferation, there are many engines that could be examined and considered for this work. To select an engine, a plurality of engine configurations were evaluated and considered, including small general purpose single cylinder engines such as those used in power equipment, large high performance multicylinder engines and even rotary engines. Importantly, the most

important design criteria were the reduced weight and size as well as specific power; in order to design a generator with a high power density, the engine must be as light and powerful as reasonably possible. In addition, the engine needs to remain simple. Rotary engines are very interesting from this point of view, because they are very compact, light, quiet, and substantially vibration free. However, they have been excluded because they have low torque and have high specific emissions. Similarly, general purpose single cylinder air cooled types were excluded as a result of their excessive bulk and weight and low specific power. Higher power multi cylinder engines were considered, including typical automotive four-stroke gasoline engines, but they were similarly rejected as a result of their excessive bulk and weight. Attention was then diverted to high performance single cylinder internal combustion engines derived from karting and motorcycling [70].

Of the engine designs considered, two-stroke and four-stroke designs were considered. The two-stroke cycle was chosen for this prototype due to its inherent advantages to heavier, less powerful, and more complex four-stroke engines [92]. Every internal combustion engine must complete the follow four phases: intake, compression, expansion, and exhaust. A four-stroke engine requires four distinct motions of the piston for each phase and to achieve a power stroke while the two-stroke requires only two. The two-stroke engine accomplishes this by combining the exhaust phase with the intake phase and the compression phase with the expansion phase. Figure 3.4 is an illustration of both two-stroke and four-stroke engine architecture.

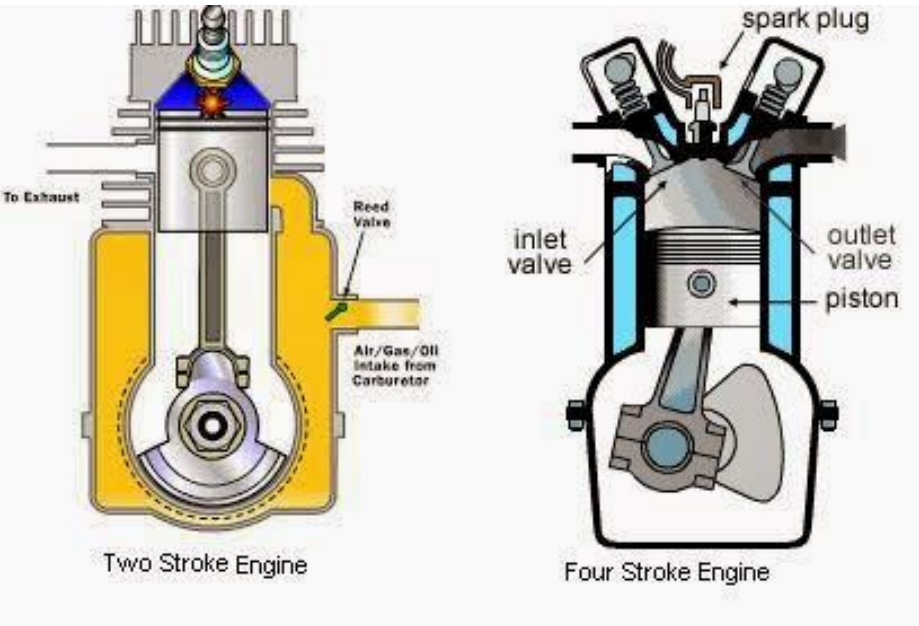

Figure 3.4: *Two-Stroke vs Four-Stroke*

Mechanically, the two-stroke engine is very simple in comparison to a four-stroke; they do not contain valves, push rods, springs, camshafts, oil pumps, and all the cumbersome structures to accomplish the four-stroke cycle. The main advantage of two-stroke engines is that they produce power on every stroke, while the four-stroke produces power on every other stroke. Further, in theory, two-stroke engines are more thermally efficient than four-stroke engines because they do not have the extra friction losses and pumping losses from the valvetrain, and they do not have dead strokes where no expansion occurs (i.e., the separate intake and exhaust stroke of four-strokes). However, outside of large-scale engines used in, for example, power generation and cargo ships, this is rarely the case because of the truncation of the expansion stroke and lower compression ratio of two-stroke engines [94]. Doubling the power stroke frequency does increase the power of the two-stroke engine per unit displacement. However, in practice, the two-stroke engine can produce about 60% more power than similarly sized four-stroke engines [92-93]. This lower than expected increase in power is due in part to the less that ideal volumetric efficiency which results from an incomplete gas exchange process [94]. The

increased frequency of power strokes also reduces the interval between power pulses and results in a smoother crankshaft torque [92]. Figure 3.5 is a diagram of the operation of a two-stroke engine.

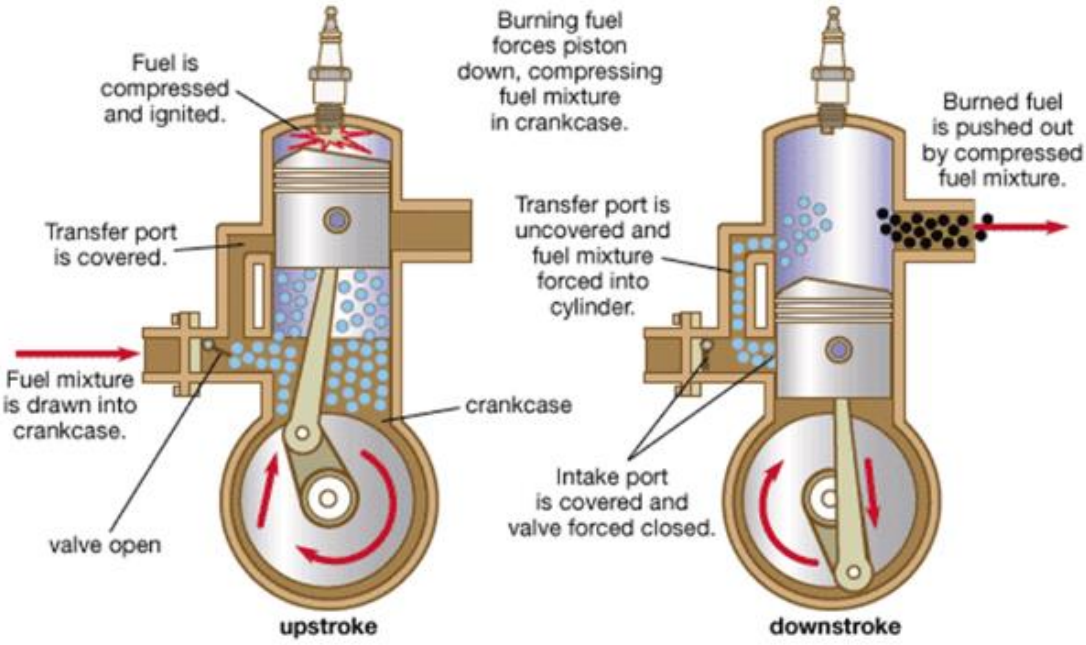

Figure 3.5: *Operation of a Two-Stroke Engine* [94]

Because two-stroke engines are far more mechanically simple than four-stroke engines, they often are much smaller and are lighter in weight. In many cases, two-stroke engines can weigh up to 50% less [92-94]. The combination of increased power per volume and reduced weight provides an engine that has a substantial advantage in power to weight over four-stroke designs. In addition, their mechanical simplicity lends itself to the engine being cheaper to manufacture and repair than similarly sized four-stroke engines. Two-stroke engines, because they do not require a dedicated oil sump, can be operated in any orientation. As long as fuel is flowing through the carburetor, a two-stroke engine can operate in any position. In lieu of an oil sump, lubricating oil is often premixed with the fuel of a two-stroke engine [92-94]. It is for at least these reasons that a two-stroke engine was chosen for use in this work.

A variety of commercially available engines were surveyed and contemplated for use for the prototype. Among these, the Yamaha KT-100 engine was selected because of its low cost, simplicity, low weight and high power, availability, and ease of adaptability. The Yamaha KT-100 is a very popular engine used in a variety of powersports including karting, motorcycling, and ultralight aircraft flight. In addition to worldwide popularity, the KT-100 has been used for decades in karting and has dedicating classes based on the engine [95]. Figure 3.6 is an image of the KT-100.

Figure 3.6: *Yamaha KT-100* [96]

The KT-100 is a single cylinder, 100cc piston port two-stroke engine. The engine is air-cooled and is lubricated via premixed fuel and oil. Importantly, the KT-100 is substantially lightweight and has a similar power output to the Honda IMA dynamo of 15 horsepower. This simple and rugged engine is carbureted by a Walboro WB-3A all-position carburetor, similar to those found on small engines such as chainsaws. The exhaust was a can-style karting exhaust

that is standard equipment for the KT-100. Table 3.2 lists the specifications of the KT-100. Figure 3.7 is a schematic view of the KT-100 [97].

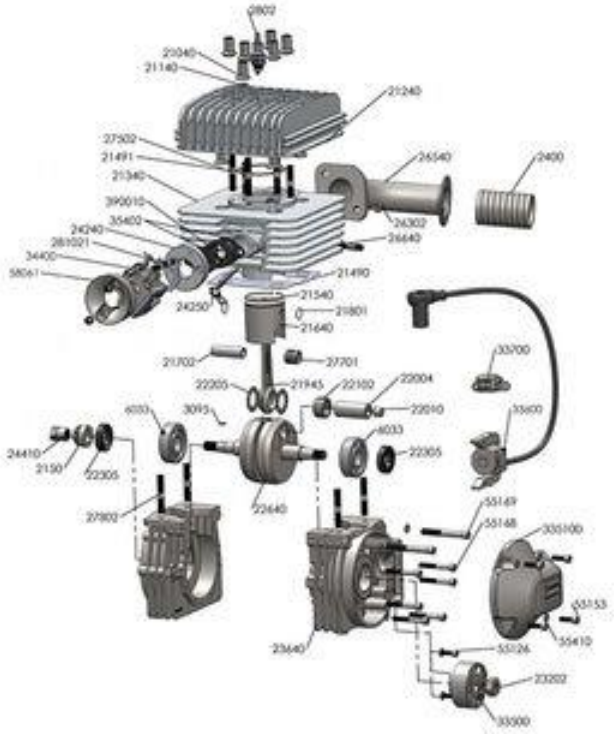

Figure 3.7: *Schematic view of the KT-100* [97]

Table 3.2: *Yamaha KT-100 Engine Specifications* [95].

Specification	Value
Engine displacement	97.6 CC
Induction	Piston Port
Compression ratio	8.3:1
Bore x Stroke	52 mm x 46 mm
Rated RPM	16,000
Cooling type	Air Cooling
Dry Weight	10 kg (21 lbs.)
Lubrication	Premix 32:1
Rated Power	11 kW @ 10,000 RPM

There are several advantages to using the KT-100 for this application that are in addition to the advantages that are inherent to two-stroke engines. First, because the KT-100 is a piston port two-stroke engine, it has one of the least complex engine architectures possible [92,95]. In a piston port two-stroke engine, the piston itself is responsible for covering and uncovering the intake ports in the crankcase absolving the need for reed or rotary valves. Because the engine is air-cooled, system cooling can easily be accomplished without requiring a cooling loop. The KT-100 is substantially powerful and lightweight and is easily tunable via adjustments to the carburetor and ignition [95]. The engine is rugged and somewhat fuel-agnostic. Two-stroke engines such as the KT-100 require very little maintenance when compared to four-stroke engines. For example, because the engine uses premixed fuel and oil, there is no need to change the oil. The KT-100 is relatively cheap and parts for the engine are readily available. It is for at least these reasons the KT-100 was chosen to power the generator. Figure 3.8 is an alternative view of the KT-100 [97].

Figure 3.8: *Alternative view of the Yamaha KT-100* [97].

3.2 Test Stand Design & Construction

With the major components of the test stand identified and acquired, a test stand was contemplated that could experimentally couple the engine and dynamo and simulate prototype operation. For the purpose of this work, a test stand is the arrangement of the components used for this prototype in a manner that allows them to be experimentally analyzed and tuned. Importantly, the test stand should provide separate positioning of the components while providing mechanical communication between the two.

In order to gain insight to the operation and performance parameters, an inline digital torque sensor was included to be installed between the engine and dynamo. An inline torque sensor is a device configured to measure the torque, power, and RPM in real time of rotary components. Inline torque sensors are disposed in the rotary assembly of the equipment they are incorporated in, such as on the crankshaft of an engine or the armature of a motor. Often these torque sensors provide digital output which can increase the accuracy of the measurements. For this work, an ATO rotary digital torque sensor was used. Table 3.3 lists the specifications of the torque sensor. Figure 3.9 is an image of the ATO Digital Rotary Torque Sensor used in this work [98].

Table 3.3: *ATO Digital Rotary Torque Sensor Specifications* [98]

Specification	Value
Capacity	100 Nm
Power supply	24 V DC
Non-Linearity	0.1% FS (Accuracy 0.001%)
Hysteresis and Repeatability	0.03% FA
Rated RPM	16,000
Output Speed	60 pulses/rev
Signal Delay	0.6 ms
Response Performance	1 kHz
Load Resistance	$\geq$ 2 kΩ

Figure 3.9: *Image of ATO Digital Rotary Torque Sensor* [98]

With the torque sensor selected, a coupling method was identified. Lovejoy connections were used to couple the engine to the torque sensor and the torque sensor to the dynamo. A Lovejoy coupling is a type of flexible coupling used to connect two shafts to transmit torque. Such couplings are widely used in industrial applications because they offer flexibility against slight misalignments, and vibration dampening, are cost-effective and robust, and are highly versatile. Figure 3.10 is an image of an exemplary aspect of the Lovejoy couplings used to provide mechanical communication for the test stand.

Figure 3.10: *Example of a Lovejoy Connection*

Because of the difference in operational RPM between the engine and dynamo, a gear reduction is required. Specifically, the engine redlines at 16,000 RPM which is much greater than the operational speed of the dynamo. Gearing configurations can be achieved through a variety of methods, each of which has its benefits. For this purpose, a timing belt drive configuration was used. Timing belts and pulleys are different than standard V-belts in that they are rated for higher speed and have teeth that engage with groves on the pulley's circumference. In addition, the teeth and groves of the timing belt reduce the chances of slippage. The high speed and high torque capacity of timing belt-style belts and pulleys make this arrangement ideal for this application. Moreover, the use of pulleys rather than gears or the like provides increases the ease of swapping the pulleys allowing the gearing ratio to be tested and optimized. What's more, the elasticity of the belt helps to absorb the jerking and vibration of the test stand.

With the major and minor components selected, the test stand layout could be planned. It is critical to plan the spacing of the elements on the test stand as the baseplates had to be machined to receive and secure the elements. To do this, each of the major and minor

components were dry fit onto the test stand and their location was recorded to establish a basic planning map. Figure 3.11 is a schematic of the basic layout of the test stand. In addition to the major and minor components of the test stand, a plurality of bearing blocks, pulleys, shaft components, and other small items were envisioned in the planning stage. A series of bearing blocks were prepared to house the rotating components. The bearing blocks comprised a pair of high-speed greaseable bearings sized to receive the shaft and spaced to cradle the primacy pulley. The combination of these various components was necessary to provide mechanical communication between the major components of the test stand. Figure 3.12 is an image of a bearing block prepared to house the primary pulley.

PART LIST		
PART NO.	PART NAME	QTY.
1	Fuel Tank	1
2	Throttle Control	1
3	Fuel Line	1
4	Ground	1
5	Carburetor	1
6	KT-100	1
7	Exhaust	1
8	Shaft Coupling	1
9	Torque Sensor	1
10	High-speed Bearing	4
11	Small Pulley	1
12	Belt	1
13	Large Pulley	1
14	Motor Generator	1
15	Motor Support	1

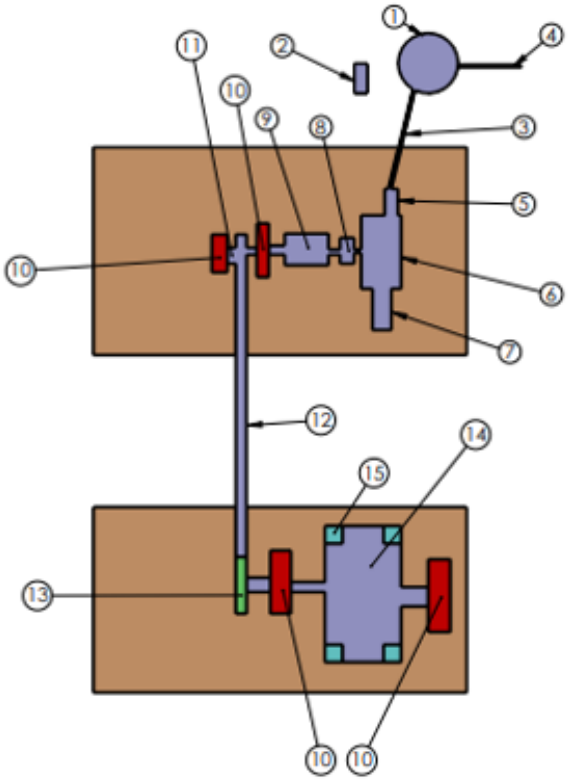

Figure 3.11: *Schematic of Test Stand Layout*

Figure 3.12: *Pulley and Bearing Block Assembly*

It was decided that the test stand would be divided into two regions; the engine side and the dynamo side. This separation was intended to divert focus to each individual component during the tuning phase. From there, each of the component's area was measured and cataloged along with the total area of the baseplates of the test stand. With these measurements, the actual location of the components could be determined. Figure 3.13 is a measured drawing of the test stand layout used during the initial design phase.

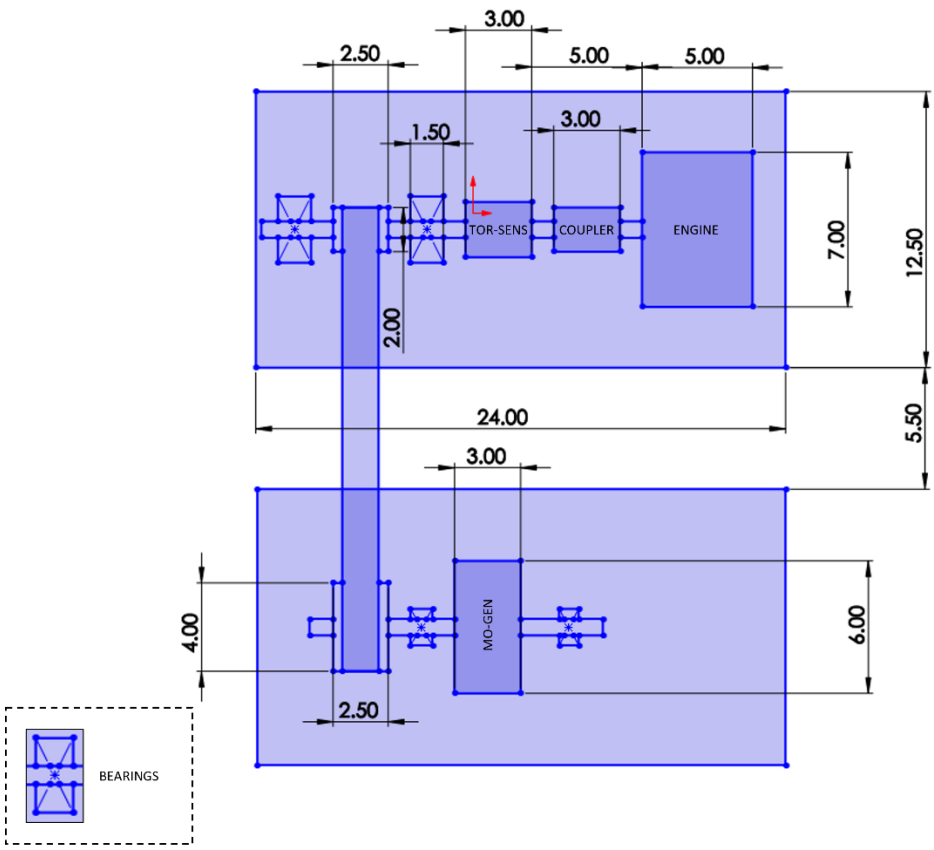

Figure 3.13: *Measured Drawing of Test Stand Layout*

With all of the components at hand and measured drawings available, machining could begin on the base plate of the test stand. To begin machining, the engine side plate was removed from the base and locations were marked based on the mounting configuration of each piece. Specifically, the engine, torque sensor, and bearing block bolt holes were located on the plate based on the measurements. Proper axial alignment in this stage was critical as the shaft crankshaft, torque sensor shaft, and pulley assembly had to share a common axis. Figure 3.14 is a collage of the engine plate machining.

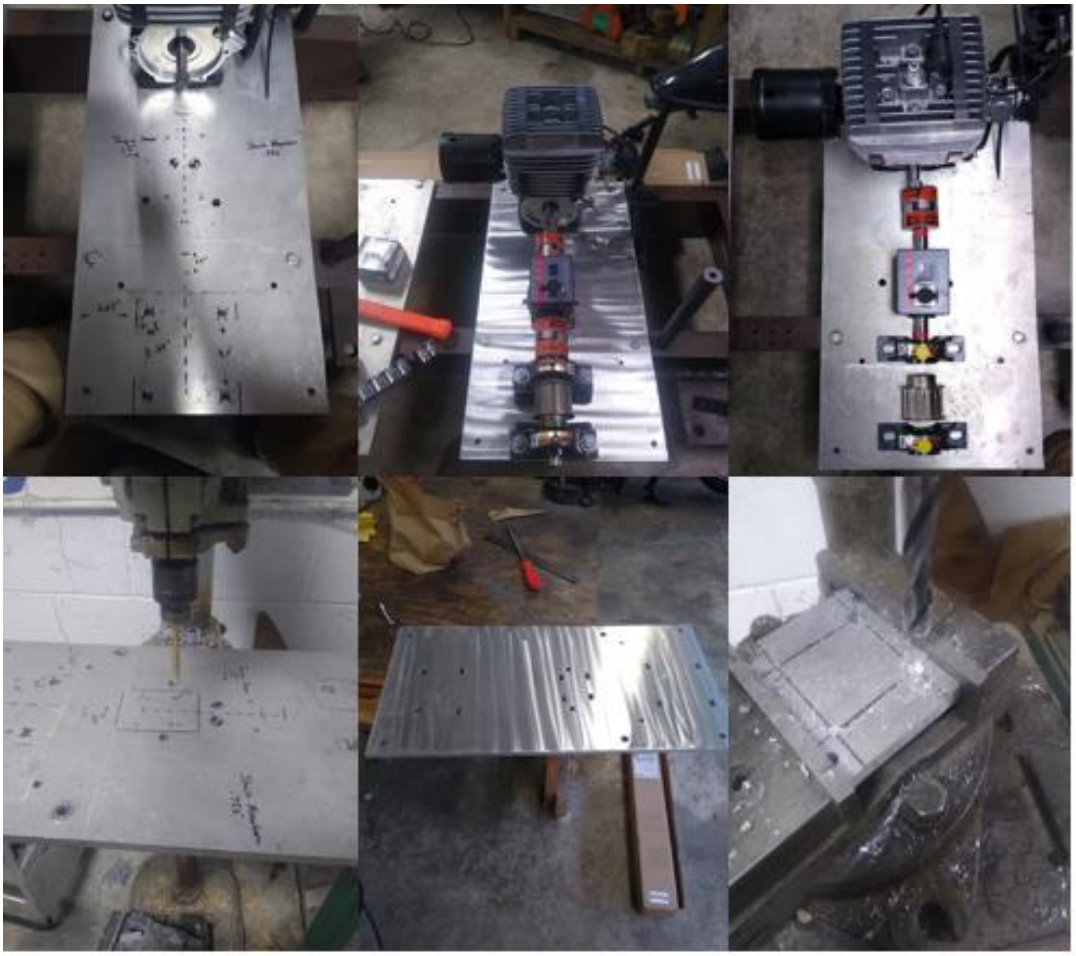

Figure 3.14: *Engine Side Plate Machining*

In addition to proper axial alignment, the components required being in vertical alignment as well. To do this, the difference in elevation was measured and a series of spacers were made to elevate the torque sensor and pulley bearing blocks. Bolts of adequate length were adapted to secure the components and their respective spacers to the mounting plate. The spacers were made out of flat stock aluminum plates. Figure 3.14 is a collage of the spacer manufacturing for the system.

Figure 3.15: *Collage of Spacer Machining*

After the alignment was correct in the axial and vertical direction, a mechanical connection had to be established between the rotating components. Specifically, an assembly had to be developed that could couple the engine to the torque sensor, and the torque sensor to the pulley assembly. The crankshaft of the KT-100 is dimensioned from the factory to receive a clutch that can drive a go kart. However, a clutch is not needed in this application as the generator is a direct drive from the engine. In addition, a series of Lovejoy fittings were used in between the engine, torque sensor, and bearing blocks. To visualize a connection means, a plan was drawn. Figure 3.16 is a schematic of the engine side driveline.

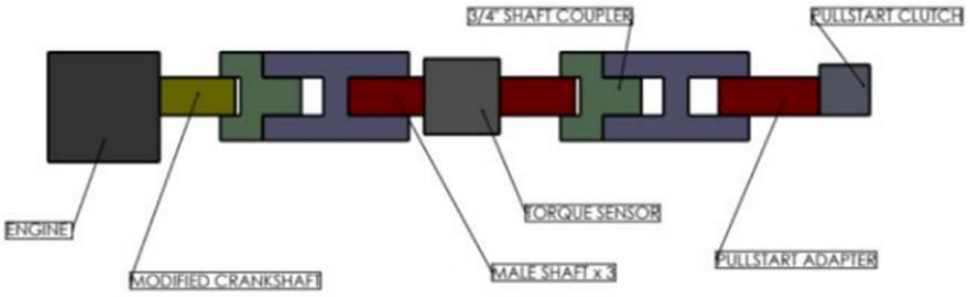

Figure 3.16: *Engine Side Driveline Schematic.*

The Lovejoy couplings were readily adaptable to the torque sensor via the keyed slot that extended from both sides. In addition, the shaft that connected the pulley to the bearing block also readily accepted the coupling. The engine, however, had to be modified to receive the Lovejoy connection. The engine was disassembled, and the crankshaft was removed from the bottom cases. From there, the crankshaft was chucked into the lathe, and the threads on the end of the crankshaft that were configured to receive the clutch were milled down. A ¾" hardened steel nut was centered and welded onto the crankshaft. A ¾" socket was sourced that could engage the nut. The socket was chucked into the lathe and machined to accept a portion of key slot rod material that was compatible with the Lovejoy couplings. The keyed shaft was milled to fit the socket, pressed in via the hydraulic press, and welded in place. The assembly comprised a nut welded onto the end of the crankshaft that was received by an adapter comprising a socket sized to engage the nut and a portion of the keyed rod. Figure 3.17 is a collage containing images of the nut welded to the crankshaft, the adapter, the machining of the two, the bearing block assembly, and the final connected unit.

Figure 3.17: *Shaft Adapter Collage*

With each of the engine side components manufactured, the engine side could be assembled. The components were placed on the engine side plate and bolted down. The engine was rested on rubber cushion blocks that reduced as much vibration as possible. The blocks were chemically resistant and consisted of foam and rubber. A hole was drilled through the rubber blocks so the bolt could pass through. The bolts that held the components on the engine side plate were secured with locknuts on the bottom side and washers between the nut and bolt head. On the side of the bearing block opposite to the Lovejoy, a ¾" nut was welded onto the shaft that could engage an external starter motor. Figure 3.18 is an image of the final engine side assembly.

Figure 3.18: *Engine Side Final Assembly*

With the engine side complete, construction could begin on the dynamo side. Unlike the engine side, the dynamo side only contained the dynamo. However, because the Honda IMA was originally designed to work in line with a Honda vehicle powertrain, it was not readily adaptable to the test stand. As a result, a special housing had to be constructed to hold the dynamo to the test stand. In addition to housing the dynamo, the housing had to also center the rotor within the dynamo. The first step in constructing the housing was to build a frame that could sandwich the dynamo. The frame was constructed out of ½" aluminum plate; it was critical to construct the

plate from aluminum and not a ferrous metal like steel to prevent any magnetic interaction between the dynamo and dynamo housing. Two vertical plates were cut from the aluminum plate that was slightly larger than the profile of the dynamo. It is imperative to the function of the dynamo that it must not move in the housing. The outer profile of the dynamo was traced onto the plates. The perimeter of the dynamo had 5 bolt locations that were asymmetrically disposed about the circumference thereof. Their position relative to the dynamo was also marked for machining. A drill bit whose diameter was exactly the diameter of the bolt holes was used to machine the bolt holes into the book-matched plates, such that the plates would mimic the bolt pattern of the bell housing that the dynamo was originally configured to engage with. Five grade 8 bolts having a diameter larger than the machined holes were sourced and machined down onto the lathe such that the shank of the bolt was a zero-tolerance fit between the housing and the dynamo. The zero-tolerance fit between the bolts, dynamo, and housing helped to ensure that the dynamo did not move relative to the housing. The bolts were accompanied with washers on both sides and lock nuts to ensure they remained tight. The dynamo was sandwiched between these two plates. A base section for each plate was formed at the bottom of the plates and welded together. Aluminum is notoriously difficult to weld because of its low melting point, high impurity level, and high heat transfer and is often done with a TIG machine. Instead of a TIG machine, a pulsed MIG welding machine was used to weld the aluminum plates. Figure 3.19 is a collage of the construction of the housing for the dynamo.

Figure 3.19: *Housing Construction Collage*

Once the housing was constructed, the assembly was test fit to ensure that the fitment was correct with no warping or binding. Importantly, when the housing was bolted together and tightened with a torque wrench to make sure that the plates were evenly taught across. Further, it was determined that approximately 30 ft-lbs. were appropriate to provide adequate torque to the structure without overtightening or warping. After the fitment was verified, the rotor assembly had to be constructed. The IMA rotor comes in two pieces: the rotor and the adaptor plate which bolts onto the rotor and couples the rotor to the armature. For this application, the adaptor was configured to work with ¾" keyed shaft as used throughout the test stand. The adaptor center hole was welded in to decrease the diameter. From there, the adapter was chucked into the lathe, and the center was milled out to ¾" to accept the shaft, which was welded in place. After the adapter was welded to the shaft, it was machined and faced to smooth out the mating surface and to decrease the rotating mass. A dial indicator was used to verify that the mating face was

substantially flat. Because of the unusual thread pitch used on the rotor, the 8 bolts around the periphery of the rotor which connected to the rotor to the shaft had to be specially ordered from Honda. Figure 3.20 is a collage of the armature manufacturing process.

Figure 3.20: *Armature Construction Collage*

After the armature was constructed, it had to be mated with the housing and remaining portion of the dynamo. This particular step requires the most care as the tolerance between the rotor and the dynamo housing was approximately .004” on either side. In addition, the strong magnetic force from the permanent magnet rotor increases the difficulty of fabrication. To mate the armature and rotor to the housing, the top plate of the housing assembly was removed, and

the rotor was set in place. A series of .004” polymer shims were placed around the circumference of the rotor to keep the rotor in place relative to the housing despite the large magnetic force. Once the rotor was centered in the housing, the assembly was transferred to the mill equipped with an edge finder and indexing tool to mark the location where the center hole would be. The location of the center hole was critical in ensuring that the armature was properly located. After double checking the location, the center hole through which the armature was received was machined. A pair of vertical bearing blocks were bolted onto the outer housing to accept the shaft. After these bearing blocks were located, the dynamo was reassembled. At this stage, the rotor could be rotated within the dynamo housing. Figure 3.21 is a collage of the final dynamo assembly.

Figure 3.21: *Final Dynamo Assembly Collage*

With the dynamo assembly completed, it could be mounted onto the test stand. Similar to the engine, the dynamo was mounted to the test stand via four grade 8 bolts, lock nuts, and washers. The dynamo was also supplied with four polymer anti-vibration pads to reduce the transmitted vibrations from the motor.

An output pulley was welded onto the armature of the dynamo and installed live with the primary pulley on the rotating assembly. Again, pulleys were used as they allow for easy interchangeability to manipulate the gearing ratio of the engine during the tuning process. A belt tensioner was made to ensure that the pulley remained taught over the course of the experiments. The belt tensioner comprised a tensioner for a serpentine belt from the parts store and a custom frame constructed from angle iron. The belt tensioner included a slot that allowed the tensioner to be tightened and loosened to remove and install the belt. A control box was installed on the opposite side of the dynamo to house the throttle and kill switch for the engine. The throttle assembly was a lawn mower style throttle that would hold the throttle opening steady. The kill switch was sourced from a Yamaha motorcycle and wired into the ignition circuit. A gas tank from a small two-stroke motorcycle was installed proximal to the control box and connected to the carburetor. The gas tank was mounted superjacent to the carburetor to promote a gravity feed of fuel. An air filter assembly was constructed from automotive intake runners and connected to the engine via a custom bell housing. A small motorcycle air filter was outfitted to the air filter assembly. Figure 3.22 is a collage of the miscellaneous items used on the test stand.

Figure 3.22: *Miscellaneous Parts Collage*

With the final miscellaneous components installed, the construction of the test stand was completed. A few preliminary tests were conducted to make sure that each of the components functioned correctly and rotated without binding. The following figures are images of the final test stand as used during the testing in this work. In some images, a cart is shown that was used to contain the test equipment. Specifically, Figures 3.23 – 3.35 are images of the final test stand configuration.

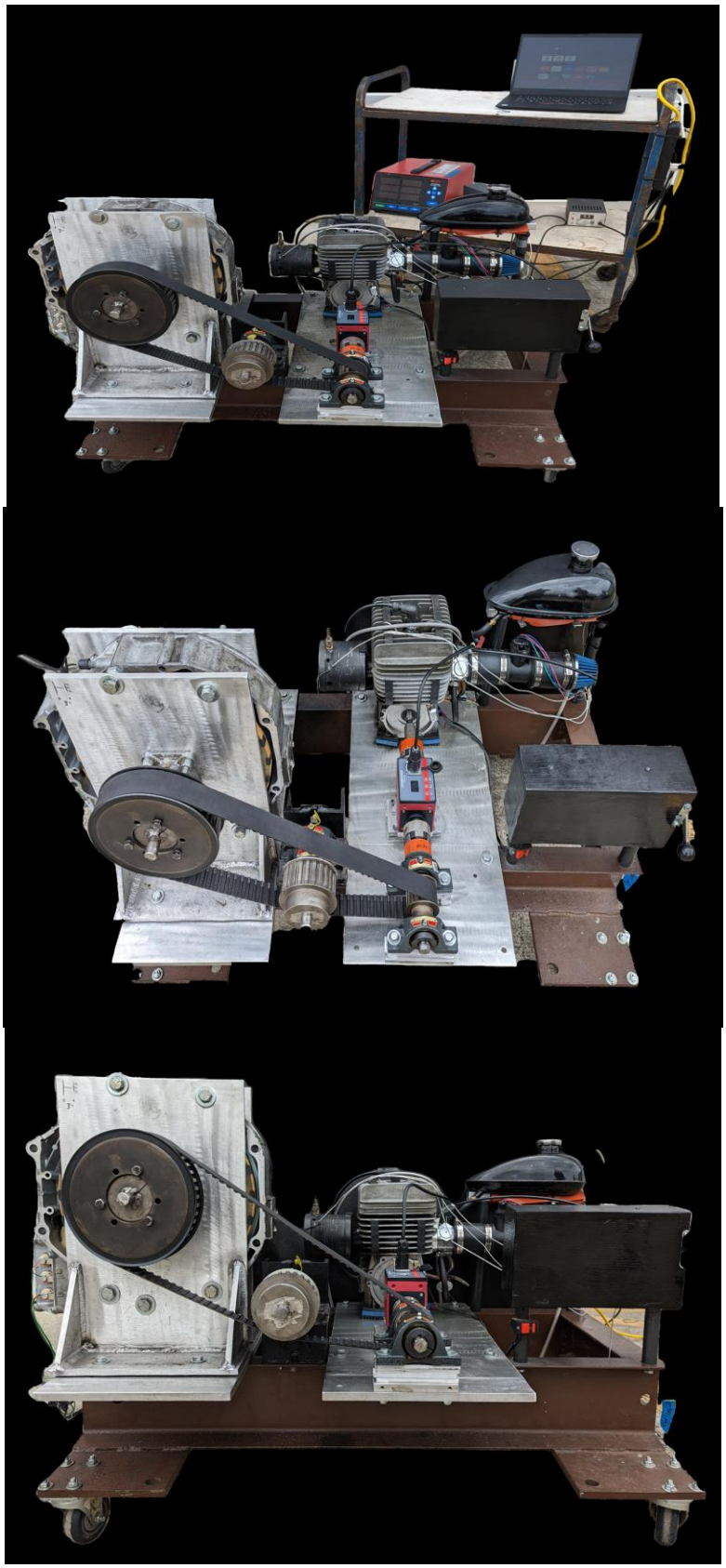

Figure 3.23 – 3.25: *Final Test Stand I,II, III*

3.4 Instrumentation & Data Collection

After the test stand was constructed, each of the components had to be instrumented and outfitted with data collection equipment for the purpose of collection experimental data. From the techniques and lessons learned from the previous work, instrumentation could be performed. The first and one of the most valuable aspects of data collection was performed by the torque sensor. The torque sensor was configured to measure brake power, brake torque, and RPM. The output from the torque sensor could be synchronized with the rotation of the crankshaft. The torque sensor could provide 3 pulses per second which was enough to generate smooth torque and power curves.

K-type thermocouples were installed in the exhaust port and cylinder head to measure temperature. K-type thermocouples are a type of temperature measuring device commonly used for measuring temperature. They are often composed of two different metal alloys which form a junction. The voltage at this junction is used to measure the temperature. Advantageously, k-type thermocouples have a wide temperature range and are highly durable. Further, they offer a rapid response time and are compatible with most DAQ systems. Understanding the cylinder head temperature and exhaust temperature is important in understanding how the engine is running, and more specifically, the state of tune of the engine. On an air-cooled engine like the one used in this work, it is critical to control and monitor the temperature to make sure that the engine does not overheat. A Bosch mass airflow sensor (MAF) was installed in the intake runner. The MAF was a hot wire style MAF and was suitable for the range of air velocities from the engine. Similarly to the thermocouples, hot wire MAF sensors offer precise airflow measurements and have a relatively quick response time. Further, they are robust and able to withstand engine

operating conditions. A calibration curve was obtained from Bosch to adjust the parameters of the MAF.

One of the most important engine operating parameters is in-cylinder pressure. In-cylinder pressure is a critical parameter to monitor and analyze in experiments because it directly shows combustion and engine performance. Moreover, these values can be used to calculate a variety of parameters. In one aspect, the in-cylinder pressure can provide insight to the combustion process; by measuring in-cylinder pressure vs time, the combustion efficiency and heat release can be calculated. In-cylinder pressure monitoring also allows for the investigation of dynamic effects that take place in the cylinder.

To measure in-cylinder pressure, an in-cylinder pressure sensor had to be installed. A Kistler model 6052A was used for this and had to be installed in the cylinder head. The cylinder head was removed, and a location was found that was thick enough to be machined and far away enough from the spark plug location. Advantageously on a carbureted two-stroke engine, since there are no valves, injectors, or other obstructions in the cylinder head other than the spark plug, locating the in-cylinder pressure sensor was relatively simple. A portion of the cooling fins were machined away to expose a flat surface. From there, a hole was bored and tapped to accept the in-cylinder pressure sensor which was threadedly secured. The data from the in-cylinder pressure sensor was synced to the crankshaft position data from the torque sensor and recorded on the DAQ. Figure 3.26 is a collage of the in-cylinder pressure sensor installation.

Figure 3.26: *In-Cylinder Pressure Sensor Installation*

Another important parameter to understanding engine performance is the exhaust emissions analysis. In one aspect, understanding the exhaust emissions and by extension the product of combustion further indicates the combustion process and efficiency of the engine. The exhaust emissions can be affected by air-fuel ration, ignition timing, combustion efficiency, and other engine parameters. In another aspect, it is critical to understand and control engine emissions from a regulatory standpoint. There are increasingly strict laws and regulations that mandate acceptable engine emissions limits and thus, it is important to understand the emission levels from the engine.

To measure the engine emissions, an Infrared Industries FGA 4000XDS exhaust gas analyzer was installed in the exhaust stream. This exhaust gas analyzer was configured to take a

small sample of exhaust gas from the exhaust manifold via a probe installed in the muffler. A pump then forces the sample across a plurality of infrared absorption sensors that measure the infrared light emitted by specific gas molecules. The exhaust analyzer used NDIR (non-dispersive infrared) to measure carbon monoxide (CO), carbon dioxide (CO_2), and unburned hydrocarbons (HC) and electrochemical cell to measure the NO_x emissions with a 1% full-scale accuracy. For HC measurements, the instrument measured methane CH_4 to approximate the HC values. Figure 3.27 is an image of the exhaust gas analyzer used in this work. The exhaust gas analyzer reports the concentration or percentage of emissions of the exhaust gas. More particularly, the EGA reports emissions species in either parts per million (PPM) or by mass percentage. To better compare the emissions performance, the data from the EGA was converted to g/kW-h. This method of comparing emissions is useful as it allows for consistent comparison. The use of the foregoing method of reporting emissions provides the conversion of emissions from volume to mass basis.

$$m_{e,i} = \frac{3600 * \mathrm{M}W_I * x_i * m_{ex}}{MW_{ex} * \dot{BP}} \qquad (3.1)$$

Figure 3.27: *Image of Exhaust Gas Analyzer*

With the data acquisition equipment in place, the data could be collected in real time. To do this, a bespoke LabVIEW program was written to collect each of the parameters that were measured. The LabVIEW program was controlled by a DAQ and computer coupled to each of the sensors and was configured to homologate the data and output in a file.

To cool the engine during testing, a fan was placed downstream of the engine to blow cooling air across the cooling fins. This fan was not used during the warmup stages to accelerate the warmup procedure. The engine was cooled via a combination of natural convection and forced air convection from the cooling fan. To start the engine, an external starting motor was used. The starting motor comprised a battery connected to a car starter with a one-way clutch installed on the armature. These starter boxes are commonly used in karting and are well suited for starting these style engines. To load the engine, a series of heating elements were electrically connected to the dyno. Heating elements are ideal for loading an engine because they are essentially pure resistive load. The heating elements were wired up to multimeters such that the voltage and current could be measured. With known voltage and current, resistive power could be calculated. To absorb and dissipate the heat generated by the heating elements, large cast iron

blocks were placed on each heater. With each of these components in place, testing could commence.

3.4 Preliminary Testing

Before the experiments with the prototype could commence, the test stand had to be validated and checked. The first step was to break in the engine. Because the engine was new, it had to have a break in cycle performed to ensure that engine life and performance was preserved. The engine was allowed to idle for about 10 minutes without any load. In addition, the fuel/oil mixture was doubled to 15:1 as per the manual recommendations. Once the engine was properly broken in, the fuel/oil mixture was returned to 32:1. The sparkplug was also replaced due to the heavy carbon deposits that accumulated as a result of the high oil ratio.

A first series of test runs were performed to ensure that the mechanical components and data collection was working properly. Through this, there were several alignment issues and excessive vibration issues that had to be resolved. The driveline was fined tuned by way of adjusting the fitment and alignment of the rotating components. With the driveline corrected, the engine could be properly tuned.

It is the nature of high-performance engines such as KT-100 used in this work to require tuning to reach optimal performance [95]. These engines are designed to be adapted to a variety of applications and thus require bespoke tuning. For example, in applications where loading varies such as in racing, the engine can have a more aggressive state of tune. In applications where the loading is continuous, such as in this application, the state of tune should be less aggressive to prevent overheating and engine damage.

The first step in tuning the engine is to adjust the ignition timing. The ignition timing refers to the position of the crankshaft when the ignition event occurs. Generally, engines can provide greater power and torque with more advanced or earlier ignition timing but will require higher octane fuel. For this application, the ignition timing was slightly retarded to lower operating temperature and fuel octane requirement. The ignition timing was adjusted by slightly moving the location of the magneto relative to the flywheel.

After the ignition timing was adjusted, the fuel/air ratio could be fine-tuned. The Walboro carburetor used with this engine was a diaphragm style carburetor commonly found on small engines such as chainsaws. These carburetors provide two tuning circuits; a low speed jet, which controls fuel mixture at lower engine speeds and a high speed jet, which controls the fuel mixture at higher engine speeds. The low speed needle was adjusted first based on the A/F and was set slightly fuel lean to promote throttle response and prevent plug fouling. The high speed jet was set moderately fuel rich to prevent overheating during extended high load operating. The tuning was adjusted based on Air/Fuel ratio readings from the exhaust gas analyzer. The carburetor was also disassembled to adjust the pop-off height. The pop-off height controls the amount of fuel introduced into the carburetor from the diaphragm pump and is controlled by fine tuning the length of the diaphragm. Figure 3.28 is a collage of the tuning process [95].

Figure 3.28: *Tuning Fuel & Ignition Collage*

After the engine was tuned and running at optimally, the driveline could be operated. During preliminary test runs, it was found that the engine was unable to reach higher RPM operating, even at lower loads. This was because the driveline ratio, or the gear reduction between the engine and dynamo of 2.73:1 was too low. The engine does not produce enough torque at lower RPMs to overcome the load of the dynamo as it, like many two-stroke engines, are intended to operate at relatively higher engine speeds. To overcome this, a series of pulleys of varying diameters were acquired and interchanged with the dynamo pulley. The drive ratio of the test stand could be configured by adjusting the pulley ratio. Different drive ratios were configured and tested. It was found that the optimal ratio for this application was a 4:1 gear reduction. As a result of the increased torque, the belt width had to be increased. With this upgraded configuration, the engine could be tuned with the dynamo. Advantageously, the setup used can essentially function as an Eddie current or electric dynamometer. The power and torque were measured from the torque sensor and plotted against RPM. Figure 3.29 is the dyno graph displaying torque and horsepower of the engine vs. engine speed from the engine after tuning.

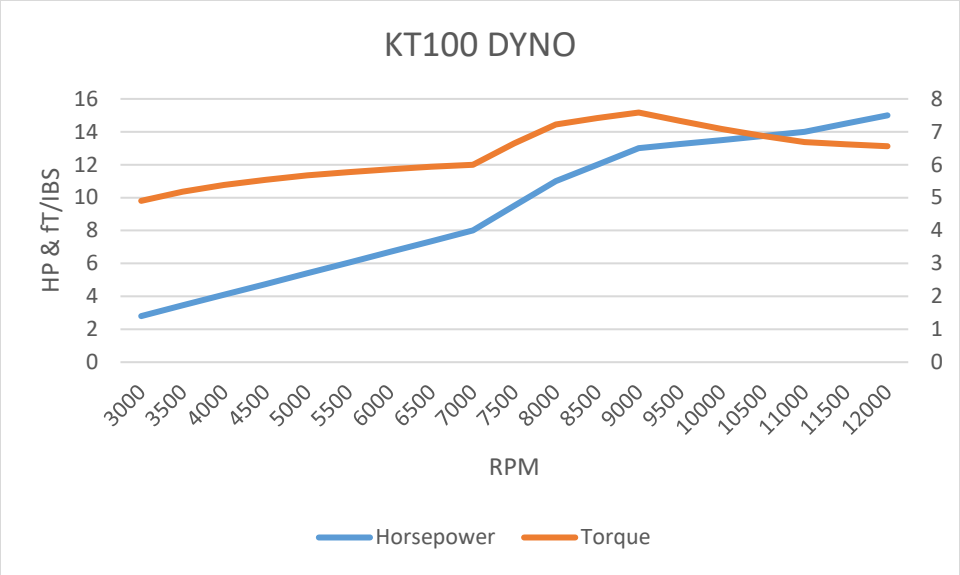

Figure 3.29: *KT-100 Dyno Results*

After the engine was prepared and the test stand was tuned, a preliminary test was conducted to check the instrumentation. The engine was motored with the starter motor and the in-cylinder pressure was measured. “Motoring” an engine refers to cranking the engine over without starting. Motoring speed is essentially the RPM of the starter motor. The pressure that is recorded is the pressure from compression only. The motoring test is important as it allows the validation of the instrumentation. The in-cylinder pressure was plotted against the crank position. Figure 3.30 shows the results from the motoring in-cylinder pressure.

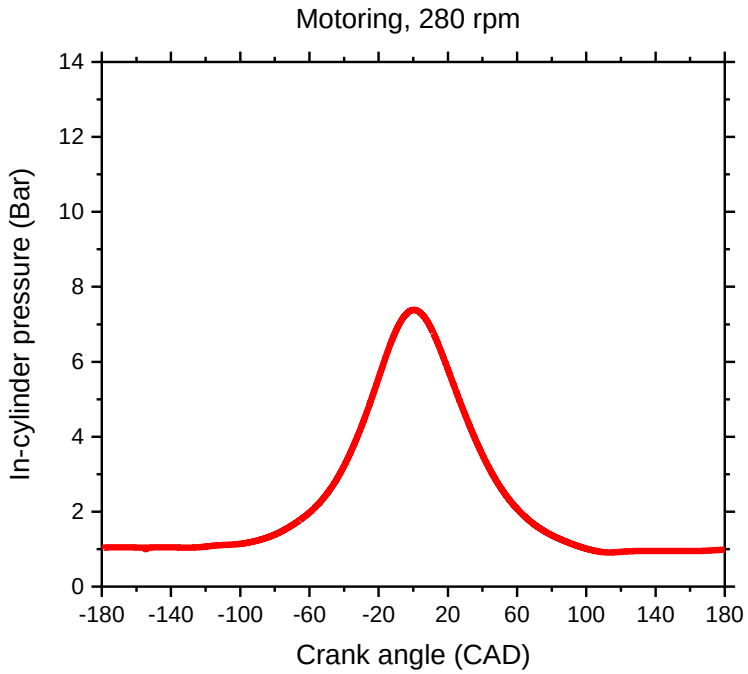

Figure 3.30: *Motoring In-cylinder Pressure Curve*

After the motoring test, a first prototype test could be conducted. The engine was loaded with a small load and test conditions were set. The in-cylinder pressure was measured from the sensor and the torque was measured from the torque sensor and were plotted against crankshaft position. In addition, the electrical power and mechanical power were also measured and reported. Importantly, the data collected from this test could be used in conjunction with the motoring data to ensure calibration of the instrumentation. The data from these tests were used to calibrate the test stand. Figure 3.31 is a graph of the preliminary calibration test results.

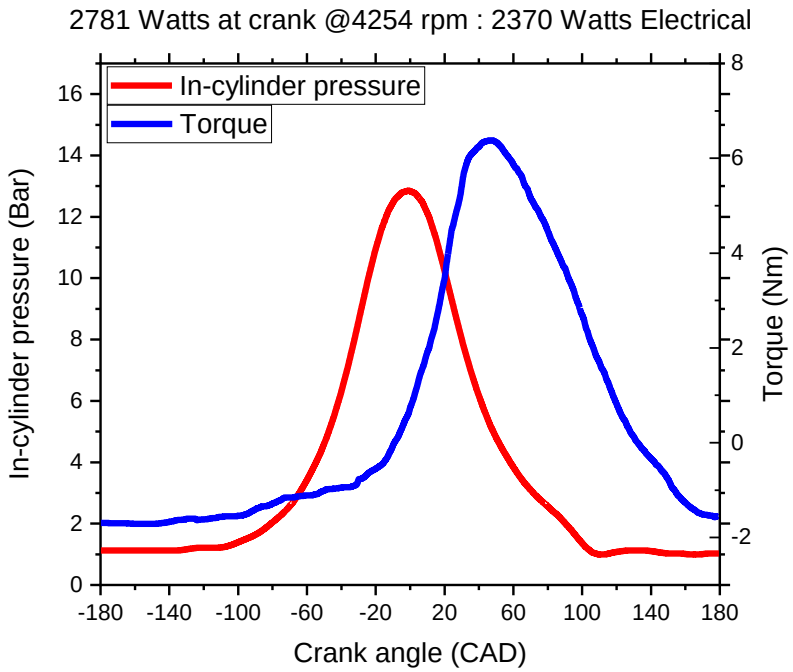

Figure 3.31: *Preliminary Calibration Test Results.*

The results of the efforts in this chapter provided a functional prototype high power density generator. The following chapters reflect the testing and experimentation using the prototype of this chapter.

CHAPTER 4: Experimental Validation: GASOLINE

4.1 Introduction

The increasing pressure from worldwide environmental concerns is motivating a transition from conventional fossil fuel-powered internal combustion engine (IC) vehicles to alternative powertrains, such as battery EVs and hybrid vehicles for the purpose of reducing anthropogenic carbon emissions. Such electric vehicles (EVs) are being introduced as a solution to the problems of dependency on fossil fuels, increasing carbon emissions, and other environmental issues [99]. The transportation sector, whose current majority comprises fossil fuel-powered vehicles, accounts for up to $1/5^{th}$ of all annual anthropogenic carbon dioxide emissions. More specifically, the transportation sector is responsible for almost 64% of global oil consumption and 23% of the energy relates to carbon emissions [99-100]. It is clear that a more viable method to fossil fuel based propulsion is necessary.

Although EV and hybrid adoption has increased over recent years, there remains a confluence of barriers that dissuade many consumers from considering EVs and plug in hybrids. Amongst these, range anxiety, or the driver's fear that the battery contains insufficient energy/battery capacity to drive the distance needed to reach a destination is predominant [103]. The conventional approach to ameliorate range anxiety includes deploying a more robust charging infrastructure, developing higher battery capacity EVs, battery swapping technology, hybrid powertrains with larger internal combustion engines, and free loan vehicles for long trips [103-104]. However, these approaches remain either long-term, impractical, or costly. Such practical issues and prices play a large role in car purchase decisions and negative sentiment toward electric vehicles and hybrid technology [105].

One solution is to adapt an electric generator as a range extender. A range extender is a fuel-based auxiliary power source that is configured to add additional drivable range to the battery of an EV independent from grid charging [106]. Another approach is to adapt the electric generator as the power source in a series hybrid vehicle. It is important to distinguish between parallel and series hybrid electric vehicles; parallel hybrid EVs utilize the energy from both an electric motor and an IC engine to propel the vehicle while series hybrid vehicles are only driven by the electric motor that receives power from the generator [107]. Importantly, the generators that could function in these configurations would not include the added weight and complexity of gearboxes, transmissions, etc., or drivetrain losses that burden conventional internal combustion engine vehicles. In addition, such a generator could operate at a single RPM and could be tuned for superior efficiency when compared to traditional IC propulsion [108]. It is common for onboard generators to be powered by conventional internal combustion engines, but many configurations have been considered including fuel cells, free-piston generators, and micro gas turbines [108-109]. In most aspects, these onboard generators are adapted to use a liquid hydrocarbon fuel, such as gasoline [109]. Thus, an EV or hybrid equipped with an onboard generator can conveniently utilize the existing network of refueling stations [10].

Unfortunately, the state of the art of powertrain generators only includes small low-power units (<5kW) that are unfit for rapid charging or driving a vehicle and can offer only small boosts in battery capacity and large permanently attached generators that can accompany certain EVs or be provided in hybrid arrangements [111]. In many cases, these permanently attached generators are prohibitively expensive, often adding up to $7000 to the purchase price of an EV that already exceeds the price of similar IC vehicles [112-113]. What's more, these generators are often bulky, complicated, and heavy which can limit their usefulness. There are many

applications, such as in UAV powertrains, motorcycles, ATVs, boats, ultralight aircraft, and more where hybrid electric power is unavailable because of the lower specific power and large size of currently available generators [114-115].

This study aims to characterize the performance of the high-power density power generator from the previous chapter to fulfill the need for a lightweight, portable, and inexpensive unit that is powerful enough to function as a range extender or as a component in a hybrid powertrain where specific power and small size is critical. For this chapter, the prototype from the previous chapter was prepared for experiments. A series of experimental analyses were performed on the prototype to understand its performance and to validate the design.

4.2 Experimental Procedure

The prototype generator underwent preparation for testing to run the experiments and performance assessment. The engine was started and allowed to run for a few minutes to reach operating temperature. Three heating elements with measurable current and voltage were adapted to impose a load on the engine. The loading elements were assembled into a load bank. Heating elements are close to ideal loads because they provide stable loading that increases linearly with voltage. These electric heating elements were wired to the dynamo via a delta configuration, where each phase was connected to a heating element. This wiring configuration was chosen because of its simplicity and balanced loading. Delta wiring configuration also experiences an increased line-to-line voltage; because the voltage across two connections is $\sqrt{3}$ times the phase voltage, the voltage to and therefore the resistance from the heating elements was magnified, making the heating elements more effective loads. A three-phase rectifier was included to transform the DC power from the dynamo to AC power for the heating elements. Large iron

castings were placed on the heaters to absorb the generated heat, ensuring a continuous load supply to the engine. The electrical power was measured at the generator. To manage engine temperature, an industrial blower was positioned adjacent to the engine, directing air over the air fins of the cylinder and cylinder head.

The system was equipped with instrumentation to record data from the engine and dynamo during operation. K-type thermocouples were affixed to the cylinder head and exhaust for temperature measurements. The Bosch mass airflow sensor in the intake measured the air mass flow rate. The cylinder head was modified to accept the Kistler model 6052A piezoelectric pressure sensor for in-cylinder pressure monitoring. An Infrared Industries FGA 4000XDS exhaust gas analyzer, utilizing NDIR for HC, CO, and CO_2 species measurements, along with an electrochemical cell for NO_x emissions with 1% full-scale accuracy, was installed in the exhaust stream. An ATO digital rotary in-line dynamic torque sensor was installed between the engine and dynamo for brake power, torque, and engine speed (in rpm) measurements. A custom LabVIEW program provided data collection and signal synchronization. MATLAB was used for subsequent data analysis and post-processing. The system provided dependable measurement results with an error margin below 5%, based on the least precise instrument. A series of experiments were conducted across varied engine speeds and throttle conditions, each repeated five times to assess repeatability and mitigate errors.

For subsequent discussions, full load is defined as the maximum electrical power before the engine stalls. Low load refers to only the power consumed to energize the coils, measured while the generator was freewheeling without electrical load and includes no load from the load bank. The low load power was maintained consistently across tested RPMs to keep the coils energized. Part load fell approximately midway between low load and full load. Slight variations

in low load and part load occurred due to the generator's limited fine control of loading. Experiments involving low load, part load, and full load conditions were conducted at three distinct RPMs with recorded data and the throttle openings were limited to up to 10% for low load, up to 50% for part load, and wide open throttle for full load. The loads were measured at the point of stall for each condition. The load power represented the power at each loading condition measured at the heating elements. It should be noted that the low load electrical power is constant between engine speeds as it is only the power required to energize the coils and includes no additional load from the load bank. Table 4.1 lists the loading conditions during testing.

Table 4.1: *Loading Conditions During Testing*

Loading Condition	RPM	Load Power (kW)
Low load	4250	.75
	6700	
	9100	
Part Load	4250	1.73
	6700	2.63
	9100	3.24
Full Load	4250	3.05
	6700	5.10
	9100	8.50

4.3 Results and Discussion

4.3.1 Brake Power & Torque Analysis

The dynamic torque sensor which was configured to measure brake torque and brake power was installed in between the engine and the dynamo allowing the brake power produced by the engine to be measured. The torque sensor was coupled to the engine via the Lovejoy

coupling and to the dynamo via the drive belt. Figure 4.1 shows the brake power measured at the crankshaft at three discrete engine speeds at low load, part load, and full load.

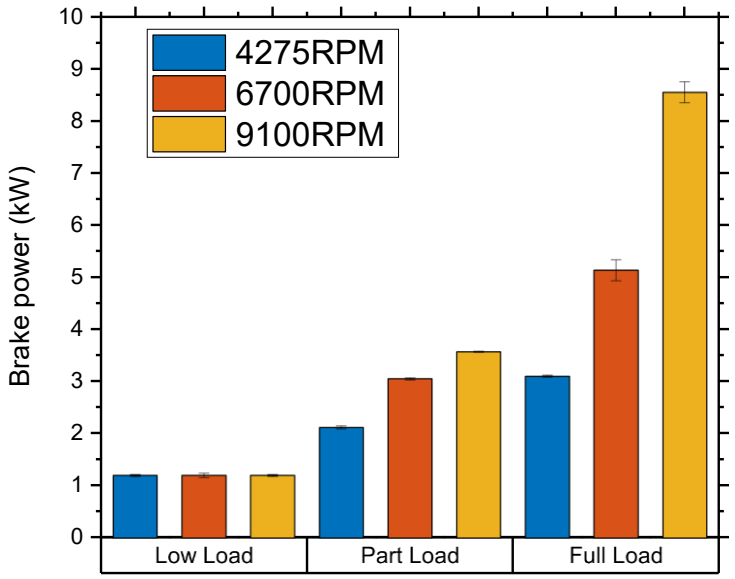

Figure 4.1: *Brake Power at Varying Loads and Engine Speeds*

From Figure 4.1, It can be seen that brake power is relatively constant at low loads at various engine speeds. At low loads, the engine is only producing enough power to rotate the assembly and energize the coils of the dynamo. The heating elements' resistance increases with voltage, and voltage is proportional to rotor speed. Because the heating elements were not engaged at low loads, only the constant load from the driveline and coil was experienced. As loading increases, the brake power produced by the engine shows an increase at each engine speed. Additionally, at full load conditions, engine speed has a profound effect on increasing engine power. This is likely because at full load the throttle is at WOT and there are minimal throttling losses. Continuing, the highest brake power is observed at full engine loading conditions at 9100 RPM. It is theorized that friction and throttling losses are predominant at

lower engine speeds and when the throttle is closed. Moreover, it is likely that at low load high-speed operations, mechanical and pumping losses dramatically affect the brake power produced by the engine. In a two-stroke engine, there is a dramatic increase in volumetric efficiency with increasing engine speed, which can explain the sharp increase in brake power with increased engine RPM [92-94].

Another aspect that affects the power out of two-stroke engines is port timing and duration. Two-stroke port timing refers to the crankshaft position when the piston uncovers the transfer and exhaust port and is controlled by the location of the ports in the cylinder. Port duration refers to how long the port is uncovered by the piston relative to the crankshaft position [92-94]. In a two-stroke engine, the port timing and duration have a profound effect on the gas dynamic during the scavenging, expansion, blowdown, and exhaust phase of the cycle, and are analogous to valve timing and duration in a four-stroke engine [92,95]. Piston-port two-stroke engines, such as the KT-100, do not incorporate rotary valves or reed valves to assist with the gas exchange and therefore have a more narrow tuning window for port timing and duration [70]. The port timing and duration scheme used on the KT-100 is optimized for high RPM power, which is common among competition engines [70]. As a result, the gas dynamics of the engine are most efficient at higher engine speeds and less efficient at lower speeds. This increase in gas exchange efficiency could participate in the increased power output at higher engine speeds.

Figure 4.2 shows the brake torque produced by the engine measured at the torque sensor. Because power is a function of torque and engine speed, the torque produced at each discrete loading condition and engine speed is related to the power at each loading condition and engine speed. More specifically, because loading is fixed, and power is a function of torque and RPM, as RPM increases at a fixed loading condition the torque decreases and power increases. It can

be observed that maximum torque occurs at full load and low engine speeds where engine efficiency is the greatest. Because the engine was power limited, and power is a function of torque and RPM, maximum torque occurs at full throttle at the lowest engine speed.

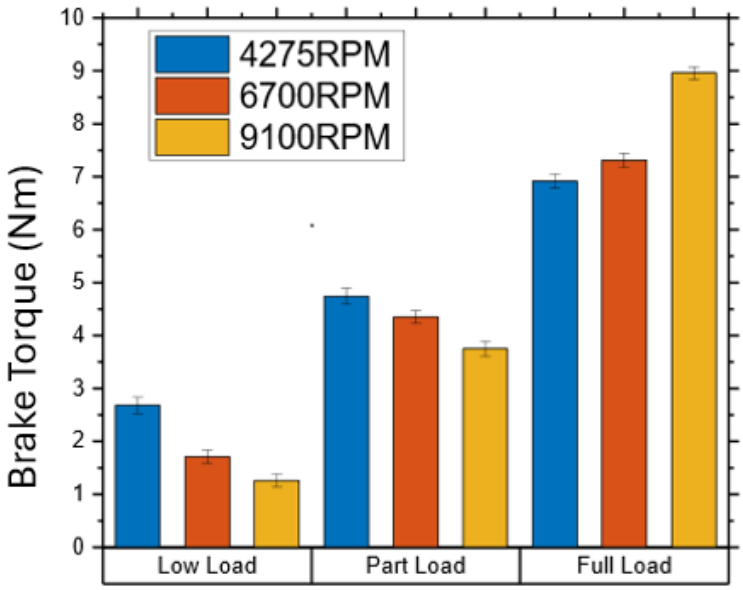

Figure 4.2: *Brake Torque at Varying Loads and Engine Speeds*

The torque produced increases with engine speed for likely the same reason power increases with engine speed. As the engine speed is increased, the volumetric efficiency increases and the fuel charge dilution decreases [92-94]. Two-stroke engines benefit from high RPM operation and generally produce greater torque at higher RPM operation. Unlike other engine architectures which can use valves or forced induction, two-stroke engines rely heavily on the momentum of the incoming fuel/air charge to breathe. Further, as the throttle is opened to meet increasing loads, throttling losses are decreased. The port timing and duration also could affect the brake torque. As a result of the port timing and duration are optimized for high engine speed operation, the increase in gas exchange efficiency at higher engine speed could contribute to the increased torque at higher engine speeds.

4.3.2 In-Cylinder Pressure

The cylinder head of the engine was machined to accept an in-cylinder pressure transducer to provide the transient combustion pressure measurements during the operation of the engine. Because two-stroke engines do not require valves in the cylinder head, the pressure sensor could be ideally placed proximal to the spark plug. The data collected was synced to the crankshaft position of the engine to provide pressure data as a function of crank angle.

Figure 4.3 shows the in-cylinder combustion pressure vs. crank angle varying loading conditions. From Figure 4.3, it is clear that as the load increases, the peak in-cylinder pressure increases with each loading condition. In addition, there is an increase in in-cylinder pressure at each loading condition as RPM increases. However, there is a more pronounced increase in in-cylinder pressure from low load to part load than from part load to full load. Similarly, there is a greater increase in in-cylinder pressure at each loading condition from 4250 RPM to 6700 RPM than from 6700 RPM to 9100 RPM. The more pronounced increase in in-cylinder pressure at lower engine speeds and loading is likely because in a two-stroke engine, at lower engine speeds, the cylinder filling efficiency and blowdown phase efficiency are low resulting in a higher concentration of diluent exhaust species remaining in the combustion chamber from cycle to cycle [92-94]. Moreover, because the port timing and duration are not optimized for low engine speed operation, the scavenging efficiency is lower at low engine speeds which results in higher levels of trapped exhaust gas in the combustion chamber [92-94]. The increase in trapped exhaust gas dilutes the fuel/air mixture and reduces pressure rise.

As engine speed and throttle openings increase, there is a pronounced increase in-cylinder filling and blowdown efficiency, in part due to the port timing and duration being optimized at these conditions. As a result, there is a lower concentration of diluent species at

higher RPM operation. Moreover, at higher engine speeds, the effects of charge dilution are lower. The lower concentration of diluents can result in higher peak pressure and pressure rise.

It is also observed that, for each loading condition, the in-cylinder pressure curve for 4275 RPM is more gradual and exhibits less of a peak than that of 6700 RPM and 9100 RPM. Again, this is likely the result of high concentrations of exhaust gas at lower engine RPMs as a result of poor gas exchange at low engine speeds. The greater concentrations of diluent exhaust gas can encourage the in-cylinder pressure rise to be more gradual [45].

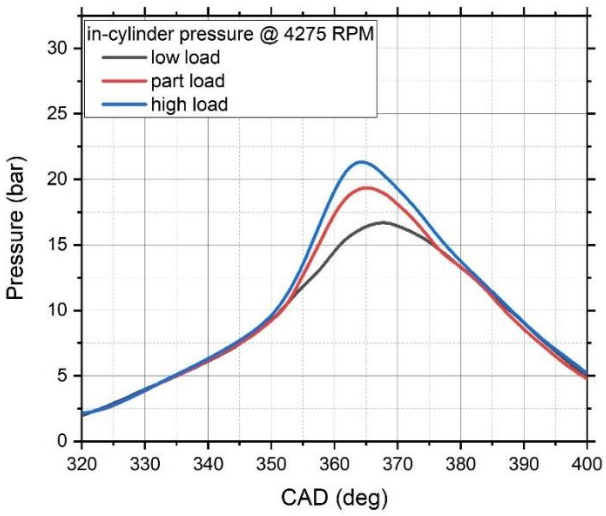

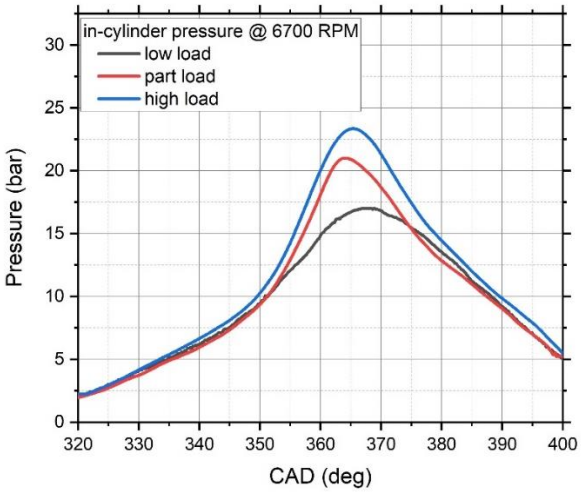

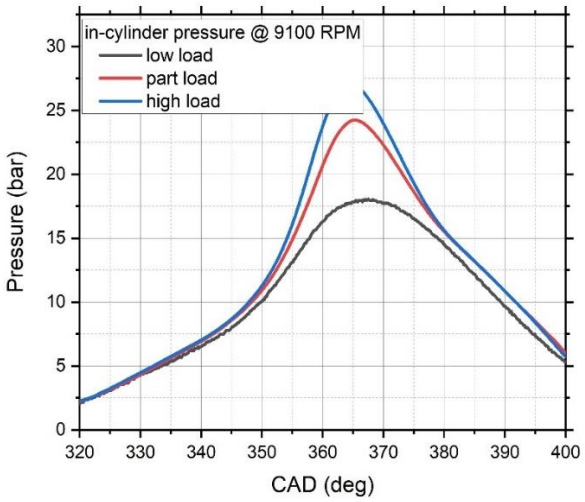

Figure 4.3: *In-Cylinder Pressure Comparison*

The in-cylinder pressure measurements were utilized to derive the heat release rate (HRR) of the fuel in the following analysis. Investigating the heat release rate is important in understanding the combustion dynamics within an internal combustion engine. This analytical approach yields important insights into combustion behavior, fuel economy, engine performance, and emissions [70]. Additionally, the heat release rate analysis provides a comparative assessment of the combustion characteristics between loading conditions. Similarly to in-cylinder pressure, the heat release rate is plotted against crank angle. The examination of heat release rate in relation to the crank angle provides details about the combustion event during its duration. Furthermore, assessing the temperature evolution of heat release offers a more empirical perspective on combustion dynamics. In this chapter, the heat release rate was calculated by using the first law heat release model proposed by *Heywood* [70]. This model calculates the heat release rate from in-cylinder pressure based on the volume of the cylinder at varying crank angles. For these calculations, the contents of the combustion chamber are modeled as an ideal gas with R held constant. A constant specific heat ratio (γ) of 1.325 as suggested by *Heywood* was used as the discrete values for γ during combustion are not well defined [70]. Equation 4.1 provides the heat release rate model.

$$\frac{dQ}{d\theta} = \frac{\gamma}{\gamma-1} P \frac{dV}{d\theta} + \frac{1}{\gamma-1} V \frac{dP}{d\theta} \qquad (4.1)$$

From Figure 4.4, it can be seen that in general, the heat release rate increases with increased loading conditions. Similarly to in-cylinder pressure, the heat release rate also increases with RPM at each loading condition. It is also observed that there is a larger increase in heat release rate from low load condition to part load condition and a more subtle increase in heat release rate from part load to full load condition, further analogous to in-cylinder pressure.

In addition, the increase in HRR between 4275 RPM and 6700 RPM is more substantial than from 6700 RPM to 9100 RPM at each loading condition. The full load operating condition showed the greatest heat release rate.

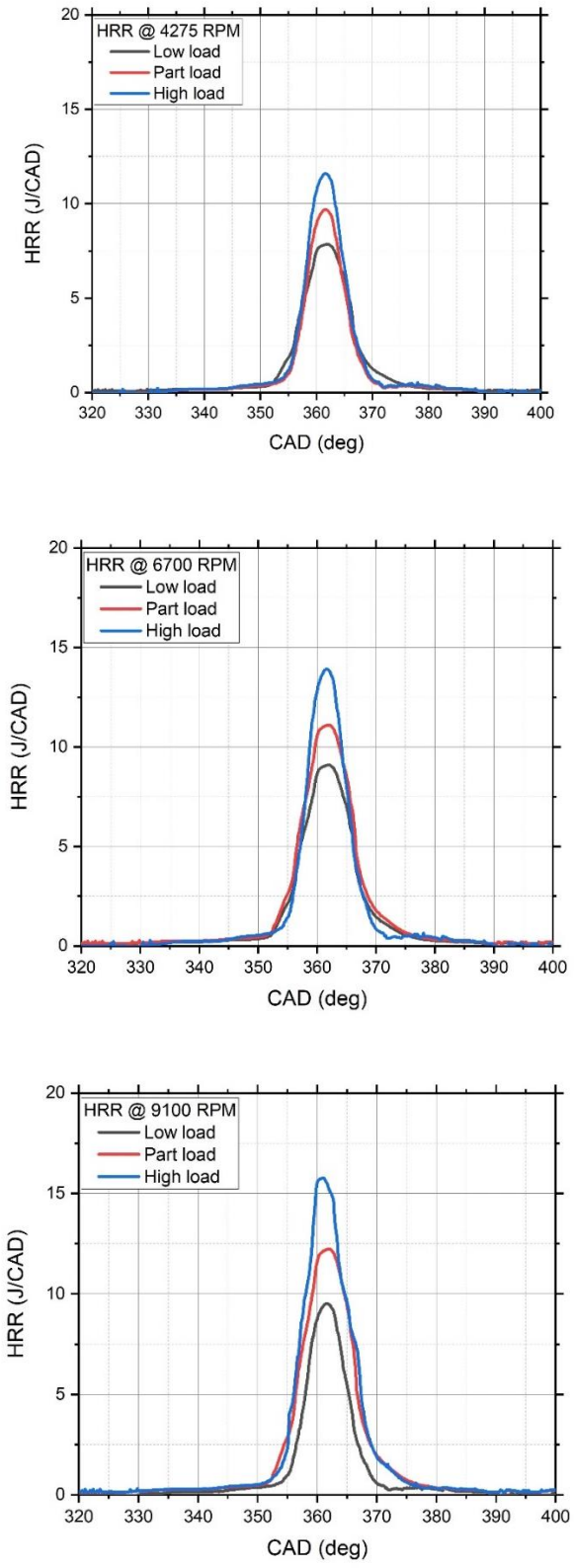

Figure 4.4: *Heat Release Rate Comparison*

The in-cylinder pressure is an important input variable when calculating the heat release rate. The parameters specific to the engine that affect in-cylinder pressure in essence likely affect the heat release rate. It is therefore theorized that differences in heat release rate are a result of the differences in gas exchange efficiencies at different loading and RPM operating conditions. In another aspect, the fuel burning rate may influence the measured HRR at each loading condition and RPM. In general, the fuel burning rate increases with increased in-cylinder turbulence [116]. The in-cylinder turbulence of the fuel charge in most engines increases with RPM. Two-stroke engines in particular experience highly turbulent flow at high RPMs because of fixed transfer port geometry [92-94]. The increase in HRR as engine speed increases may also be a result of increased turbulence.

The cumulative heat release is the sum of the heat release rate throughout the cycle. Cumulative heat release generally represents the total heat generated inside the cylinder per cycle. Cumulative heat release is also an important parameter in providing a comparison between loading and engine speed experiments. The heat release rate data was used to calculate the cumulative heat release at the specified loading conditions.

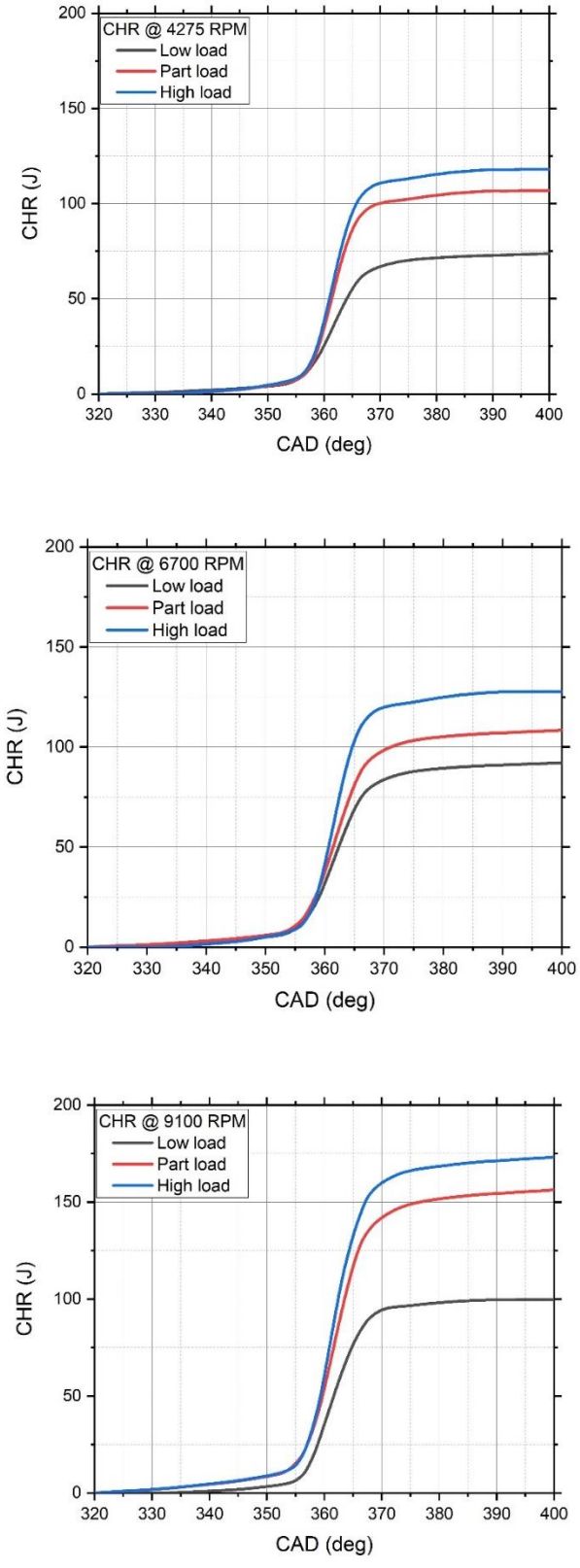

Figure 4.5: *Cumulative Heat Release Rate Comparison*

Figure 4.5 shows the cumulative heat release rate results for different engine loads. From Figure 4.5, it is clear that a similar trend to heat release rate can be identified between loading conditions wherein the cumulative heat release increases with increasing loading conditions. What's more, there is a greater increase in cumulative heat release between low load and part load conditions than between part load and full load conditions, likely as a result of the reasons discussed above. In continuation, full load conditions exhibited the greatest cumulative heat release. When compared to gasoline operation, methanol showed slightly higher cumulative heat release.

4.3.3 Efficiency Analysis

Examining the thermal efficiency of the prototype is important for understanding its effectiveness. Thermal efficiency serves as a practical metric to gauge various efficiency aspects, including fuel efficiency and mechanical conversion efficiency, consolidating them into a single measure. It is defined as the ratio of work performed to absorbed heat [70].

The indicated thermal efficiency was calculated from the pressure data taken from the in-cylinder pressure sensor. Indicated thermal efficiency is the ratio of indicated power to fuel power. Indicated thermal efficiency is important as it provides a measure of how well the engine converts the heat energy from fuel into mechanical work. Further, indicated thermal efficiency ignores the losses in the system and provides an idealized efficiency value. Table 4.2 displays the calculated indicated thermal efficiency of the engine. For this work, the indicated thermal efficiency is defined in Equation 4.2 provided from *Heywood* [70].

$$n_{f,i} = \frac{W_{e,i}}{m_{f*}\, Q_{LHV}} \qquad (4.2)$$

Table 4.2: Calculated Indicated Thermal Efficiency

Loading	4275 RPM	6700 RPM	9100 RPM
Low load	12.45%	14.54%	16.21%
Part Load	13.20%	15.15%	18.25%
Full Load	13.74%	16.24%	21.02%

From Table 4.2, it can be seen there is an increase in indicated thermal efficiency as engine speed increases. Further, as loading increases, the indicated thermal efficiency also increases. In one aspect heat transfer likely controls the indicated thermal efficiency; the indicated efficiency can increase with increased RPM because there is less time for heat transfer to take place. Higher rates of heat transfer can lower the thermal efficiency of the engine because energy that could be converted to mechanical work escapes as heat. Because the operating temperatures of the engine are generally hotter at higher loading and RPM, the thermal gradient is lower which can further limit heat transfer and increase thermal efficiency. The engine of this work utilizes air cooling to control engine temperatures. For this application, air cooling is preferred because of its simplicity and ruggedness. However, air-cooled engines are often subjected to uneven temperature distribution across the engine and fluctuating operating temperatures [70]. It is theorized that, if the engine were switched to liquid cooling, the indicated thermal efficiency would increase. It has been shown that liquid-cooled engines generally have greater thermal efficiency than air-cooled engines [92-95]. It is important to note that the indicated thermal efficiency is an idealized value that calculates the work done inside the cylinder and does not account for various losses that are present in a real engine, such as friction, heat losses, and pumping and powertrain losses. Brake thermal efficiency is used to account for these losses and can provide an idea of the useful work, such as crankshaft work.

The brake thermal efficiency is the measured efficiency of the engine at the crankshaft. Brake thermal efficiency can be more useful in certain aspects because it indicates the mechanical efficiency of the engine. More generally, brake thermal efficiency takes into consideration the mechanical losses that burden the engine. The brake thermal efficiency is the ratio of mechanical power measured at the crankshaft to fuel power. Figure 4.6 lists the brake thermal efficiency of the prototype generator at varying loads and engine speeds (shown in RPM). For this work, the indicated thermal efficiency is defined in Equation 4.3 provided from *Heywood* [70].

$$n_{f,b} = \frac{W_{e,b}}{m_{f^*} Q_{LHV}} \qquad (4.3)$$

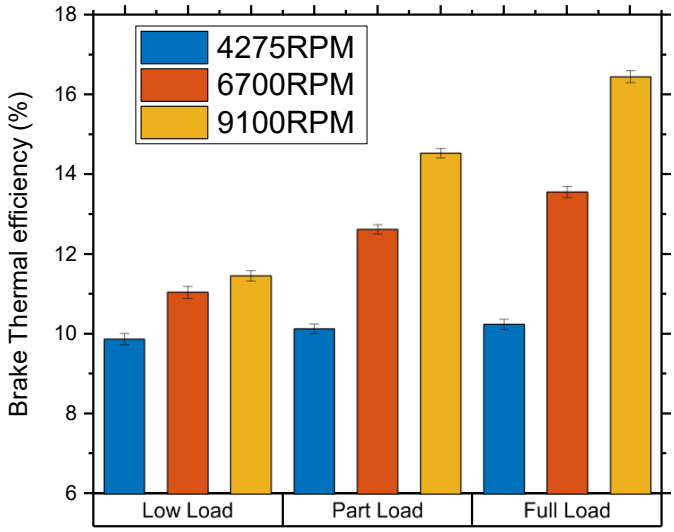

Figure 4.6: *Brake Thermal Efficiency Comparison*

From Figure 4.6 it is shown that for each loading condition, as engine speed increases, the brake thermal efficiency increases. More particularly, as engine loading increases the difference between the brake thermal efficiency as engine speed increases also increases. The

increase in efficiency is likely because as engine speed increases, volumetric efficiency increases. This is because on a two-stroke engine certain tuning parameters, such as the port shape and timing, are tuned to operate most efficiently at a certain RPM range, and as the engine speed approaches this RPM, the efficiency increases [70]. Many two-stroke engines have narrow RPM ranges at which they operate most efficiently [95]. For the KT100, a marked increase in thermal efficiency and power output is observed as the engine approaches and operates in its tuned highest efficiency RPM range, at around 9k RPM. When the engine is operating in its RPM of highest efficiency, cylinder filling, and combustion efficiency increases while fuel charge dilution decreases [92-94].

High load, high speed operation shows the greatest power and efficiency while low load, low speed shows the worst power and efficiency. Apart from the engine operating far outside its optimum tuning window at these speeds, the dynamo may contribute to poor performance low speed low load performance because the effects of uneven coil loading become more pronounced. Considering the data contained in Figure 4.6, it can be concluded that the generator should be operated at the highest possible engine speed during operation. The engine is capable of engine speeds in excess of 16k RPM. Such high engine speeds were not explored as they showed a decrease in efficiency and an increase in undesirable noise, harshness, and vibration.

The brake thermal efficiency is relatively high because of the simplicity of the drive line. Without a complex transmission, drivetrain, or other components to introduce sources of mechanical loss, the generator can minimize power lost to friction and maintain relatively higher brake thermal efficiency. Other tuning parameters encourage the efficiency of the engine to increase with engine speed and throttle opening, such as the port geometry, duration, and timing. Many two-stroke engines, when compared to other engine types, have a narrower range of RPM

in which they operate efficiently [92-94]. It is common for two-stroke engines to be tuned to operate most efficiently at high RPM and wide-open throttle conditions, which is the case for the KT-100 [95]. In a steady-state application, such as the generator of this work, this can be a particular advantage.

The mechanical efficiency of an engine is the ratio of brake power to indicated power. Mechanical efficiency is affected by the friction and pumping losses that reduce the useful work. The friction can result from the piston-to-cylinder interaction, bearing drag, and other friction introduced by various mechanical components. Table 4.3 calculates the mechanical efficiency of the engine at each loading condition. Equation 4.4 provides the mechanical efficiency.

$$n_{f,b} = \frac{n_{f,b}}{n_{f,i}} \quad (4.4)$$

Table 4.3: *Calculated Mechanical Efficiency in Percent (%)*

Loading	4275 RPM	6700 RPM	9100 RPM
Low load	86.6	89.7	91.5
Part Load	80.7	83.4	87.9
Full Load	80.8	83.8	87.1

Friction power depends largely on throttle position and engine speed. As the throttle is opened, fewer pumping losses occur. Friction increases as engine speed increases because friction is proportional to the square of engine speed. In addition, as engine power increases, the forces that act on the ring and piston can cause higher rubbing forces that result in more friction losses. It can be seen that mechanical efficiency increases with engine speed. This is likely because there are lower pumping losses. Mechanical efficiency also decreases with engine

loading. This is likely a result of the higher combustion forces increasing the force that the ring and piston engage the cylinder wall with, which creates more friction [94].

In addition to evaluating the engine efficiency, the dynamo efficiency was analyzed. The efficiency of the dynamo can be calculated by comparing the output power supplied to the dynamo to the electrical power produced. Higher dynamo efficiency means that there is less wasted energy and more available power to the application. The dynamo efficiency can also be called conversion efficiency as it is a measure of how efficiently the dynamo can convert mechanical power into electrical power. Specifically, the dynamo efficiency is the ratio of mechanical power supplied to electrical power produced. The efficiency of the dynamo was calculated and plotted as a function of efficiency vs output power. It should be noted that the electrical efficiency is shown as a curve because the dynamo efficiency is constant across engine loading. Figure 4.7 shows the measured dynamo efficiency.

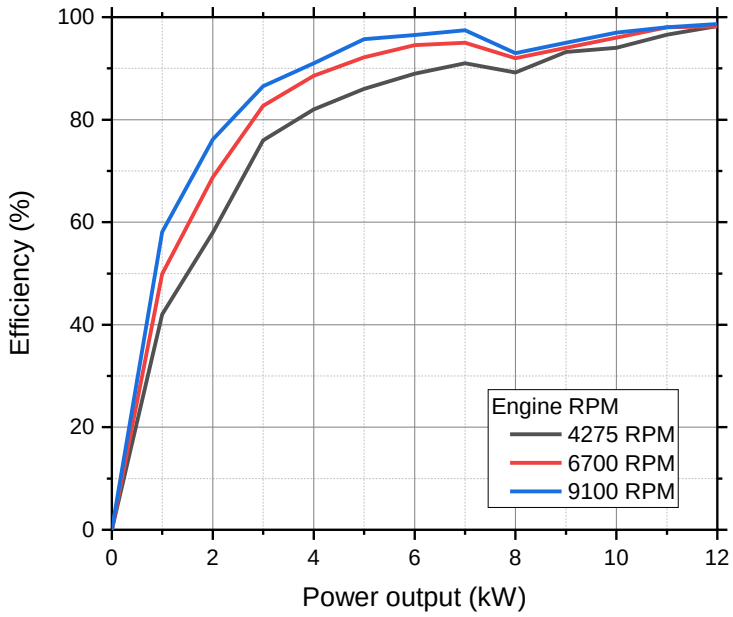

Figure 4.7: *Calculated Dynamo Efficiency*

From Figure 4.7, it can be seen that as the power output increases, the dynamo conversion efficiency increases. This is because at lower speeds, a larger proportion of the power supplied to the dynamo is used to energize the coils and overcome friction and losses. The power consumed to energize the coils is fixed and does not increase with increased speed or loading. Therefore, the proportion of power lost to energize the coil diminished and the dynamo efficiency increased with RPM and loading. Advantageously, high conversion efficiency occurs around the maximum power output and target operation speed of the generator system. Table 4.4 lists the discrete dynamo efficiency at each loading condition and engine speed.

Table 4.4: *Electrical Efficiency at Discrete Loading and Engine Speeds*

Loading Condition	RPM	Electrical Efficiency (%)
Low load	4250	62.5
	6700	
	9100	
Part Load	4250	70.6
	6700	85.3
	9100	90.0
Full Load	4250	97.3
	6700	97.0
	9100	96.1

In view of the engine and dynamo performance, it can be concluded that the generator should operate at a relatively steady high RPM and high loading conditions to achieve maximum efficiency and power. Table 4.5 lists the measured parameters of engine performance of the prototype generator at 9100 RPM.

Table 4.5*: *Generator Performance at 9100 RPM

Loading (9100 RPM)	Brake Torque (Nm)	Brake Power (kW)	Electrical Power (kW)
Low load	1.24	1.25	.75
Part Load	3.75	3.61	3.18
Full Load	8.95	8.65	8.5

The electrical power of the system was measured at the loads based on the voltage and current draw of each heating element. The measured power at low load is the measured electrical power to energize the coil and does not include measured electrical power at the load bank of heating elements. Part load and full load include the power measured at the load bank and the coil energizing power. For each loading condition, three engine speeds were tested and kept constant. The throttle openings were limited to 10% for low load, 50% for part load, and wide open throttle for full load. The loads were measured at the point of stall for each condition. The electrical load was increased at each loading condition until stall. From Table 4.5, it is shown that the prototype produced a maximum of 8.5 kW of electrical power at full loading and high RPM conditions. Given that the generator has a proposed weight of 21 kg, the power density of the prototype range extender on gasoline is calculated at .405 kW/kg, it can be concluded that, in many scenarios, the generator's performance is sufficient to function as a hybrid generator or range extender.

4.3.4 Emissions Analysis

In this study, the exhaust emissions from the prototype generator were sampled and tested for the purpose of understanding engine emissions performance and combustion characteristics. An exhaust gas analyzer was incorporated in the exhaust stream to measure unburnt

hydrocarbons (HC), carbon monoxide (CO), carbon dioxide (CO_2), and oxides of nitrogen (NO_x). For comparison, all values are presented in units of grams per kilowatt hour (g/kW-h).

Unburnt Hydrocarbons

Figure 4.8 shows the HC emissions for different loading conditions and operating RPMs. From Figure 4.8, The results indicate that HC emissions are reduced considerably with an increase in engine RPM. Further, HC emissions decrease with an increase in engine load.

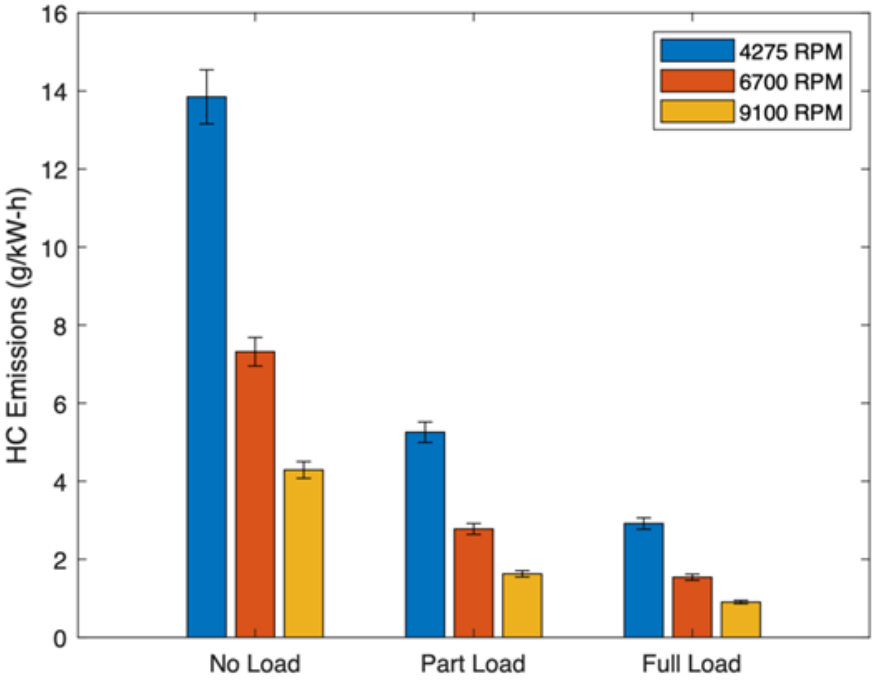

Figure 4.8: *Unburnt Hydrocarbon Emissions*

In two-stroke engines, HC emissions are arguably the most concerning emissions species. In a crankcase compression two-stroke engine, such as the engine KT-100, a significant amount of the fuel may short-circuit during the scavenging and blowdown process resulting in fresh charge escaping through the exhaust port. Fuel short-circuiting in two-stroke engines refers to the tendency for a portion of the fuel/air charge to escape through the exhaust port during the scavenging phase after exhaust blowdown [92]. This happens because, in a two-stroke when the

piston is at BTC, the transfer port and exhaust port are open at the same time. A substantial portion of the measured HC emissions are likely a result of fresh fuel-air escaping through the exhaust port during the scavenging phase. Additionally, there are often regions in the combustion chamber where fuel can be trapped during the normal combustion process and escape burning [92]. These effects are greatly exaggerated under light load operation when conditions for combustion are poor and when flame propagation may be incomplete and under low engine speed operation when port timing is not optimized to prevent short-circuiting events from dominating. The effect of the foregoing is apparent in the HC emissions measured during operation, where peak HC emissions occurred at low load/low rpm operation. It can be seen that as engine RPM and loading increase, the concentration of HC decreases. The concentration of HC emissions is the highest at low load, low speed operation where the gas exchange is the least efficient. This is likely because, under these conditions, the portion of the fuel that is subject to short-circuiting is the highest. Unburnt hydrocarbon emissions are also influenced by incomplete combustion. When the fuel is not completely consumed during the combustion event, it is emitted at HC emissions [74]. Incomplete combustion often occurs at lower loads, smaller throttle openings, and lower engine speeds as a result of lower in-cylinder and combustion temperatures. In a two-stroke engine, the larger concentration of trapped exhaust gases at lower engine speeds and loading conditions can lower combustion temperatures and promote incomplete combustion. As loading and engine speed increase, the combustion temperatures increase which decreases the occurrence of incomplete combustion. As a result, the concentration of unburnt fuel decreases.

In addition, a potentially significant component of HC emissions in crankcase-scavenged two-stroke engines is the lubricating oil mixed that is mixed with the fuel. At lower engine

speeds and loads, the lubricating oil carried by the scavenged air stream may escape the cylinder unburned and be exhausted. At higher loading, a substantially larger portion of the lubricating oil is combusted resulting in a decrease in HC emissions with increasing loading and engine speed [74]. Overall, a large portion of the HC emissions are generated from lubricating oil that is partially combusted and expelled from the exhaust; this exhausted oil is measured with and adds to the total concentration of HC emissions.

Carbon Monoxide

Figure 4.9 shows the CO emissions for different engine speeds and loading conditions. A similar trend can be observed to HC emissions, where CO concentration decreases with engine speed and loading conditions. However, the change in concentration is much less pronounced with the CO species in comparison to HC. In two-stroke engines, the gas exchange and therefore volumetric efficiency is linearly related to engine speed. As previously discussed, because the engine porting and timing is optimized for high RPM operation, low-speed gas exchange is relatively inefficient. The poor gas exchange at lower engine speeds results in a higher concentration of trapped exhaust gas from cycle to cycle [92-94]. It is likely that the higher concentration of diluent species lowers combustion temperature and increases the likelihood of incomplete combustion. As engine speed is increased the gas exchange becomes more efficient and the concentration of diluents is lower resulting in more complete combustion [75]. At lower engine speeds and loading conditions, there can be areas of the cylinder wall that are locally cooler. These regions can cause locally rich conditions. The rich regions resulting from deviation from stoichiometric mixtures and poor trapping efficiency may contribute to the increase of CO emissions at lower loads and engine speeds as rich regions also promote incomplete combustion.

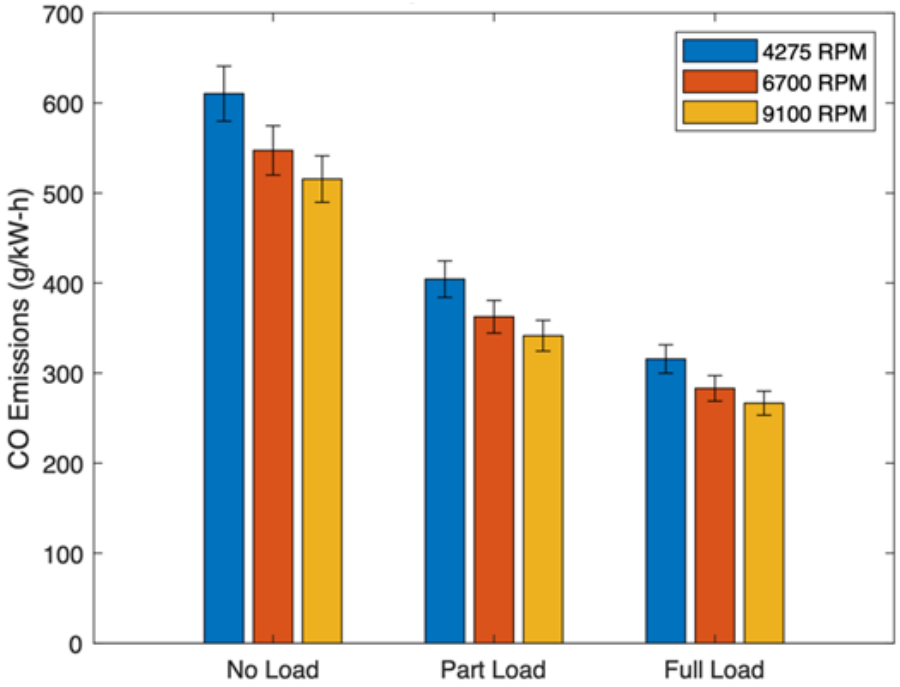

Figure 4.9: *Carbon Monoxide Emissions*

Carbon Dioxide

Figure 4.10 shows the relative amount of CO_2 from each loading condition and engine RPM. Similar to HC and CO, there is a decrease in the concentration of CO_2 emissions with increasing engine speed, but in contrast, there is a relatively constant concentration of CO_2 across different loading conditions. In general, the concentration of CO_2 increases as the A/F ratio approaches stoichiometric conditions, while fuel-rich mixtures show a decrease in CO_2 emissions [76]. The Walbro carburetor used in this work operates with a low-speed and high-speed jet. To prevent the engine from overheating during high power operation, the high-speed jet was set slightly richer than the low-speed jet. The extra fuel from the rich conditions helps to control engine temperatures by increasing the latent heat of vaporization of the fuel in the

combustion chamber. As engine RPM increased, the engine transitioned from the close to stoichiometric low speed jet to the fuel-rich high-speed jet. As the fuel/air mixture is richened, there is a noticeable decrease in CO_2 concentration. The fuel-rich conditions likely result in incomplete combustion and limit the formation of CO_2.

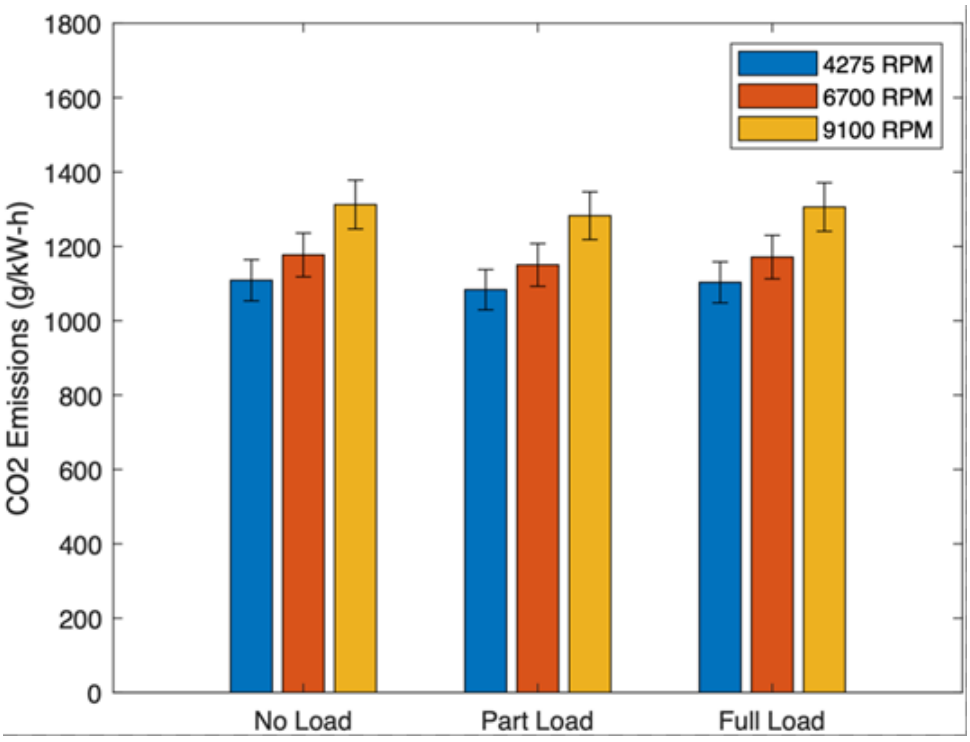

Figure 4.10: *Carbon Dioxide Emissions*

Oxides of Nitrogen

Figure 4.11 shows the relative amounts of NO_x emissions present during the operation of the generator. Unlike the previous species, NO_x shows an increasing concentration with an increase in engine speed and loading. In some aspects, NO_x formation is a function of cylinder temperature. Further, the formation of nitrogen emissions generally follows the Zel'dovich mechanism which posits that the reaction rate and resulting concentration of NO_x is a function of

engine temperature [117]. Generally, at higher loads and power outputs, there is an increase in combustion temperature [92-94]. This increase in combustion temperature likely encourages the formation of NO_x. It is therefore reasonable to expect an increase in NO_x emissions as engine RPM and loading increase, as shown by Figure 4.11 Additionally, extensive data from four-stroke SI engines has established that other critical engine variables that affect NO_x emissions are the amount of burned gas in the in-cylinder mixture of fuel and air, residual gas such as EGR, and relative air/fuel ratio [92,95]. As discussed, in a two-stroke engine, as engine load and RPM decrease, the cylinder filling efficiency and gas exchange rate also decrease. As a result, there is a higher concentration of burned residual gas in the combustion chamber that dilutes the fuel charge and lowers flame temperature. This natural EGR effect may influence the decrease in NO_x emissions at lower engine loading and RPM.

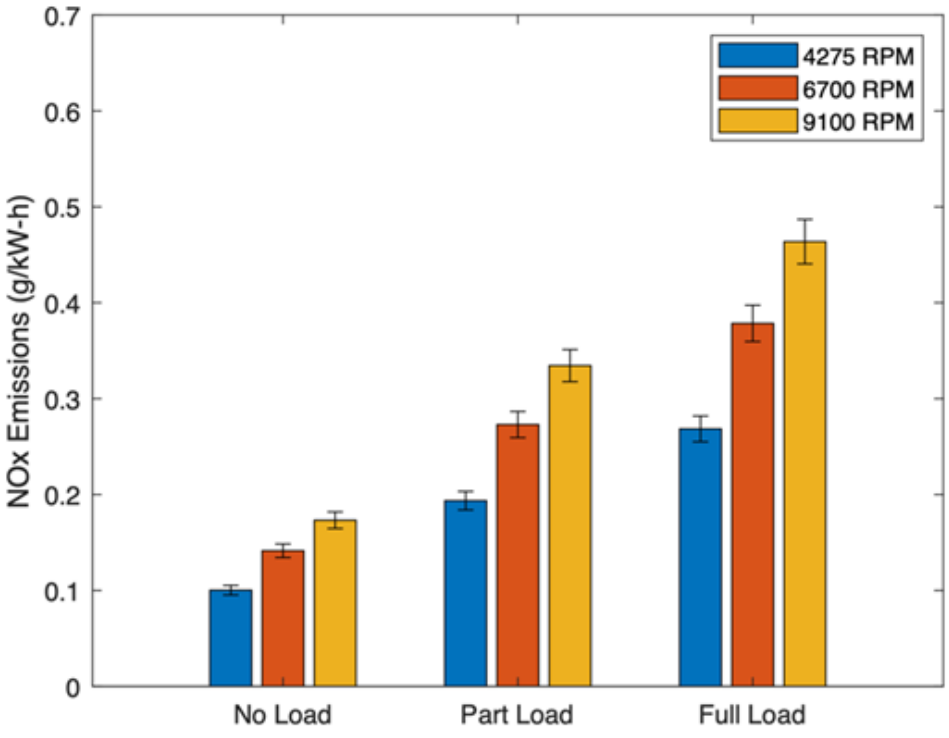

Figure 4.11: *Oxides of Nitrogen Emissions*

4.4 Conclusions

The high-performance portable generator that has the potential to function as a range extender for an EV or a component in a hybrid powertrain that was designed in Chapter 3 was tested in this chapter. The test of the design was intended to characterize the combustion, performance, and emissions, as well as to evaluate the viability of the generator. It was found that the prototype generator produced 8.5 kW of electrical power while having a weight of only 21 kg. As a result, the generator yields sufficient power density to function in the intended functions. It was found that the thermal efficiency, mechanical efficiency, and power output of the generator increased with increasing RPM, most likely as a result of the state of tune of the engine. Further, the generator demonstrated a reduction in HC and CO emissions with increasing load. However, as load increases, there is an increase in NO_x emissions. It was shown that the generator may be suitable for the intended applications but may be hamstrung because of the high overall emissions. In the next chapter, methods to reduce emissions and increase performance are investigated.

CHAPTER 5: Experimental Validation: METHANOL

5.1 Introduction

As the automotive industry continues to move toward electrification, the increased cost and limited vehicle range EVs and hybrid vehicles continue to burden consumers. In some countries, the future sales of internal combustion engine-based vehicles have been restricted. While electric vehicles and hybrid vehicles have certain benefits related to sustainability, they also have disadvantages. A novel high power density electric generator that can function as a range extender for EVs or as a component in a series hybrid powertrain has been presented in previous chapters of this dissertation. In previous chapters, the prototype was designed, constructed, and evaluated. Because of the high specific power demonstrated by the prototype, it may have the potential to fill a not yet met vacancy in the state of the art. The generator is particularly useful in scenarios where high specific power, portability, compactness, and small size are appreciated. For example, the prototype generator of this dissertation may be incorporated as a portable EV range extender, as a component in a UAV or drone powertrain, or as a component in a series hybrid powertrain where power density is critical, such as in motorcycles, ATVs, dirt bikes, small vehicles, ultralight aircraft, or marine applications [118-119]

One of the key components to the high power density of the generator presented in this dissertation is the two-stroke engine. The two-stroke engine is able to accomplish a combustion cycle in only one revolution of the crankshaft. The simplicity of the two-stroke allows it to be cheaper, lighter, and more power-dense than four-stroke engines. Although it is almost never the case, from a theoretical standpoint, two-stroke engines are inherently more efficient than four-

stroke engines because they do not have the friction and heat losses associated with non-power strokes, or parasitic pumping losses from the valve train [120]. Most importantly, the increased specific power of the two-stroke is the main advantage over four-stroke engines. The high specific power of the engine used in the prototype contributed to the overall power density of the prototype.

However, in some aspects, the use of two-stroke engines is controversial because of their high emissions [121]. Two-stroke engines can emit higher levels of unburnt hydrocarbons and carbon monoxide when compared to four-stroke engines. Even a small handheld two-stroke engine can emit more specific pollution than four-stroke automobile engines [123-124]. On larger engines, emissions control can be accomplished, for example, by lean burn control schemes, catalytic converters, exhaust gas recirculation, lean burn technology, fuel injection, and selective catalytic reduction. Although the emissions of two-stroke engines can be improved through these means, the incorporation of such would increase the cost, weight, and complexity and decrease the reliability of the engine [92, 125]. Clearly, the incorporation of these technologies would decrease the advantages provided by the engines and thus are not an option. Further, these solutions provide limited usefulness when applied to smaller engines [126-127]

The reduction of carbon emissions is vital for the viability and continued use of two-stroke engines. Without the availability of large scale emissions reduction methods, other strategies must be explored. Moreover, methods such as fuel injection, catalytic converters, and exhaust after treatment are otherwise impractical for use with small engines. The use of alternative fuels has been shown to be a promising solution to reducing carbon emissions in automobile engines. The use of alternative fuels does not require major overhauls to the engine architecture to achieve emissions reduction [128-129]. Many types of alternative fuels have been

presented as replacements for gasoline, including for example compressed natural gas (CNG), liquefied petroleum gas (LPG), ethanol, and hydrogen [130-132]. While these fuels are promising, there is a vacancy in the state of the art for the evaluation of performance and emissions reduction on small scale two-stroke engines. Moreover, there exists a vacancy in the state of the art for high power density generators that operate on renewable fuel. The work in the following chapter details the adaptation of the generator to function on methanol fuel. In addition, the performance and emissions characteristics of methanol combustion are examined.

5.2 Methanol Fuel

5.2.1 Methanol as a Fuel

Methanol was chosen for use as an alternative fuel for the engine in pursuit of lowering emissions and potentially increasing performance. Methanol (CH_3OH) is a simple oxygenated hydrocarbon that is among the top five most widely traded chemicals in the world and is an attractive option as a fuel for use in internal combustion engines for a variety of reasons [133]. The scalability of methanol is one of the main advantages of methanol as a fuel. The efficiency at which methanol can be synthesized coupled with its viability for use in an internal combustion engine make methanol a promising candidate [134-135]. Most internal combustion engines can be readily adapted to operate on methanol. In addition, methanol is a liquid fuel and is relatively safe to store and dispense [136]. Thus, it would require little modification of existing fuel station infrastructure to provide methanol fuel. In general, methanol also has the potential to offer increased thermal efficiency and increased power output than gasoline [137]. Methanol has many desirable attributes in view of its use as a fuel, such as high heat of vaporization or latent heat, low stoichiometric fuel/air ratio (6.42:1 as compared to 14:7:1 for gasoline), higher laminar

flame speed, high molar expansion ratio, low combustion temperature, and high hydrogen-to-carbon ratio [138-140]. However, the energy density of methanol compared to gasoline is much lower (43.4 MJ/kg for gasoline and 20.1 MJ/kg for methanol). Methanol also has a lower in-cylinder combustion rate than gasoline [137]. The properties of methanol make it a highly desirable fuel for use in internal combustion engines. Methanol is an alcohol and is a colorless flammable liquid. One attribute in particular associated with methanol that makes it an excellent candidate for use as an internal combustion engine fuel is its high octane rating (109 RON) [141]. Methanol has a superior octane rating when compared to gasoline and exhibits a greater heat of vaporization [141-142]. As a result, methanol is a suitable fuel for high compression high output engines because the higher-octane rating permits a significant increase in compression ratio while the high latent heat of vaporization cools the combustion chamber which together increases the volumetric and thermodynamic efficiency and power output of the engine [143]. Notably, methanol has a lower volumetric energy density than gasoline or diesel [143].

In some aspects, methanol can be considered a net carbon zero fuel or "E-fuel." Although methanol is traditionally produced from fossil fuels, it can be produced from biomass, such as wood, biomass, organic waste, or other organic sources that remove carbon from the atmosphere, or man-made carbon-capturing techniques that actively remove carbon from the atmosphere [144]. When methanol is produced from organic material or from carbon-capturing techniques, it is often referred to as "bio-methanol" or "e-methanol" [145]. Bio-methanol is chemically identical to the methanol produced from fossil fuels and can function as an internal combustion engine fuel in a similar way [146]. Bio-methanol has been shown to give rise to significantly lower greenhouse gas emissions during its lifecycle than fossil fuels [147-150]. The increase in popularity of bio-methanol is a direct result of efforts to decrease emissions from internal

combustion engines. The production of methanol from biomass or carbon-capturing techniques does not involve experimental technology and can be commercially available. Further, the sources used to produce bio-methanol are generally considered to be sustainable and readily available [151].

The energy required to synthesize methanol can be sourced from either fossil fuel based sources or renewable sources. For example, the energy required for the hydrogenation of methane during methanol synthesis can be sourced from a renewable energy source, such as wind or solar [152]. In an example aspect, methanol could be created by sourcing carbon from renewable biomass or by absorbing carbon from the atmosphere. The energy required to synthesize the methanol could be sourced from green energy. The carbon that is released from combustion would be roughly equivalent to the carbon absorbed during methanol synthesis and would not include the release of sequestered carbon [152]. Therefore, the use of methanol can in many aspects be a net zero carbon fuel. Methanol was chosen for use as an alternative fuel in the following work. It should be noted that the castor premix oil that was mixed with the methanol fuel is a vegetable oil pressed from castor beans and is biodegradable and renewable.

One important consideration with methanol as a fuel is methanol's toxicity and the potential for toxic exhaust emissions. Although there are toxic exhaust emissions associated with petroleum combustion, methanol combustion can introduce toxic exhaust emissions species that are not associated with conventional fuel. Amongst these, formaldehyde and formic acid are most notable. Both formaldehyde and formic acid can be formed at very low concentrations as a product of incomplete combustion of methanol [152]. Formaldehyde can interact with molecules on cell membranes and in body tissue and fluid, such as proteins and DNA. High concentrations of formaldehyde can result in cell death. Importantly, it should be noted that methanol

experiences less incomplete combustion than conventional fuels and that an individual would have to inhale a substantial about of methanol exhaust to be damaging. Moreover, methanol itself is a highly toxic substance and should be handled carefully. Methanol can be toxic if inhaled or ingested and has a potentially lethal dose of 1 gram per kilogram of bodyweight. The same products of incomplete combustion are formed in the body when methanol is ingested which can cause blindless and cellular death. The hazards associated with methanol can be reduced or eliminated with proper combustion chamber design, exhaust aftertreatment, and fuel injection schemes to lower toxic methanol emissions as well as safe storage and transport of methanol fuel to lower methanol exposure.

5.2.2 KT-100 Methanol Conversion

There were several modifications that had to be made to the engine to convert it from gasoline combustion to methanol combustion. The differences between alcohol fuel and hydrocarbon fuels are such that the fueling and ignition schemes for both are incompatible. As a first matter, the engine was completely disassembled for inspection after the gasoline experiments and cleaned. On a two-stroke crankcase scavenged engine, residual gas and oil can linger in the crankcase, which could potentially interfere with the methanol data. The engine was cleaned and reassembled. The gas tank and fuel lines were similarly drained and flushed with methanol to ensure no cross-contamination of fuels.

The major step to convert the engine was replacing the Walboro carburetor with a methanol carburetor. In its stock configuration, the Walboro carburetor is not sufficient for methanol operation. Because stochiometric methanol combustion requires a richer A/F ratio (6.46:1 as compared to 14.7:1 for gasoline), the carburetor must feed more fuel to the engine

than the Walboro operable on gasoline. The Walboro carburetor is not suitable for this for because of at least two reasons: the diaphragm lacks the capacity to move the fuel from the tank to the engine, and the jets are not large enough to provide the proper fuel flow. In lieu of modifying the Walboro, a carburetor configured for methanol operation was sourced and installed. A small spacer was made to adapt the carburetor to the engine intake.

The Buller Atomizer carburetor, made by Buller Race Engines, is commonly used in kart racing and other applications for methanol engines [153]. The Buller Atomizer carburetor is similar in function and design to the Walboro but is structured for methanol fuel. The Atomizer is a bolt on replacement for the stock carburetor and works with the existing controls. The Atomizer has a dual-stage diaphragm pump, increased pilot and main jet dimensions, and a larger venturi with a more exaggerated vacuum. According to their website, “This alcohol carb begins as a WB3A but has the entire venturi area machined out and a CNC machined insert installed. The insert atomizes the alcohol with 10 equally placed outlets around the venturi.” [153]. Figure 5.1 is an image of the Bullet Atomizer carburetor.

Figure 5.1: *Image of Buller Atomizer Methanol Carburetor* [153]

In addition to the carburetor, the sparkplug was exchanged with a colder heat range plug which had a recessed electrode to prevent detonation, as is commonly recommended with methanol kart engines. The spark plug was upgraded from an NGK BR9EIX to an NGK BU8H model. Methanol engines require spark plugs with lower heat ranges to prevent pre-ignition, larger electrode diameters to produce a more reliable spark, and recessed electrodes and grounds in case engine compression is increased. The methanol plug is also adapted to withstand the corrosive effects of methanol fuel. In general, alcohol fuels, such as methanol as used in this work, have more ignition delay than gasoline. Often, the ignition on alcohol engines is advanced to account for the greater ignition delay. For this application, the ignition timing was advanced by two degrees from gasoline settings [95]. Importantly, the type of oil had to be changed for methanol operation. During gasoline operation, a synthetic petroleum based two-stroke premix oil was used. Because alcohol fuels are hygroscopic and highly polar, petroleum two-stroke

premix oils are not miscible in alcohol fuels and therefore are incompatible; petroleum based two-stroke premix oils can cause lubrication failures in alcohol engines. Therefore, the methanol fuel was mixed with a castor based two-stroke premix oil. Castor based two-stroke oils are bio-based oils that come from castor bean plants and are miscible in gasoline and alcohol fuels. The highly polar fatty acids of castor oils readily form hydrogen bonds with and are dissolved by the polar OH groups in alcohols [95]. These castor based oils often comprise fatty triglycerides, specifically triester of glycerol and ricinoleic acid, and are characterized by their excellent film strength and lubricity. Castor oils, such as the Klotz BeNol used in this work, are excellent lubricating oils and have a higher wetting ability than synthetic, petroleum, or ester-based oils. Moreover, Castor oils have an increased tendency to migrate toward locally hotter areas of the cylinder and in many cases provide enhanced lubrication over other oil types [95]. Castor oils are not as widely used as synthetic oils because they tend to leave carbon deposits behind. This carbon formation is a result of low engine temperatures and poor oil mitigation. Carbon buildup that results from oil residue is problematic for two-stroke engines that incorporate power valves. The KT-100 is a good candidate for castor oils because of its higher operating temperature which results from air cooling, and because it does not have a power valve [95].

After the engine was configured with methanol equipment, it was re-tuned to realize optimal performance. The same tuning procedures that were used in the preceding chapters were repeated with the methanol setup. However, the tuning parameters were slightly different with methanol. As a first matter, the low speed needle was tuned fuel lean to promote easy starting. Alcohol fuels can tend to foul plugs and can be hard to start with fuel rich conditions at low speeds. The high speed needle was set fuel rich to prevent overheating. The extra fuel at higher loads and RPMs can prevent overheating due to the increased latent heat cooling effects. With

the engine converted and tuned for methanol, the investigation of methanol as an alternative fuel could begin. Figure 5.2 is a collage of the methanol conversion on the engine during the tuning process.

Figure 5.2: *Methanol Conversion Collage*

5.3 Experimental Procedure

The prototype was prepared on the test stand for experimentation and performance testing. A series of heating elements, who's current and voltage could be measured, were adapted to provide a constant load to the engine. To simulate this operational load, these electric heating elements were connected to the generator. Large iron castings were placed on the heaters to absorb the heat produced to ensure they could continuously provide load to the engine. The

electrical power was measured at the generator. To cool the engine, an industrial blower was mounted adjacent to the engine to force air across the air fins of the cylinder and cylinder head.

The system was instrumented to record the parameters of the engine and dynamo during operation. K-type thermocouples were installed on the cylinder head and exhaust to measure temperatures. The Bosch mass airflow sensor was included in the intake to measure air mass flow rate. The cylinder head was modified to accept the Kistler model 6052A piezoelectric pressure sensor to monitor the in-cylinder pressure. An Infrared Industries FGA 4000XDS exhaust gas analyzer was used in the exhaust stream. The exhaust analyzer used NDIR (non-dispersive infrared) to measure HC, CO, and CO_2 species. The analyzer also used an electrochemical cell to measure the NO_x emissions with a 1% full-scale accuracy. An ATO digital rotary in-line dynamic torque sensor was installed between the engine and dynamo to measure brake power, torque, and engine speed in rpm. Data from each sensor was collected with a bespoke LabVIEW program; the program was used to record the data and synchronize the signals. The collected data was post-processed and analyzed with MATLAB. The system delivers reliable measurement results with an error of less than 5% based on the least accurate instrument. A series of experiments were conducted at varying engine speeds and throttle conditions. Each experiment at each condition was repeated five times to evaluate repeatability and eliminate errors.

The loading was provided by the heating element connected to the dynamo. For all the discussions below, full load is defined as the maximum electrical power measured before the engine stalls. Low load is defined as the electrical power consumed to energize the coils and measured only while freewheeling the generator with no electrical load connected. The low load power is kept constant between the RPMs tested. Part load is approximately in the middle

between low load and full load. The engine speeds were kept constant and throttle openings were limited to up to 10% for low load, up to 50% for part load, and wide open throttle for full load. The loads were measured at the point of stall for each condition. There are some variations in the low load and part load as the generator does not allow for very fine control of loading. Low load, part load, and full load loading condition experiments were conducted at three discrete and constant RPMs, while the data was recorded. The load power is the power at each loading condition measured at the load bank. Table 5.1 describes the loading conditions during testing.

Table 5.1: *Loading Conditions During Testing*

Loading Condition	RPM	Load Power (kW)
Low load	4250	.78
	6700	
	9100	
Part Load	4250	1.88
	6700	3.02
	9100	6.12
Full Load	4250	4.34
	6700	5.98
	9100	9.80

5.4 Results and Discussion

5.4.1 Brake Power & Torque Analysis

The dynamic torque sensor which was configured to measure brake torque and brake power was installed in between the engine and the dynamo allowing the brake power produced by the engine to be measured. The torque sensor was coupled to the engine via the Lovejoy coupling and to the dynamo via the drive belt. Figure 5.3 shows the brake power measured at the crankshaft at three discrete engine speeds at low load, part load, and full load.

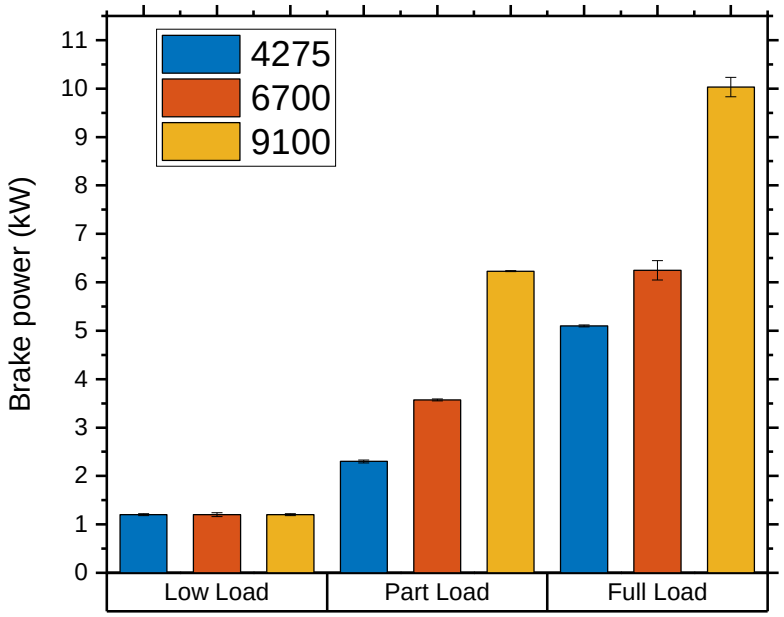

Figure 5.3: *Brake Power at Varying Loads and Engine Speeds*

From Figure 5.3, It can be seen that brake power is relatively constant at low loads at various engine speeds. At low loads, the engine is only producing enough power to rotate the assembly and energize the coils of the dynamo. As loading increases, the brake power produced by the engine shows an increase at each engine speed. At full load conditions, engine speed has a profound effect on increasing engine power. Further, the highest brake power can be observed at full throttle, which is full engine RPM, and full load conditions. It is theorized that friction and throttling losses are predominant at lower engine speeds. Moreover, it is likely that at low load high-speed operations, mechanical and pumping losses dramatically affect the brake power produced by the engine. In a two-stroke engine, there is a dramatic increase in volumetric efficiency with increasing engine speed, which can explain the sharp increase in brake power with increased engine RPM [92-94].

In another aspect, and as previously discussed in Chapter 4, the port timing and duration likely have a profound effect on the performance of the prototype at different engine speeds. Because the KT-100 is a piston port two-stroke, the port timing, duration, and shape are limited to being optimized in a narrower range of operating speeds. Because of the limited tuning window and in view of the KT-100 being a competition engine, the porting is tuned for high RPM efficiency and high RPM output. This is an advantage for high RPM operation and a disadvantage for low RPM operation. The brake power measurements in Figure 5.3 reflect the state of tune of the engine; it can be seen that the engine produces more peak power at higher engine speeds.

When compared to gasoline operation, the engine on methanol produced greater power throughout each loading condition. More specifically, through the use of methanol fuel, peak power was increased from 8.5 kW to 9.8 kW, which is an observed 15.3% more peak power at full-throttle operation. Even though methanol has a lower energy density than gasoline, its operating air/fuel ratio is much lower. As a result, there is much more methanol in the fuel charge, and therefore the total energy of the fuel charge can be greater. The higher heat of vaporization can increase the density of the incoming air charge [135]. In addition, the extra oxygen that is introduced by the fuel can increase power. The engine may also be producing more power as a result of greater ignition advance. In addition, the premix oil used during methanol operation was castor-based, which unlike the synthetic premix oil used during gasoline operation, contributes a measurable amount of energy to the combustion event [92-94].

Figure 5.4 shows the brake torque produced by the engine measured at the torque sensor. Because power is a function of torque and engine speed, the torque produced at each discrete loading condition and engine speed is related to the power at each loading condition and engine

speed. More specifically, because loading is fixed, and power is a function of torque and RPM, as RPM increases at a fixed loading condition the torque decreases and power increases. It can be observed that maximum torque occurs at full load and low engine speeds where engine efficiency is the greatest. Because the engine was power limited, and power is a function of torque and RPM, maximum torque occurs at full throttle at the lowest engine speed.

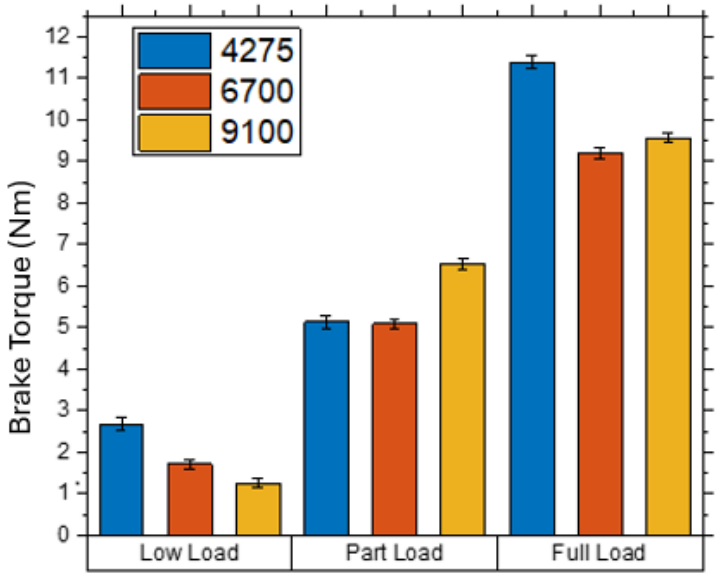

Figure 5.4: *Brake Torque at Varying Loads and Engine Speeds*

The torque produced increases with engine speed for likely the same reason power increases with engine speed. As the engine speed is increased, the volumetric efficiency increases and the fuel charge dilution decreases [92-94]. Unlike other engine architectures which can use valves or forced induction, two-stroke engines rely heavily on the momentum of the incoming fuel/air charge to breathe. As a result, two-stroke engines benefit from high RPM operation and generally produce greater power and torque at higher RPM operation. Further, there is a decrease in throttling losses as the loading is increased which results. The port timing

and duration also could affect the brake torque. As stated, because the port timing and duration are optimized for high engine speed operation, the increase in gas exchange efficiency at higher engine speed could contribute to the increased torque at higher engine speeds.

When compared to gasoline operation, the prototype when operated on methanol produced greater torque across each loading condition. Specifically, the engine operable on methanol produced 21.7% more peak torque than the engine operable on gasoline. Similarly to gasoline, the increase in torque is likely a result of the higher total energy in the combustion charge with methanol combustion, resulting in slightly higher BMEP. Similarly to peak power, the advanced ignition timing likely increased peak torque. The castor oil necessary for methanol operation also adds a small but measurable amount of energy to the combustion event, whereas the synthetic oil used during gasoline experimentation does not [98].

5.4.2 In-Cylinder Pressure

The cylinder head of the engine was machined to accept an in-cylinder pressure transducer to provide the transient combustion pressure measurements during the operation of the engine. Because two-stroke engines do not require valves in the cylinder head, the pressure sensor could be ideally placed proximal to the spark plug. The data collected was synced to the crankshaft position of the engine to provide pressure data as a function of crank angle.

Figure 5.5 shows the in-cylinder combustion pressure vs. crank angle at three discrete loading conditions. From Figure 5.5, it is clear that as the load increases, the peak in-cylinder pressure increases with each loading condition. In addition, there is an increase in in-cylinder pressure at each loading condition as RPM increases. However, there is a greater increase in in-cylinder pressure from low load to part load than from part load to full load. There is likewise a

greater increase in in-cylinder pressure at each loading condition from 4250 RPM to 6700 RPM than from 6700 RPM to 9100 RPM. The greater increase in in-cylinder pressure at lower engine speeds and loading is likely because in a two-stroke engine, at lower engine speeds, the cylinder filling efficiency and blowdown phase efficiency are low resulting in a higher concentration of diluent exhaust species remaining in the combustion chamber from cycle to cycle [92-94]. Moreover, because the port timing and duration are not optimized for low engine speed operation, the scavenging efficiency is lower at low engine speeds which results in higher levels of trapped exhaust gas in the combustion chamber [92-94].

More generally, at lower engine speeds and partial throttle openings, there is a greater concentration of exhaust gas that remains trapped in the cylinder from cycle to cycle. The high concentration of trapped exhaust gas can lower the in-cylinder pressure rise. As engine speed and throttle openings increase, there is a dramatic increase in-cylinder filling and blowdown efficiency, in part due to the port timing and duration being optimized at these conditions. As a result, there is a lower concentration of diluent species at higher RPM operation. Moreover, at higher engine speeds, the effects of charge dilution are lower. The lower concentration of diluents can result in higher peak pressure and pressure rise.

It is also observed that, for each loading condition, the in-cylinder pressure curve for 4275 RPM is more gradual and exhibits less of a peak than that of 6700 RPM and 9100 RPM. Again, this is likely the result of high concentrations of exhaust gas at lower engine RPMs as a result of poor gas exchange at low engine speeds. The greater concentrations of diluent exhaust gas can encourage the in-cylinder pressure rise to be more gradual [30].

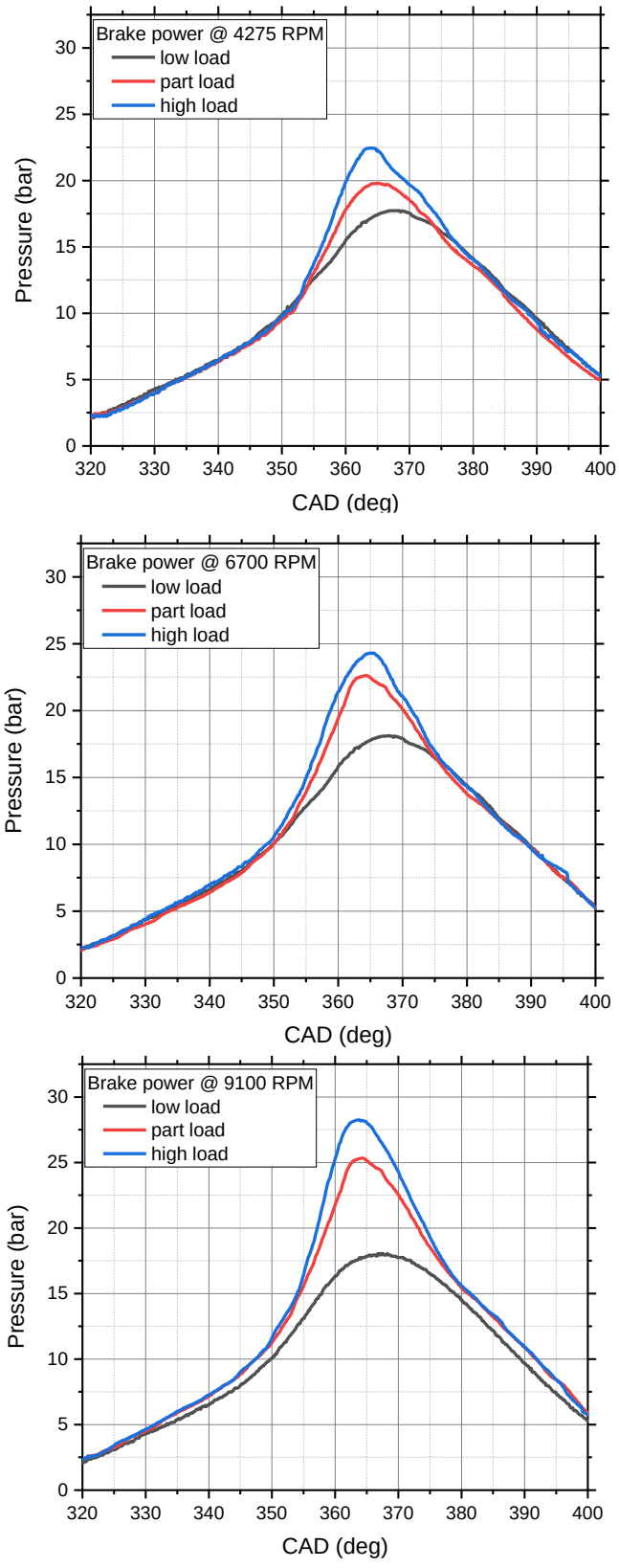

Figure 5.5: *In-Cylinder Pressure Comparison*

When compared to gasoline operation, there is a more pronounced rise in peak pressure from part load to full load. In addition, the peak pressure values for methanol operation are slightly higher than for gasoline operation. Methanol can operate at much lower air/fuel ratios than gasoline. In other words, a larger quantity of fuel can be combusted during the combustion event. Despite its lower energy density, the methanol fuel charge can contain a higher total energy and produce a greater pressure rise [135]. More generally, methanol and gasoline experience similar pressure curves. Further, methanol experiences a slightly earlier peak pressure during the stroke for each loading condition and RPM when compared to gasoline. This is likely a result of the timing being advanced slightly more than what is required to compensate for the slower burning rate and ignition delay.

The data collected from the in-cylinder pressure measurements was next used to calculate the heat release rate (HRR) of the methanol fuel. The heat release rate is an important approach in examining the combustion process of an internal combustion engine. The HRR analysis provides valuable information on the combustion behavior that can affect fuel economy, engine performance, and emissions [154]. The HRR analysis can also provide a comparison of the combustion behavior of methanol and gasoline. A further understanding of methanol fuel performance and prototype performance was gathered by comparing the heat release rate to the crank angle. Moreover, by evaluating the evolution of heat release per unit of time, a more empirical view of combustion dynamics can be provided. In this chapter, the heat release rate was calculated by using the first law heat release model proposed by *Heywood* [70]. This model calculates the heat release rate from in-cylinder pressure based on the volume of the cylinder at varying crank angles. For these calculations, the contents of the combustion chamber are modeled as an ideal gas with R held constant. A constant specific heat ratio (γ) of 1.325 as

suggested by *Heywood* was used as the discrete values for γ during combustion are not well defined [70]. Equation 5.1 provides the heat release rate model.

$$\frac{dQ}{d\theta} = \frac{\gamma}{\gamma-1} P \frac{dV}{d\theta} + \frac{1}{\gamma-1} V \frac{dP}{d\theta} \qquad (5.1)$$

In a similar way to in-cylinder pressure, the heat release rate between the discrete loading conditions at varying RPMs was compared. Figure 8 shows the comparison between heat release rate at varying loading and RPM conditions.

From Figure 5.6, it can be seen that in general, the heat release rate increases with increased loading conditions. The heat release rate also increases with RPM at each loading condition. It is also observed that there is a larger increase in heat release rate from low load condition to part load condition and a more subtle increase in heat release rate from part load to full load condition, similar to in-cylinder pressure. In addition, the increase in HRR between 4275 RPM and 6700 RPM is more substantial than from 6700 RPM to 9100 RPM at each loading condition. The full load operating condition showed the greatest heat release rate.

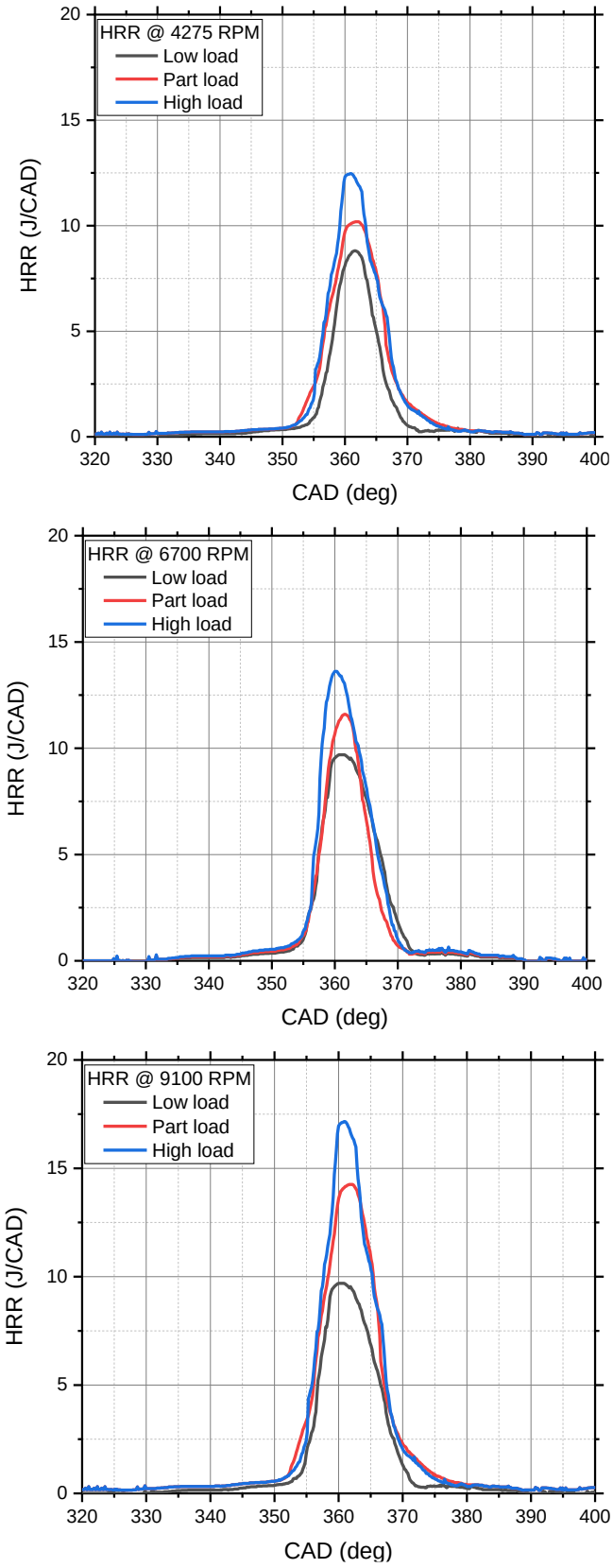

Figure 5.6: *Heat Release Rate Comparison*

The in-cylinder pressure is an important input variable when calculating the heat release rate. The parameters specific to the engine that affect in-cylinder pressure in essence likely affect the heat release rate. It is therefore theorized that differences in heat release rate are a result of the differences in gas exchange efficiencies at different loading and RPM operating conditions. In another aspect, the fuel burning rate may influence the measured HRR at each loading condition and RPM. In general, the fuel burning rate increases with increased in-cylinder turbulence [70]. The in-cylinder turbulence of the fuel charge in most engines increases with RPM. Two-stroke engines in particular experience highly turbulent flow at high RPMs because of fixed transfer port geometry [92-94]. The increase in HRR as engine speed increases may also be a result of increased turbulence.

When compared to gasoline operation, the engine on methanol exhibited a slightly higher peak heat release rate. This is likely a result of the extra oxygen (OH radicals) that participate in combustion. It has been shown that OH radicals are able to increase the reaction rate of premixed combustion [117]. In addition, methanol experiences a slightly earlier peak heat release rate than gasoline, a likely result of the advanced ignition timing. However, gasoline experienced a greater total heat release rate. It should be noted that the heat release rate of these fuels may be influenced in part by the premix oil and oil ratio used in the fuel; methanol fuel requires an alcohol-solvable castor-based oil which, unlike synthetic two-stroke oils, participates in the combustion event [92-94]. Methanol operation also requires slightly different jetting than gasoline, which could further influence the heat release rate [95]. Specifically, methanol engines must operate fuel-rich at high load high RPM conditions to prevent overheating. These rich operating conditions could affect the measured heat release rate. It was also found that methanol

experiences a slightly later peak in heat release rate in crank angle than gasoline, likely because of the slower combustion of methanol.

The cumulative heat release is the sum of the heat release rate throughout the cycle. Cumulative heat release generally represents the total heat generated inside the cylinder per cycle. Cumulative heat release is also an important parameter in providing a comparison between gasoline and methanol. The heat release rate data was used to calculate the cumulative heat release at the specified loading conditions.

Figure 5.7 shows the cumulative heat release rate results for different engine loads. From Figure 5.7, it is clear that a similar trend to heat release rate can be identified between loading conditions wherein the cumulative heat release increases with increasing loading conditions. What's more, there is a greater increase in cumulative heat release between low load and part load conditions than between part load and full load conditions, likely as a result of the reasons discussed above. In continuation, full load conditions exhibited the greatest cumulative heat release. When compared to gasoline operation, methanol showed slightly higher cumulative heat release, likely a result of the greater total energy content of the methanol fuel charge.

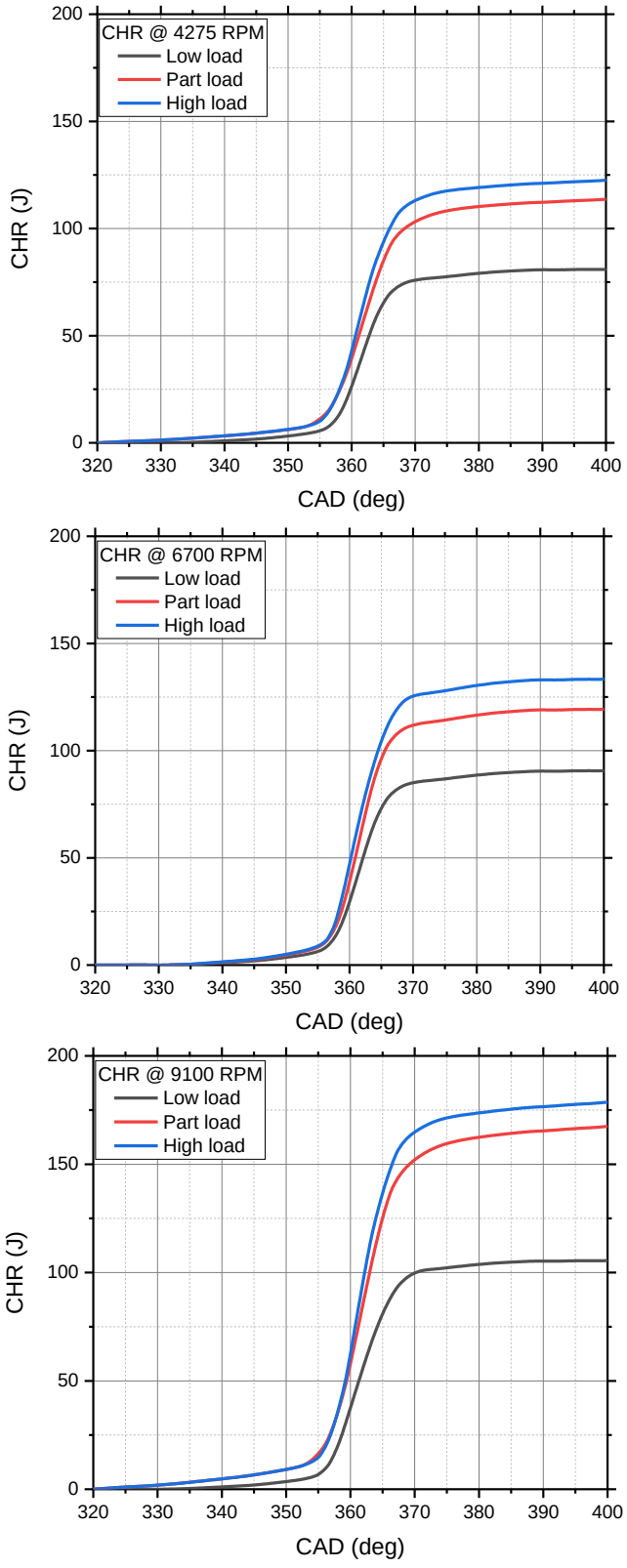

Figure 5.7: *Cumulative Heat Release Rate Comparison*

5.4.3 Efficiency Analysis

It is important to consider the thermal efficiency of the system to understand its overall effectiveness. Thermal efficiency is a reasonable way to understand a variety of efficiency parameters, such as fuel efficiency, mechanical conversion efficiency, etc. with one metric. Thermal efficiency can be defined as the ratio between work done to heat absorbed [27].

The indicated thermal efficiency was calculated from the pressure data taken from the in-cylinder pressure sensor. Indicated thermal efficiency is the ratio of indicated power to fuel power provided. Indicated thermal efficiency is important as it provides a measure of how well the engine converts the heat energy from fuel into mechanical work. Further, indicated thermal efficiency ignores the losses in the system and provides an idealized efficiency value. Table 5.2 displays the calculated indicated thermal efficiency of the engine. For this work, the thermal energy is defined in Equation 5.2 provided from *Heywood* [70].

$$n_{f,i} = \frac{W_{e,i}}{m_{f^*} Q_{LHV}} \quad (5.2)$$

Table 5.2: Calculated Indicated Thermal Efficiency

Loading	4275 RPM	6700 RPM	9100 RPM
Low load	9.99%	10.90%	11.45%
Part Load	11.75%	12.95%	13.09%
Full Load	12.14%	13.9%	16.81%

From Table 5.2, it can be seen that as RPM increases, the indicated thermal efficiency increases. Further, as loading increases, the indicated thermal efficiency also increases. In one aspect, the indicated efficiency can increase with increased RPM because there is less time for

heat transfer to take place. More heat transfer can lower the thermal efficiency of the engine because the heat energy is lost. Continuing, the engine is generally hotter at higher loading and RPM which can further limit heat transfer and increase thermal efficiency. It is important to note that the indicated thermal efficiency is an idealized value that calculates the work done inside the cylinder and does not account for various losses that are present in a real engine, such as friction, heat losses, and pumping and powertrain losses. Brake thermal efficiency is used to account for these losses and can provide an idea of the useful work, such as crankshaft work.

When compared to gasoline, the prototype experiences slightly lower indicated thermal efficiency. Specifically, the prototype experiences a roughly 20% decrease in peak indicated thermal efficiency. Methanol likely has a lower thermal efficiency for a few reasons. First, because the rate of combustion is lower for methanol, there is more time for heat transfer to take place, which results in more heat losses. Because methanol is a single-component fuel, water forms earlier during the combustion process [137]. Because water exists for a longer duration with methanol combustion than with gasoline, it can absorb more heat and lower the in-cylinder temperature and pressure rise. In addition, there are about 1.75 times as many moles of water per unit of energy in methanol combustion as in gasoline combustion; the extra water content when compared to gasoline can absorb heat and lower efficiency. It is likely that the combination of the increased concentration of water during the combustion event in addition with the water forming earlier during the combustion event may absorb more heat and lower the indicated thermal efficiency. The latent heat of methanol is about 3 times greater than gasoline [137]. The increased latent heat could further absorb some of the heat from the combustion event [137]. The engine was tuned richer during methanol combustion when compared to gasoline. *Heywood* suggests that fuel rich conditions, such as those present during methanol operation, can decrease

the combustion efficiency, and lower the indicated thermal efficiency [92]. The stock cylinder head was designed for gasoline combustion and is not optimized for methanol; it is likely the cylinder head design could have lowered combustion efficiency which could affect thermal efficiency. Methanol, as a result of being highly hygroscopic, could introduce water into the combustion process. The additional introduced water could lower indicated thermal efficiency. It is important to note that methanol fuel has a much higher octane than gasoline fuel [137]. The higher octane of methanol allows it to function in engines with much higher compression ratios than what would be possible with gasoline. If the compression ratio was increased, the indicated thermal efficiency would likely be increased above that of gasoline [137]. It should be further noted that utilizing liquid cooling may increase the indicated thermal efficiency because it can decrease the heat lost through the cylinder [94].

The brake thermal efficiency is the measured efficiency of the engine at the crankshaft. Brake thermal efficiency can be more useful in certain aspects because it indicates the mechanical efficiency of the engine. More generally, brake thermal efficiency takes into consideration the mechanical losses that burden the engine. The brake thermal efficiency is the ratio of brake power measured at the crankshaft to fuel power. Figure 5.8 lists the brake thermal efficiency of the prototype generator at varying loads and engine speeds (shown in RPM). For this work, the indicated thermal efficiency is defined in Equation 5.3 provided from *Heywood* [70].

$$n_{f,b} = \frac{W_{e,b}}{m_{f^*} Q_{LHV}} \quad (5.3)$$

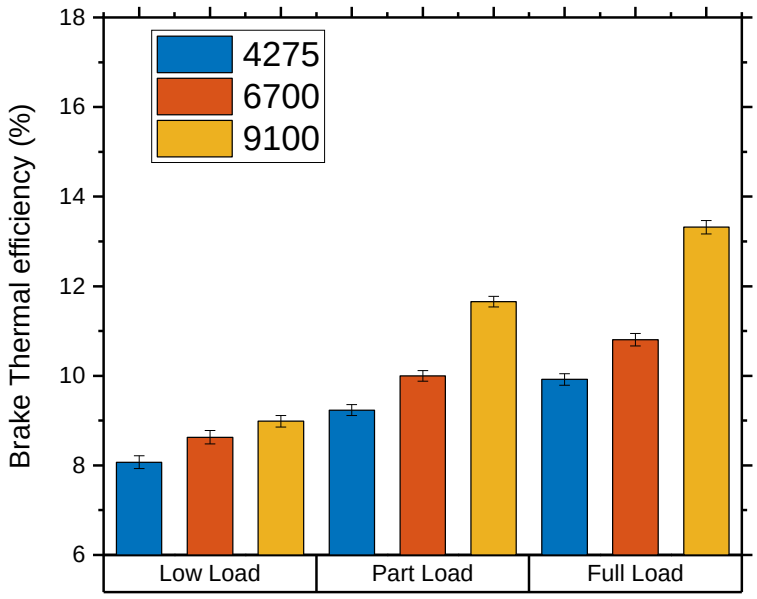

Figure 5.8: *Brake Thermal Efficiency Comparison*

From Figure 5.8, it is shown that similar to indicated efficiency, for each loading condition, as engine speed increases, the brake thermal efficiency increases. Further, the brake thermal efficiency increases with an increase in RPM. There is an increase in both indicated and thermal efficiency as both engine RPM and loading increase. In another aspect, as engine loading increases the difference between the brake thermal efficiency at increasing engine speed also increases; the difference between low load and full load efficiency at 9100 RPM is much more exaggerated than the difference between the same at 4275 RPM. The increase in brake thermal efficiency likely results from the same parameters that affect indicated thermal efficiency. The friction and mechanical losses that decrease brake thermal efficiency are generally constant across engine RPM [92].

When compared to other powertrains, the brake thermal efficiency is close to the indicated thermal efficiency as a result of few mechanical losses due to of the simplicity of the drive line. Without a complex drivetrain to introduce sources of mechanical loss, the generator

can minimize power lost to friction and maintain relatively higher brake thermal efficiency. Other tuning parameters encourage the efficiency of the engine to increase with engine speed and throttle opening, such as the port geometry, duration, and timing. Most two-stroke engines are tuned to operate most efficiently at a certain RPM range, and as the engine speed approaches this RPM, the efficiency increases [92-94]. Many two-stroke engines are also tuned to operate most efficiently at high RPM and wide-open throttle conditions [94]. As a result, their efficiency is the greatest in these conditions. In a steady-state application, such as the generator of this work, this can be a particular advantage. It should be noted that, similar to indicated thermal efficiency, the brake thermal efficiency could be increased by increasing the compression ratio [94].

Similarly to the indicated thermal efficiency, when compared to gasoline operation, the prototype operating on methanol experiences slightly lower brake thermal efficiency. Specifically, the prototype generator experienced 18% lower thermal efficiency on methanol. The decrease in brake thermal efficiency is a result of the same parameters that decrease indicated thermal efficiency. The brake thermal efficiency of methanol is lower than that of gasoline due to the properties of combustion of methanol. The slower combustion and extra water content as a byproduct of methanol combustion lower the combustion efficiency which affects thermal efficiency. Once again, it should be noted that, because of methanol's superior octane rating to gasoline, the thermal efficiency of the generator on methanol could likely be increased above that of gasoline by increasing the compression ratio. The generator could also experience an increase in indicated power and torque with further ignition advance. It is contemplated that the thermal efficiency could be increased with the introduction of water cooling, which would limit the heat lost to the air fins from a more constant operating temperature.

The mechanical efficiency of an engine is the ratio of brake power to indicated power. Mechanical efficiency is affected by the friction and pumping losses that reduce the useful work an engine can provide. The friction can result from the piston-to-cylinder interaction, bearing drag, and other friction introduced by various mechanical components. Table 5.3 calculates the mechanical efficiency of the engine at each loading condition in percentage (%). Equation 5.4 provides the mechanical efficiency.

$$n_{f,b} = \frac{n_{f,b}}{n_{f,i}} \quad (5.4)$$

Table 5.3: *Calculated Mechanical Efficiency in Percent (%)*

Loading	4275 RPM	6700 RPM	9100 RPM
Low load	89.1	92.4	94.0
Part Load	83.2	85.9	90.4
Full Load	83.3	86.3	89.6

Friction power depends largely on throttle position and engine speed. As the throttle is opened, fewer pumping losses occur. Friction increases as engine speed increases because friction is proportional to the square of engine speed. In addition, as engine power increases, the forces that act on the ring and piston can cause higher rubbing forces that result in more friction losses. It can be seen that mechanical efficiency increases with engine speed. This is likely because there are lower pumping losses. Mechanical efficiency also decreases with engine loading. This is likely a result of the higher combustion forces increasing the force that the ring and piston engage the cylinder wall with, which creates more friction [94]. Specifically, higher gas pressures can act on the ring through the ring end gap and force it to expand, which increases the normal force between the ring and the cylinder [92]. When compared to gasoline, there is a

slightly greater average mechanical efficiency of about 2.5%. This is likely a result of the extra lubricity of the oil; castor oils tend to have a higher film strength than petroleum-based oils which can reduce the friction between the piston and cylinder [94].

Considering the data from the power and efficiency analysis, it can be concluded that the generator should be operated at the highest possible engine speed during operation. The engine is capable of engine speeds of more than 16,000 RPM. However, such high engine speeds were not explored as they showed negligible increase in efficiency and an increase in undesirable noise, harshness, and vibration (NHV).

In addition to evaluating the engine efficiency, the dynamo efficiency was analyzed. Similarly to in Chapter 4, The efficiency of the dynamo can be calculated by comparing the output power supplied to the dynamo to the electrical power produced. Higher dynamo efficiency means that there is less wasted energy and more available power to the application. The dynamo efficiency can also be called conversion efficiency as it is a measure of how efficiently the dynamo can convert mechanical power into electrical power. Specifically, the dynamo efficiency is the ratio of mechanical power supplied to electrical power produced. The efficiency of the dynamo was calculated and plotted as a function of efficiency vs output power. It should be noted that the electrical efficiency is shown as a curve because the dynamo efficiency is constant across engine loading. It should also be noted that the dynamo efficiency is unchanged from what was measured in Chapter 4 because the only modifications were to the engine. Figure 5.9 shows the measured dynamo efficiency.

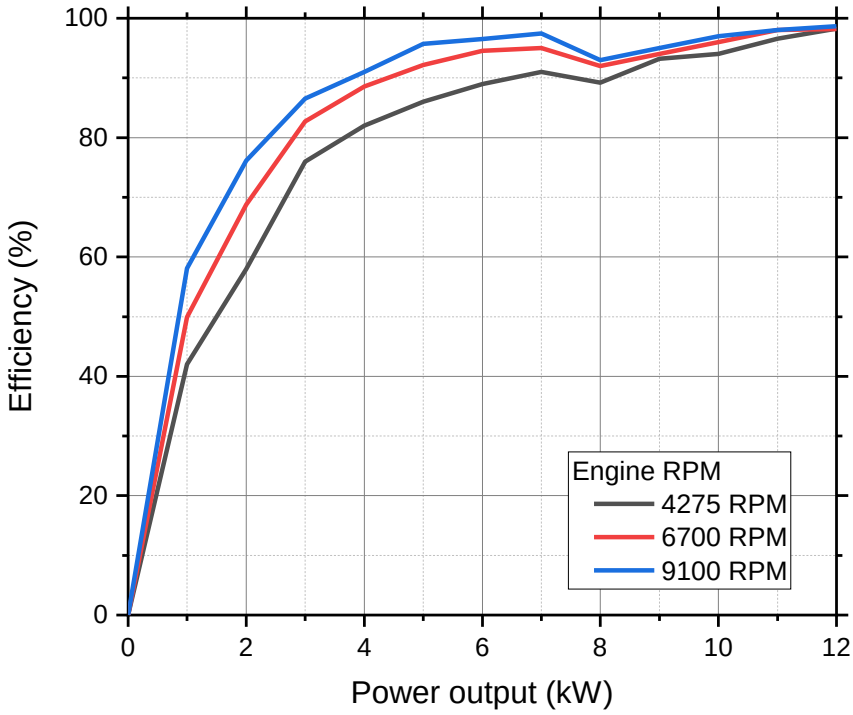

Figure 5.9: *Calculated Dynamo Efficiency*

From Figure 5.9, it can be seen that, similarly to the dynamo efficiency reported in Chapter 4, the power output increases, the dynamo conversion efficiency increases. This is because at lower speeds, a larger proportion of the power supplied to the dynamo is used to energize the coils and overcome friction and losses. The power consumed to energize the coils is fixed and does not increase with increased speed or loading. Therefore, the proportion of power lost to energize the coil diminished and the dynamo efficiency increased with RPM and loading. Advantageously, high conversion efficiency occurs around the maximum power output and target operation speed of the generator system. When compared to gasoline, the electrical conversion efficiency was slightly greater. This is a result of the generator providing more mechanical input power to the generator. Table 5.4 provides the electrical conversion efficiency at discrete loading conditions and engine speeds.

Table 5.4: *Electrical Efficiency at Discrete Loading and Engine Speeds*

Loading Condition	RPM	Electrical Efficiency (%)
Low load	4250	63.2
	6700	
	9100	
Part Load	4250	71.6
	6700	86.5
	9100	90.8
Full Load	4250	97.4
	6700	97.1
	9100	96.4

In view of the engine and dynamo performance, a similar conclusion to that presented in Chapter 4 can be drawn, where it can be concluded that the generator should operate at a relatively steady high RPM and high loading conditions to achieve maximum efficiency and power. Table 5.5 lists the measured parameters of engine performance of the prototype generator at 9100 RPM.

Table 5.5**:** *Generator Performance at 9100 RPM*

Loading (9100 RPM)	Brake Torque (Nm)	Brake Power (kW)	Electrical Power (kW)
Low load	1.50	1.25	.78
Part Load	6.55	6.35	6.12
Full Load	9.55	10.05	9.8

From Table 5.5, it is shown that the prototype produced a maximum of 9.8 kW of electrical power at full loading and high RPM conditions. When compared to gasoline operation, the methanol engine produced 15.3% more electrical power. This is a direct result of the engine producing more power through the use of methanol fuel. Importantly, the generator weight did not change between gasoline and methanol operation. Therefore, the use of methanol increased

the power density of the generator. The increase in power density is a certain benefit as it increases the usefulness of the generator. Given that the generator has a proposed weight of 21 kg and provides 9.8 kW of electrical power, the power density of the prototype range extender with methanol is calculated at .466 kW/kg, which exceeds the prototype's power density when using gasoline of .405 kW/kg. The generator, when operable on methanol fuel, showed a 15.3% increase in power density. This increase in power density further exemplifies that the prototype of this work would be suitable for use as a generator where high specific power is required, such as for use as a range extender for EVs or a component in a high-performance series hybrid powertrain. It can be concluded that, in many scenarios, the generator's performance is sufficient to function as a hybrid drive or range extender [15]. Importantly, the performance of the generator could be further increased by reconfiguring the engine architecture for methanol combustion, for example by increasing the compression ratio or modifying the combustion chamber for methanol combustion [95].

To understand the usefulness of the generator, its performance can be compared to a pure battery range extender system to define a breakeven point. The breakeven point exists where a pure battery range extender maintains a higher power density than the generator system. To perform this calculation, the following assumptions must be made. First, no additional weight, such as battery structures, thermal management, fuel tanks, control systems, etc., will be included in the weight assumptions of the battery or generator. Second, the battery and generator will power the same traction motor; the only parameter to be analyzed will be specific power of the architecture. Currently, the average lithium-ion battery maintains a specific power of about .72 MJ/kg [15]. Assuming the battery was equivalent in weight to the generator, Equation 5.5 shows that a battery equal in weight to the generator would provide 15.12 MJ of energy.

$$(21\ kg) * \left(.72 \frac{MJ}{kg}\right) = 15.12\ MJ \qquad (5.5)$$

Given that the generator yields a brake thermal efficiency of about 15%, and that the specific energy of methanol is about 22 MJ/kg, Equation 5.6 provides that the generator would need to carry 4.58 kg of methanol to provide equivalent energy to a pure battery range extender.

$$\frac{15.12\ MJ_{battery}}{22 \frac{MJ}{kg} * .15} = 4.58\ kg \qquad (5.6)$$

Assuming that methanol has a density of .7918 g/cc, Equation 5.7 shows that the generator would need carry 1.52 gallons of methanol to have equivalent energy to a pure battery range extender of the same weight.

$$\frac{4.58\ kg}{.7918\ kg/l} * \frac{1\ l}{3.3.785 \frac{l}{gal}} = 1.524\ gal \qquad (5.7)$$

From equations 5.6 and 5.7, it is shown that if the generator is supplied with less than about 1.5 gallons of fuel it is more practical to utilize a pure battery to supply power to the drive motor. Likewise, if the generator is supplied with more than about 1.5 gallons of fuel, it is more practical to utilize the generator of this work. Given that a user would likely carry more than 1.5 gallons of fuel, and that refueling is accomplished at a fraction of the rate of recharging, it is suggested that the generator considered in this work maintains a practical advantage over a pure battery configuration.

5.4.4 Emissions Analysis

In this study, the exhaust emissions from the prototype generator were sampled and tested for the purpose of understanding engine emissions performance and combustion characteristics. An exhaust gas analyzer was incorporated in the exhaust stream to measure unburnt hydrocarbons (HC), carbon monoxide (CO), carbon dioxide (CO_2), and oxides of nitrogen

(NO_x). For comparison, all values are presented in units of grams per kilowatt hour (g/kW-h). A comparison between gasoline emissions and methanol emissions is provided.

Unburnt Hydrocarbons

Figure 5.10 shows the HC emissions for different loading conditions and operating RPMs. From Figure 5.10, it can be seen that as engine loading increases, HC emissions decrease. It can also be seen that HC emissions decrease at each loading condition with increased engine speed.

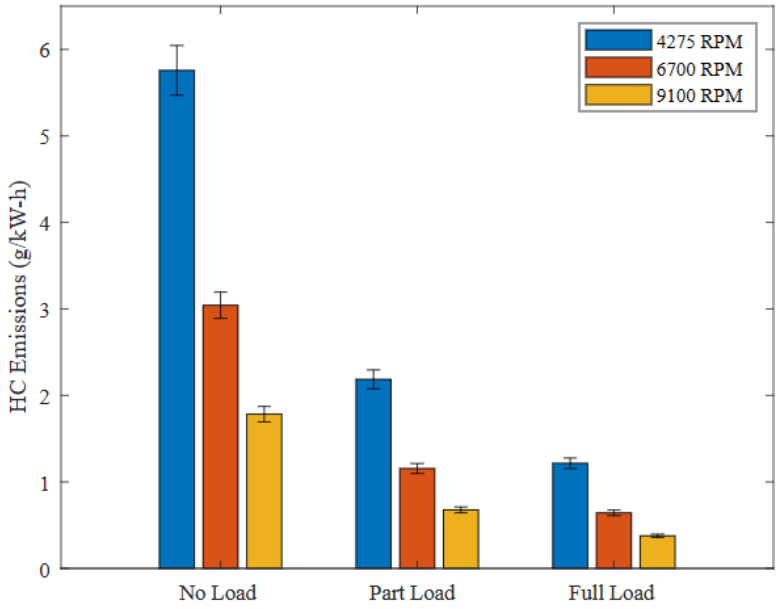

Figure 5.10: *Unburnt Hydrocarbon Emissions*

From Figure 5.10, it can be seen that there is a decrease in HC emissions as loading increases. There is also a decrease at each loading condition as engine speed is increased. As previously stated, in two-stroke engines, HC emissions are arguably the most problematic emissions species. High levels of HC emissions burden many two-stroke engines and limit their usefulness. In a premixed crankcase scavenged two-stroke engine, such as the engine incorporated for this prototype, a significant amount of the fuel may short circuit. Short-

circuiting refers to the fuel charge escaping the combustion chamber through the exhaust port during the scavenging phase after blowdown [92]. When a two-stroke engine is at the bottom of its stroke, the transfer port and exhaust port are simultaneously open. A portion of the incoming fuel charge may escape the combustion chamber during this stage. Further, there are often places where fuel can escape the flame front during the normal combustion process and escape burning [92]. These effects are greatly exaggerated under low throttle openings when conditions for combustion are poor and when flame propagation may be incomplete and under low engine speed operation when port timing is not adequate to prevent short-circuiting events from dominating. The effect of the foregoing is apparent in the HC emissions measured during operation, where peak HC emissions occurred at low load/low rpm operation. It should be noted that there is a pronounced difference in HC emissions between low load low speed operation and full load high speed operation. This substantial decrease in HC emissions is a result of the decrease in fuel short circuiting and further encourages high RPM high load operation of the generator. The highest concentration of HC emissions can be seen at low speed low load conditions where the effects of fuel short-circuiting are the most pronounced. As engine speed and loading increase, the amount of fuel that is subject to fuel short-circuiting is decreased which results in lower concentrations of HC emissions.

As previously discussed, unburnt hydrocarbon emissions are also influenced by incomplete combustion. When the fuel is not completely consumed during the combustion event, it is emitted as HC emissions [74]. Incomplete combustion often occurs at lower loads, smaller throttle openings, and lower engine speeds as a result of lower in-cylinder and combustion temperatures. In a two-stroke engine, the larger concentration of trapped exhaust gases at lower engine speeds and loading conditions can lower combustion temperatures and promote

incomplete combustion. As loading and engine speed increase, the combustion temperatures increase which decreases the occurrence of incomplete combustion. As a result, the concentration of unburnt fuel decreases.

In addition, a potentially significant component of HC emissions in crankcase-scavenged two-stroke engines is the lubricating oil mixed that is mixed with the fuel. The lubricating oil that escapes through the exhaust is often partially combusted and is emitted as blue smoke. In a two-stroke engine, as the fuel charge enters the crankcase, the oil in the fuel separates from the fuel charge and migrates through the engine [92]. At lower engine speeds and loads, there is less heat to fully combust the oil, and the lubricating oil carried by the air stream may escape the cylinder unburned and be exhausted as smoke or oil droplets. At higher loading, a substantially larger fraction of the lubricating oil is combusted. This likely contributes to the decrease in HC emissions with increasing loading and engine speed [74]. Overall, it is theorized that a large portion of the HC emissions are generated from lubricating oil that is partially combusted and expelled from the exhaust; this exhausted oil is measured with and adds to the total concentration of HC emissions.

When compared to gasoline operation, the engine operable on methanol produced significantly lower unburnt hydrocarbon emissions. HC emissions are often a result of incomplete combustion [95]. Methanol is a more simple, single-component molecule than gasoline and often experiences more complete combustion. In addition, the extra oxygen content of methanol may further promote complete combustion. HC emissions are also correlated with richer A/F ratios. The engine was tuned fuel lean on the low-speed setting on the carburetor which resulted in lean A/F ratios in the low engine speed, low loading conditions where the HC emissions are the highest. This leaner low speed A/F ratio with methanol likely participated in

the reduction of HC emissions. It is theorized that most of the HC emissions from the generator on methanol are a result of short-circuiting and not incomplete combustion, whereas with gasoline incomplete fuel combustion contributed to HC emissions.

Carbon Monoxide

Figure 5.11 shows the CO emissions for different engine speeds and loading conditions. A similar trend can be observed in HC emissions, where CO concentration decreases with engine speed and loading conditions. However, the change in concentration is much less pronounced with the CO species. As previously discussed, in two-stroke engines, the gas exchange and therefore volumetric efficiency are linearly related to engine speed. As previously discussed, because the engine porting and timing is optimized for high RPM operation, low-speed gas exchange is relatively inefficient. The poor gas exchange at lower engine speeds results in a higher concentration of trapped exhaust gas from cycle to cycle [70]. It is likely that the higher concentration of diluent species lowers combustion temperature and increases the likelihood of incomplete combustion. As engine speed is increased the gas exchange becomes more efficient and the concentration of diluents is lower resulting in more complete combustion [92]. In another aspect, the rich regions that form in the cylinder resulting from deviation from stoichiometric mixtures and poor trapping efficiency may contribute to the increase of CO emissions at lower loads and engine speeds as richer fuel mixtures encourage incomplete combustion.

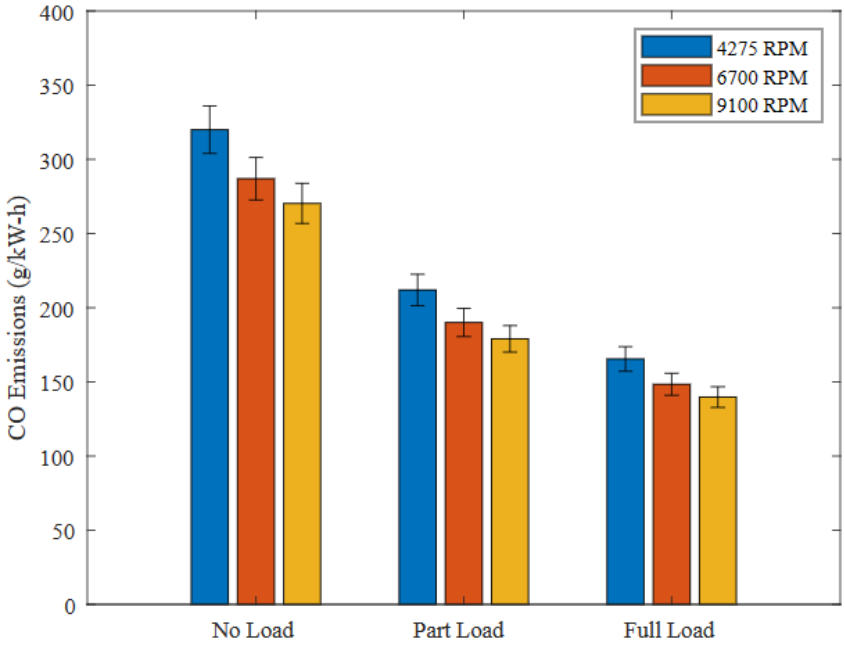

Figure 5.11: *Carbon Monoxide Emissions*

When compared to gasoline, methanol produces slightly less CO. CO emissions essentially depend on air/fuel ratio. With methanol, CO emission is reduced due to oxygen enrichment resulting from methanol. In some respects, the higher hydrogen to carbon ratio of methanol combustion may influence the presence of CO. The greater concentration of hydrogen atoms lowers the formation potential of CO [75]. Methanol is an oxygenated fuel and can introduce extra oxygen in the form of OH radicals which also encourage the oxidation of CO to CO_2. The formation of CO is similar to HC, which often results from incomplete combustion of fuel. Similar to the measured HC emissions, methanol may provide a decrease in CO emissions because it achieves more complete combustion as a result of its chemical simplicity and carried oxygen content.

Carbon Dioxide

Figure 5.12 shows the measured amount of CO_2 from each loading condition at discrete engine RPMs. Similar to HC and CO, there is a decrease in the concentration of CO_2 emissions with increasing engine speed, but in contrast, there is a relatively constant concentration of CO_2 across different loading conditions. In general, the concentration of CO_2 increases as the A/F ratio approaches stoichiometric conditions [70]. The Buller Atomizer carburetor used in this work operates with a low-speed and high-speed jet. To prevent the engine from overheating, the high-speed jet was set slightly richer than the low-speed jet. As engine RPM increased, the engine transitioned from the close to stoich low-speed jet to the slightly richer high-speed jet. It is likely that, as engine RPM increased, the fuel mixture became richer resulting in a decreased concentration of CO_2. Engines that operate on methanol or other alcohol fuels are often tuned with fuel lean low speed A/F ratios to reduce the difficulty of starting the engine [95]. The engine of this work was likewise tuned fuel lean on the low-speed jet. These lean low speed fuel ratios could have exaggerated the transition from lean to rich with increasing RPM.

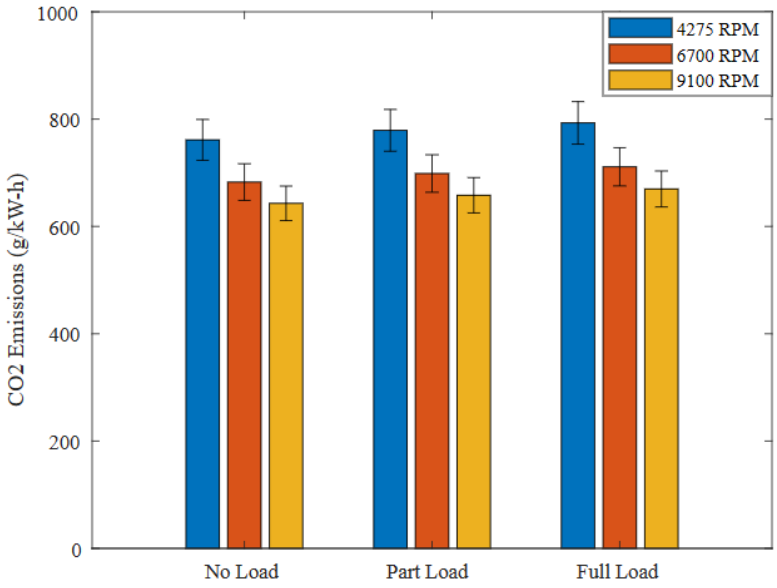

Figure 5.12: *Carbon Dioxide Emissions*

Importantly, depending on the method of production, methanol can be a net-zero carbon fuel. Certain carbon capturing techniques could be utilized in the production of methanol fuel. The CO_2 emissions generated during operation of the engine can be balanced by an equivalent amount of CO_2 removed or sequestrated during the production of the fuel. With the use of net-zero carbon fuel, the engine has the potential to provide a net-zero impact on atmospheric CO_2 levels and thus the measured CO_2 levels are moot.

Oxides of Nitrogen

Figure 5.13 shows the measured amounts of NO_x emissions during the operation of the generator. Unlike the previous species, NO_x shows an increasing concentration with an increase in engine speed and loading. In addition, for each loading condition, NO_x levels increase with increased engine RPM.

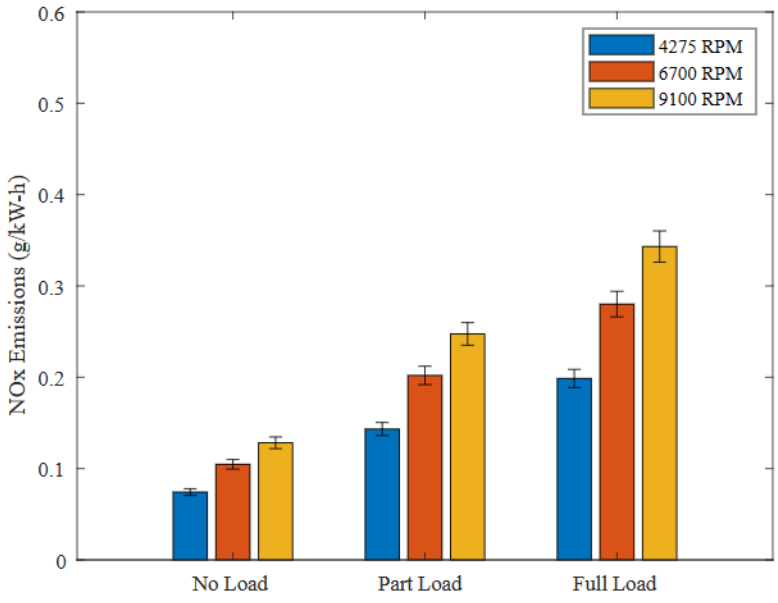

Figure 5.13: *Oxides of Nitrogen Emissions*

Extensive data from four-stroke SI engines has established that the critical engine variables that affect NO_x emissions are combustion temperatures. Several parameters that can

affect in-cylinder combustion temperatures include the mass fraction of burned exhaust gas in the in-cylinder mixture of fuel and air, residual gas such as EGR, and relative air/fuel ratio [45,70]. As discussed, in a two-stroke engine, at lower engine loads and speeds, the cylinder filling efficiency and gas exchange rate is low. As a result, there is a higher concentration of burned residual gas in the combustion chamber that dilutes the fuel charge and lowers the flame temperature. The result of the foregoing generates similar in-cylinder conditions to an engine equipped with an exhaust gas recirculation (EGR) system. EGR systems are structured to lower NO_x emissions by increasing the dilution ratio of the fuel charge and lower in-cylinder temperatures. This natural EGR effect may influence the decrease in NO_x emissions at lower engine loading and RPM. As shown above, during low load, low RPM operation where the fuel charge may be more diluted by trapped exhaust gas, there are lower measured levels of NO_x. Additionally, the lower flame temperature resulting from the cooler combustion and high latent heat of hydrogen reduces the formation of thermal NO_x when compared to gasoline [77].

When compared to gasoline operation, the prototype on methanol, the NO_x emissions were slightly lower. This is most likely because the maximum temperature of the thermodynamic cycle is lower with methanol as a fuel than gasoline. The adiabatic flame temperature of methanol combustion is lower because of the lower specific energy of methanol and because of the higher latent heat of vaporization [137]. NO_x emissions increase in positive correlation with increasing combustion temperature due to their formation mechanism. NO_x emissions could potentially be lowered further in a methanol engine by leaning the fuel mixture. This is made especially feasible with methanol fuel due to its wider flammability range when compared to gasoline. Because the A/F ratio of methanol is lower than gasoline, there is less air and therefore less nitrogen in the combustion chamber to form NO_x. It should be noted that the NO_x emissions

an engine produces are not associated with the fuel used because the nitrogen source is the air. Rather, the NO_x emissions are often a result of in-cylinder combustion conditions and are otherwise outside the scope of control with alternative fuels, such as methanol.

Emissions Reduction Through Methanol

Due to their high-power density, small footprint, simplistic constriction, and low cost, two-stroke engines may remain the most suitable choice for high power density generators like the prototype discussed in this work. However, due to their high specific emissions, it is difficult for gasoline-powered crankcase scavenged two-strokes to meet emission requirements in most jurisdictions. In many applications, it is not practical to outfit these often small engines with common emissions reduction technology, such as fuel injection or exhaust after treatment. A potential solution to this is to adapt the engine to operate on a renewable fuel that provides lower carbon emissions. For this work, the engine of the prototype generator was modified to operate on methanol, which is a net carbon-zero renewable fuel. In view of other emission reduction methods such as exhaust catalytic aftertreatment, fuel injection, lean burn techniques, etc., alternative fuels are favorable because they require little to no modification and do not add complexity and weight to the powertrain.

In summary, when comparing the gasoline operated prototype and methanol operated prototype, it was found that peak NO_x emissions from the methanol experiments were 26.3% lower than the gasoline experiments. Further, peak CO emissions were approximately 53.2% lower and peak HC emissions were approximately 42.6% lower with methanol than with gasoline. The average CO_2 emissions were reduced by 40.3%. In general, CO and HC emissions form during incomplete combustion during the combustion event. Because methanol experiences

more complete and perfect combustion, CO, and HC emissions are generally lower. However, because the engine utilizes a fuel oil blend where the oil is composed of fatty triglycerides, it is likely the combustion is less ideal than pure methanol combustion. It should be noted that certain elements of HC emissions are a result of short circuiting and would not be affected by the combustion chemistry.

Further, though there is a significant reduction in HC emissions, some levels of HC emissions are unavoidable regardless of the fuel with this engine architecture due to fuel short-circuiting. As discussed, during the scavenging phase when the piston is at BDC, the transfer ports and exhaust ports are open simultaneously which results in unburned fuel escaping from the exhaust. There does, however, exist a plurality of solutions that could be incorporated to reduce the quantity of HC escaping from the exhaust. Amongst these, the incorporation of a tuned expansion chamber is the least costly and invasive and would potentially provide a significant reduction in HC emissions while providing a boost in specific power. Tuned exhaust pipes include an expansion chamber that are dimensioned to reverberate the exhaust pressure wave back to the exhaust port. When this happens, the exhaust port is substantially sealed, and fuel short-circuiting is limited. In addition to decreasing the emissions of the engine, tuned pipes are often operable to provide significant increases in volumetric efficiency and cylinder filling of two-stroke engines, which would further increase the output power, efficiency, and energy density of the prototype.

5.5 Conclusions

The high-performance prototype electric generator that has the potential to function as a range extender for an EV, hybrid vehicle generator for powersports or power equipment, UAV

propulsion or the like from the previous chapters was converted to operate on renewable fuel in pursuit of emissions reduction is presented in this chapter. The prototype electric generator from the previous chapters was modified to function with methanol fuel and the experiments from Chapter 4 were repeated to characterize the combustion, performance, and emissions of the prototype while using methanol fuel. It was found that the prototype electric generator produced 9.8 kW of electrical power while having a proposed weight of only 21 kg. Further, the prototype demonstrated certain increases in power while simultaneously demonstrating a decrease in certain emissions species when compared to gasoline operation. As a result, the power density and effectiveness of the prototype generator was increased over gasoline. The prototype operable on methanol exceeded the power density when operated on gasoline. Further, the generator demonstrated a reduction in HC, NO_x, and CO emissions when compared to gasoline operation. It was shown that the generator may be suitable for applications where high specific power, low cost, and low weight are critical. In addition, there still remain avenues for increased power, thermal efficiency, and emissions reduction. The generator may additionally be suitable for applications with strict emissions requirements, in particular, if used in combination with net-zero emissions methanol fuel.

CHAPTER 6: Conclusions & Future Work

6.1 Conclusions

The major objective in this dissertation is to explore the experimental development and performance of a prototype high power density electric generator, and more generally, explore the protentional to source energy from alternative fuels. The high power density electric generator of this work can be used in a variety of applications, for example as a range extender for electric vehicles, as a component in a hybrid powertrain for powersports and off road equipment, and a UAV range extender [155]. To achieve this goal, the state of the art for high power density electric generator was investigated and contemplated. Preliminary experiments were conducted with a gasoline generator where the generator was modified to operate on a synthetic gaseous alternative fuel. The fuel in the preliminary experiments comprised inert and flammable components. The performance and emissions of the generator operable on alternative was measured and evaluated.

With the knowledge and techniques from this preliminary work and literature review, a prototype high power density generator was constructed and arranged in a test stand. The test stand was operated and optimized and prepared for experimentation. The first series of experiments were conducted with the generator operable on conventional gasoline fuel. The performance and emissions data during gasoline operation was collected and analyzed. After the gasoline experiments were conducted, the engine of the test stand was modified to operate on renewable methanol fuel. The experiments were then repeated, and the data was recollected. The performance and emissions data from methanol operation was analyzed and compared with gasoline. It was found that the prototype high power density generator would theoretically yield

the highest power density of any similar generator both known and theoretical. Moreover, there was a substantial reduction in major emissions species as well as slight performance increases when the generator was converted to methanol fuel. A final design of the prototype was proposed and submitted in this work. At the completion of this dissertation, the following major contributions to the field have been made and corresponding conclusions are summarized as follows (more detailed findings should be found in the conclusions of each chapter):

New fundamental insights have been obtained into the viability of gaseous fuels which comprise high levels of diluent species have been obtained. Many engines are currently equipped with exhaust gas recirculation devices that reintroduce the inert products of combustion back into the engine in an attempt to reduce certain exhaust emissions. However, these systems often only introduce small quantities of diluent gas into the fuel charge. This work provides insights to possibility of adapting modern engines to operate on fuels that are almost 50% diluent exhaust gas. This work provides techniques and lessons for the adaptation of existing engines to use fuels of this type and provides experimental validation of the same. Specifically, it was found that through light to moderate modification, existing engines can become adapted to use gaseous fuels with a high diluent charge. In addition, this work provides data that suggests that similar levels of performance can be achieved in addition to the reduction of certain exhaust emissions.

A new fundamental design for a high power density electric generator that can be used in a variety of applications, such as a range extender or in combination with a hybrid powertrain was presented. The design and development of the generator is provided in this dissertation as well as experimental techniques and data. Further, this work demonstrates that the prototype generator has one of the highest power densities of any known generator that is available. It was concluded that the prototype has the potential to function as a range extender for an EV, a hybrid

powertrain for power equipment and small vehicles such as motorcycles, ATVs, or PWCs, and UAV range extenders. A prototype based on the design was constructed to characterize the combustion, performance, and emissions, as well as to evaluate the viability of the generators. It was found that the prototype generator produced 8.5 kW of electrical power while having a weight of only 21 kg. It was found that the thermal efficiency, mechanical efficiency, and power output of the generator increased with increasing RPM. Further, the generator demonstrated a reduction in HC and CO emissions with increasing load. However, as load increases, there is an increase in NO_x emissions.

The last focus of this dissertation involves the modification and operation of the engine on renewable fuels. This dissertation submits new techniques and findings and enhances the state of the art of engines and power generation for hybrid powertrains and high power generators using renewable fuel. The engine was modified to operate on methanol, which is a potentially net carbon zero fuel. The engine was then returned and optimized for methanol fuel, and the experiments of the previous section were repeated to characterize the combustion, performance, and emissions of the prototype while using methanol fuel. It was found that the prototype electric generator produced 9.8 kW of electrical power, showing a 15.3% increase in power when compared to gasoline operation. As a result, the generator yields the highest power density of any theoretically proposed or commercially available generator considered in this work. It was found that the power output and peak torque of the generator increased with increasing RPM. Further, the generator demonstrated global reduction in measured emissions, including a reduction in HC, NO_x and CO emissions when compared to gasoline operation. It was shown that the generator may be suitable for applications where high specific power, low cost, and low weight are critical. In addition, there still remain avenues for increased power, thermal

efficiency, and emissions reduction. The generator may additionally be suitable for applications with strict emissions requirements.

6.2 Future Work

Based on the findings of the work of this dissertation, it can be concluded, through the efforts of this dissertation, the prototype satisfied the scope of this work. However, there are several technologies and modifications that can and should be made to continue to improve the performance of the prototype.

The first action that should be taken to advance this work is to complete a commercially viable final design of the generator. The prototype of this work demonstrated that it is feasible to produce a high power density electric generator for use in, for example, a hybrid powertrain or range extender. The components that would be included in the final design have been validated on the test stand and can be incorporated into a consumer-ready package. Thus, it is envisioned that the final design would incorporate the essential elements demonstrated on the test stand. It should be emphasized that the final design should focus on minimizing the size and weight of the generator. In one aspect, the final design can remove some of the weight associated with the stand as the aluminum used to build the dynamo was not optimized for weight. A planetary gearbox or other gear reduction could be used in the place of the belt drive to lower weight and reduce the final size. Cooling could be achieved by way of a small cooling fan in unity with a cooling duct to direct cooling air around the cylinder head. A polymer casing could be included to house the components. Figure 6.1 is a collage of CAD models of one embodiment of a potential final design.

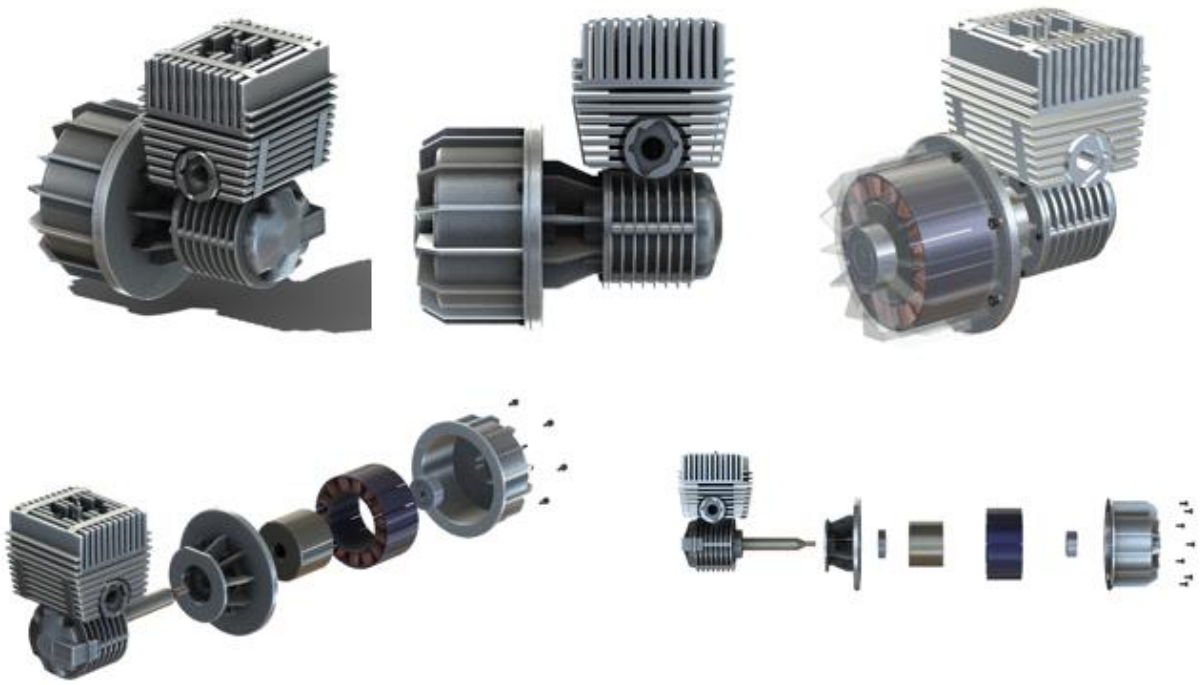

Figure 6.1: *CAD Model of Proposed Final Desing*

It has been shown in this work that conventional some conventional engines can be modified to operate on alternative renewable fuels to gasoline or diesel. It is contemplated that future work could include the use of other alternative fuels to operate the generator. Some alternative fuels, either gaseous or liquid, may further decrease certain emissions species or improve performance in some aspects. Ammonia (NH_3) has been shown to be a promising alternative to gasoline as an alternative fuel [156]. While ammonia is mainly used for fertilizer production, it stands as a promising alternative to hydrocarbon fuels due to its high energy density and ease of storage. Ammonia can be affordably produced from fossil fuels, such as natural gas or coal, or biomass similar to methanol. As a result, ammonia stands to be another potentially net zero carbon fuel if carbon capturing techniques are incorporated. Moreover, ammonia delivers an energy density comparable to fossil fuels, around 22.5 MJ/kg [157]. It is theorized that similar techniques to those used in this work could be applied to the generator or

other engines to convert them to ammonia combustion. Ammonia's properties allow it to be used in internal combustion engines with minor engine modifications. Moreover, similarly to methanol, fuel stations would require little conversion to dispense ammonia fuel [158]. The nature of nitrogen based fuels is such that ammonia can be used within a dual-fuel concept, for example in combination with gasoline, diesel, methanol, ethanol, and others while handing over promising results in terms of emissions and performance [160]. Thus, the consideration of ammonia as a fuel for this engine and others is encouraged.

In one aspect, the dynamo could be improved or replaced with a smaller more powerful dynamo. The commercially available dynamos are either prohibitively expensive or have a power density that is too low. In some of the works considered in this dissertation, custom dynamos were made and coupled to the engine which increased the global power density of the generator. Therefore, the potential to increase the performance, power density, and decrease the size and weight of the generator by way of alternative or custom generators should be explored.

In another aspect, modifications to the engine can be made that could dramatically increase the performance both on methanol and gasoline. The engine could be blueprinted, which refers correcting the manufacturing tolerances which are relatively loose to lower costs [95]. The compression ratio on the stock KT-100 is relatively low as a result of Karting rules which govern the manufacture of the engine. The compression ratio could be increased which would increase MEP and thermodynamic efficiency. Increasing the compression ratio is especially useful for methanol operation; because of methanol's high octane rating (109 RON), the compression ratio can be increased above what would be possible with gasoline which can further increase thermodynamic efficiency and power. This can be achieved by milling the cylinder head. Further, the squish band of the engine, which refers to the geometry of the combustion chamber,

could be optimized for methanol operation which would further increase the performance of the engine. Finally, the operational RPM of the prototype could be increased past 9100 RPM. The power an engine produces is in many ways a function of RPM. This engine was restricted to 9100 RPM for NHV considerations. The prototype could be outfitted with sound and vibration dampening equipment that would allow the engine to operate at a higher RPM. It is theorized that higher RPM operation may also increase thermodynamic efficiency as evidenced by the thermodynamic efficiency trend from this work.

There are several technologies, some simple and some complex, that could be configured with the engine to increase performance. In a first aspect, the exhaust could be upgraded on the engine from a can style silencer to an expansion chamber. Expansion chambers are commonly equipped on two-stroke engines to increase their volumetric efficiency [92,95]. As previously stated, it is a common misconception that two-stroke engines emit higher levels of emissions because they utilize a total loss lubrication system where the oil is mixed with the fuel and combusted in the cylinder. However, most of the increased levels of emissions result from the transfer port and exhaust port being open at the same time when the piston is at the bottom of the stroke. An expansion chamber is a tuned exhaust pipe comprising a series of cones and nozzles that optimize the Cadence effect to reflect the exhaust pulse wave back towards the exhaust port, effectively sealing the port and preventing fuel short circuiting [92]. Once the piston falls and uncovers the exhaust port, the exhaust pulse travels down the expansion chamber. Once the exhaust pule reaches the expansion chamber, it is then reflected by the expansion chamber and returns back to the exhaust port where it meets the escaping fresh fuel charge and substantially prevents fresh fuel from bypassing the combustion chamber. Figure 6.2 is a schematic of the operation of a two-stroke expansion chamber.

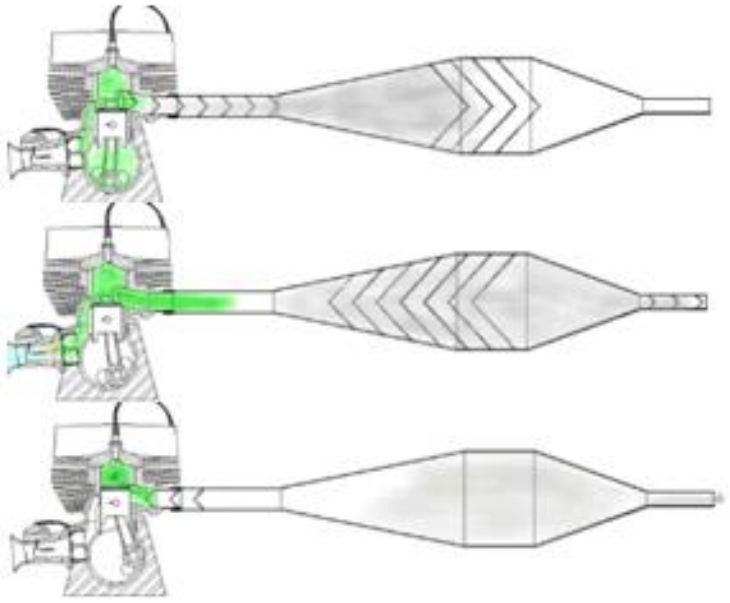

Figure 6.2: *Two-Stroke Expansion Chamber Schematic* [92]

Expansion chambers exhausts can increase the volumetric efficiency of a two-stroke engine past 100% and in some applications increase the specific power by up to 100%, commonly 50%. One particular advantage to a tuned expansion chamber is that they can decrease HC emissions by preventing fuel short circuiting. Expansion chambers prevent the fresh fuel charge from escaping the engine [92]. Moreover, expansion chambers can be tuned to increase the power at specific RPM ranges or broaden the powerband of the engine; the prototype generator of this work could benefit from a tuned exhaust pipe in terms of increased power output and lowered HC emissions. Figure 6.3 is an image of a two-stroke expansion chamber on a Yamaha Yz250. Figure 6.4 is an example of a tuned pipe for a karting engine similar to the KT-100. It is theorized that a tuned pipe could be constructed that is similar in design to the exhaust pipes presented in Figures 6.3 and 6.4.

Figure 6.3*: Yamaha Yz250 Two-Stroke Expansion Chamber*

Figure 6.4: *Example of a Tuned Pipe* [97]

There are a few other technologies that should be explored in future works to increase the performance of the prototype that would be less invasive than those previously presented. Firstly, the engine could be equipped with a power valve. A two-stroke power valve is a mechanical valve that is in the exhaust port and is structured to alter the exhaust valve timing, and in some cases, tuned length of the exhaust. These devices are often governed by the RPM of the engine

and function similarly to variable valve timing in four-stroke engines. These valves a can increase the power output of the engine over a greater RPM range and have the protentional to reduce certain emissions species. Future iterations of the prototype of this should consider the use of a power valve. Figure 6.5 is an image of a two-stroke power valve.

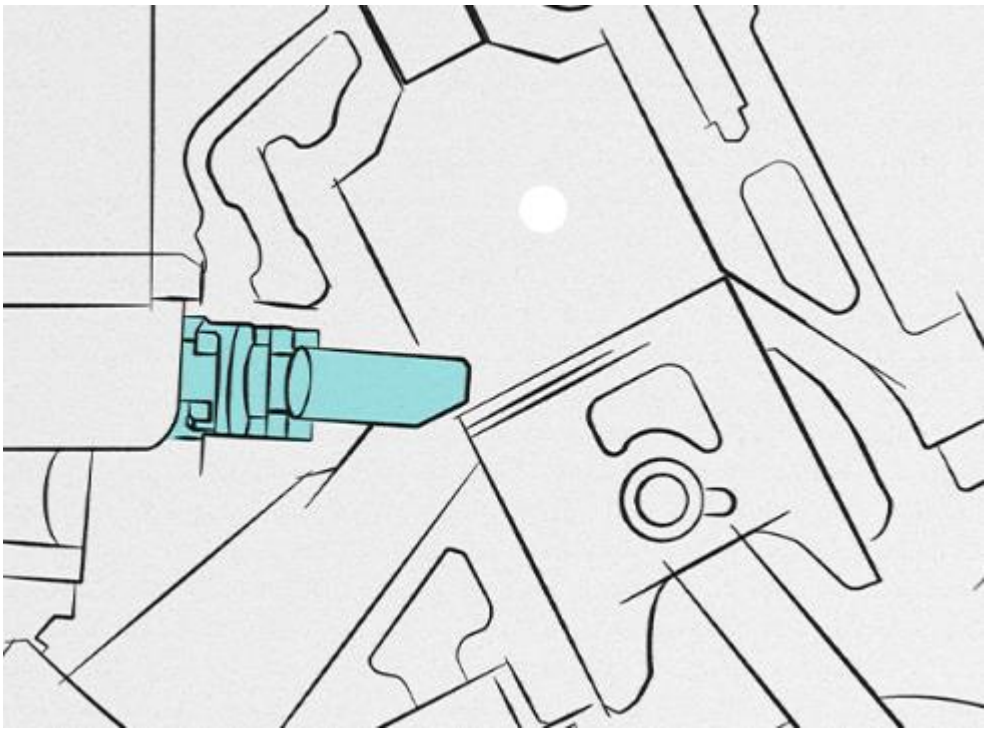

Figure 6.5: *Schematic of Two-Stroke Power Valve* [161]

Certain electrics can be included in the engine to further increase power and reduce emissions. It is theorized that catalytic aftertreatment could be incorporated into the exhaust to further increase certain exhaust species, such as HCs. These catalytic aftertreatment systems have been successfully scaled down and incorporated into small engines, such as chainsaws with good success in reducing HC emissions. In addition, lean burn strategies could be incorporated to reduce nitrogen and carbon emissions. There are several outboard manufactures who produce two-stroke power heads which incorporate these lean burn strategies. The engine could be outfitted with a separate oil pump to inject lubricating oil directly into the engine which removes

the need to mix fuel and oil. This technology could reduce oil consumption and emissions by reducing the amount of oil injected during low load and low RPM operation where excess oil is not required. Each of these technologies should be investigated as future improvements to the generator of this work.

Fuel injection techniques are increasingly common with two-stroke engines and have shown great potential in reduction of emissions. KTM, an Austrian motorcycle manufacturer, has shown that fuel injected two-stroke engines have the potential to decrease certain exhaust emissions to that of comparably sized four-stroke units [162]. KTM offers a variety of models with throttle body fuel injection and transfer port fuel injection. Transfer port fuel injection is of particular interest as it has shown that locating fuel injectors in the transfer ports of the cylinder can reduce the amount of fuel that is lost in short circuiting. Further, the use of transfer port fuel injection has been shown to work well with lean burn strategies and should be investigated in future works. Figure 6.6 is a schematic of a Transfer Port Injection (TPI) scheme.

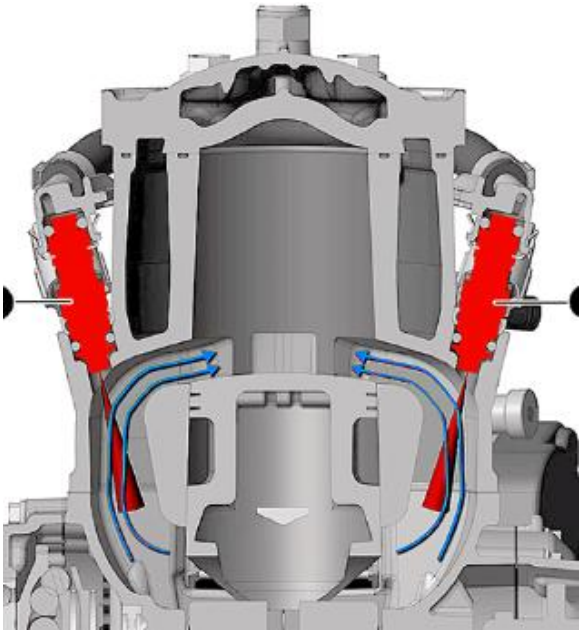

Figure 6.6: *KTM Transfer Port Fuel Injection Schematic* [162]

However, these fuel injection schemes fail to completely solve issues of fuel short circuiting. Regardless of the injection technique, combustion scheme, or exhaust apparatus, there is always the potential for some fuel to escape through the exhaust port with these methods. Direct injection, which refers to locating a fuel injector directly in the cylinder poses to completely solve fuel short circuiting in two-strokes. Figure 6.7 is a schematic of a direct injected two-stroke cylinder.

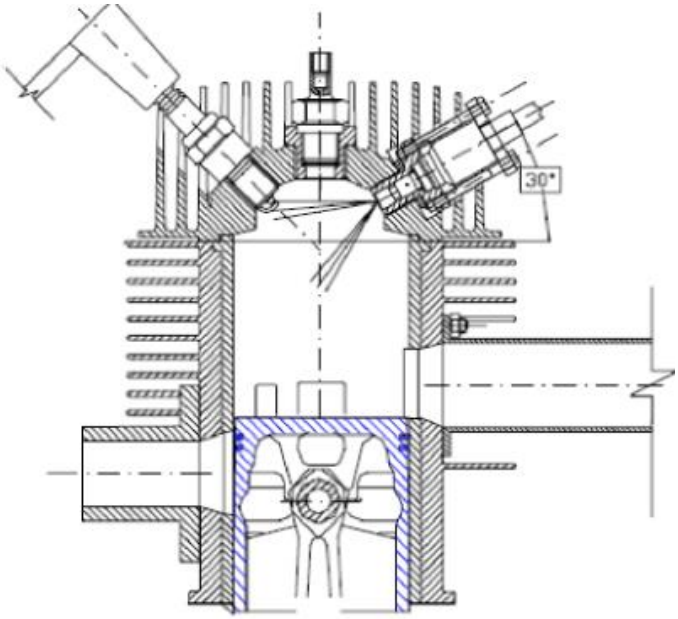

Figure 6.7: *Schematic of Direct Injected Two-Stroke* [163]

With direct injection, the fuel injection event can take place after the exhaust port is sealed by the piston, which means that only fresh air and products of combustion are expelled through the exhaust port when both ports are simultaneously open. Bombardier Recreational Products, or BRP has shown through their E-TEC direct injection technology that direct injection schemes can be successfully applied to two-strokes with high levels of emissions reduction [163]. The E-TEC engines are used extensively in their snowmobile and outboard engines and have shown that the direct injected two-stroke can meet or exceed emissions standards and actually offer lower emissions than comparable four-stroke engines. Moreover, direct injection

opens up the potential for forced induction on crankcase scavenged two-stroke engines because of the elimination of fuel short circuiting. Figure 6.8 is an image of an E-TEC 800cc parallel twin direct injection two-stroke engine.

Figure 6.8: *Image of BRP E-TEC Direct Injected Two-Stroke* [126]

It is evident that there is a bright future for two-stroke engines. The lightweight, simplistic design, and high specific power are advantages that cannot be matched by alternative engine configurations in certain applications. The two-stroke engine is a key element in the success of this work, and continues to play a crucial role in powersports, power equipment, off highway equipment, and a variety of other applications. It, therefore, should continue to be researched and developed at least until an alternative to internal combustion engines is viable. Long live the two-stroke engine.

REFERENCES

1. Z. Rezvani, J. Jansson, J. Bodin. Advances in Consumer Electric Vehicle Adoption Research: A Review and Research Agenda, Volume 34,2015, Pages 122-136, ISSN 1361-9209. https://doi.org/10.1016/j.trd.2014.10.010.
2. G. Krishna. Understand and Identifying Barriers to Electric Vehicle Adoption Through Thematic Analysis. Volume 10, 2021. 100364. ISSN 2590-1982. https://doi.org/10.1016/j.trip.2021.100364.
3. O. Egbue, S. Long. Barriers to Widespread Adoption of Electric Vehicles: An Analysis of Consumer Attitudes and Perceptions, Energy Policy, Volume 48, 2012, Pages 717-729, ISSN 0301-4215, https://doi.org/10.1016/j.enpol.2012.06.009.
4. Eberle, Ulrich & Helmolt, Rittmar. (2010). Sustainable Transportation Based on Electric Vehicle Concepts: A Brief Overview. Energy & Environmental Science. 3. 689. 10.1039/C001674H.
5. Jena, R. (2020). An Empirical Case Study on Indian Consumers' Sentiment Towards Electric Vehicle: A Big Data Analytics Approach." Industrial Marketing Management 90 (2020): 605-616.
6. 2018, M.-K.; Bhatti, A.; Vrolyk, R.; Wong, D.; Panchal, S.; Fowler, M.; Fraser, R. A Review of Range Extenders in Battery Electric Vehicles: Current Progress and Future Perspectives. World Electr. Veh. J. 2021, 12, 54. https://doi.org/10.3390/ wevj12020054
7. Husain, I. Electric and Hybrid Vehicles Design Fundamentals, 2nd ed.; CRC Press Taylor & Francis Group: Boca Raton, FL, USA, 2011.
8. Szybist, J.; Wagner, R.; Curran, S. Internal Combustion Engines for Hybrid Electric Configurations; National Transportation Research Center: Knoxville, TN, USA, 2017.

9. Heron, A.; Reinderknecht, F. Comparison of Range Extender Technologies for Battery Electric Vehicles. In Proceedings of the 2013 8th International Conference and Exhibition on Ecological Vehicles and Renewable Energies, Stuttgart, Germany, 27–30 March 2013.
10. Friedl, H.; Friedl, G.; Hubmann, C.; Sorger, H.; Teuschl, G.; Martin, C. Range Extender Technology for Electric Vehicles. In Proceedings of the 2018 5th International Conference on Electric Vehicular Technology, Surakarta, Indonesia, 30–31 October 2018.
11. Vortisch, Peter; Chlond, Bastian; Weiß, Christine; Mallig, Nicolai (June 2015). "Electric Vehicles with Range Extender as a Suitable Technology (EVREST)". Karlsruher Institut für Technologie. Retrieved 2015-05-18.
12. Adepetu, A., Keshav, S. The relative importance of price and driving range on electric vehicle adoption: Los Angeles case study. Transportation **44**, 353–373 (2017). https://doi.org/10.1007/s11116-015-9641-y.
13. Andwari, A.M.; Pesiridis, A.; Rajoo, S.; Martinez-Botas, R.; Esfahanian, V. A review of battery electric vehicle technology and readiness levels. Renew. Sustain. Energy Rev. **2017**, 78, 414–430.
14. 014 BMW I3 Electric Car: Why California Set Range Requirements Engine Limits. Available online: https://www.greencarreports.com/news/1087888_2014-bmw-i3-electric-car-why-california-set-range-requirements-engine-limits (accessed on 22 June 2020).
15. Borghi, M.; Mattarelli, E.; Muscoloni, J.; Rinaldini, C.A.; Savioli, T.; Zardin, B. Design and experimental development of a compact and efficient range extender engine. Appl. Energy **2017**, 202, 507–526.

16. Imai, K., Ashida, T., Zhang, Y., Minami, S.: “EV Range Extender: Better Mileage Than Plug-in Hybrid?” - IEEE Vehicle Power and Propulsion Conference (VPPC), September 3-5, 2008, Harbin, China Book.
17. Chan, C.C., Chau, K.T., “Modern Electric Vehicle Technology”, Oxford University Press, New York, 2001. 7. Badin, F., Jeanneret, B., Trigui, R., Harel, F.: “Hybrid Vehicles, Should We Plug Them to The Grid or Not?”
18. Shamsi, H.; Tran, M.-K.; Akbarpour, S.; Maroufmashat, A.; Fowler, M. Macro-level optimization of hydrogen infrastructure and supply chain for zero-emission vehicles on a Canadian corridor. J. Clean. Prod. 2021, 289, 125163.
19. Perera, P.; Hewage, K.; Sadiq, R. Are we ready for alternative fuel transportation systems in Canada: A regional vignette. J. Clean. Prod. 2017, 166, 717–731.
20. Evelyn, Evelyn, Abd Rashid Abd Aziz, and Poetro Lebdo Sambegoro. "A Review of Range Extender Technologies in Electric Vehicles." International Journal of Sustainable Transportation Technology 3.1 (2020): 7-11.
21. MAHLE Powertrain. (2022, May). Range Extender Demonstrator Vehicle. MAHLE Powertrain. Retrieved from https://www.mahle-powertrain.com/media/mahle-powertrain/news-&-press/brochures/range-extender/mpt-range-extender-demonstrator-vehicle-2.pdf.
22. ROTAX (09.05.2014). Range Extender for Electrified Vehicles; Combined Expertise. ROTAX BRP. Retrieved from https://www.rotax.com/detail/range-extender-for-electrified-vehicles-combined-expertise.html.
23. Turner, J., Blake, D., Moore, J., Burke, P. et al., "The Lotus Range Extender Engine," SAE Int. J. Engines 3(2):318-351, 2010, https://doi.org/10.4271/2010-01-2208.10.

24. Capaldi, P., "A Compact 10 kW Electric Power Range Extender Suitable for Plug-In and Series Hybrid Vehicles," SAE Technical Paper 2011-24-0085, 2011, https://doi.org/10.4271/2011-24-0085.

25. Gang BG, Kim K-B. Performance evaluation of a compact designed electric power system composed of a two-stroke gasoline engine, generator, and battery for high-endurance unmanned aerial vehicles. Energy Sci Eng. 2022;10:4071-4084. Doi:10.1002/ese3.1271.

26. Lopez JJ, Molina S, Garcia A, Valero-Marco J, Justet F. Analysis of the potential of a new automotive two-stroke gasoline engine able to operate in spark ignition and controlled autoignition combustion modes. Appl Therm Eng. 2017;126:834-847.

27. Wang X, Zhao H. A high-efficiency two-stroke engine concept: the boosted uniflow scavenged Direct-Injection gasoline (BUSDIG) engine with air hybrid operation. Engineering. 2019;5:535-547.

28. Range extender – Quaternium. (n.d.). https://www.quaternium.com/range-extender/.

29. Simpson, S. (2022, September 6). Range extender for hybrid drones released. Unmanned Systems Technology. https://www.unmannedsystemstechnology.com/2022/09/range-extender-for-hybrid-drones-released/Serrao, l., Pisu, P., Rizzoni, G., Analysis and Evaluation of a Two Engine Configuratino Hybrid Electric Vehicle. Proceedings or IMECE2006 2006 ASME International Mechanical Engineering Congress and Exposition. November 5-10, 2006, Chicago, Il USA.

30. hirthX. (2019, October 2). Perfect partners: The sky’s the limit for two-stroke engines and electric hybrids - Hirth Engines. Hirth Engines. https://hirthengines.com/perfect-partners-the-skys-the-limit-for-two-stroke-engines-and-electric-hybrids/.

31. Kebriaei, Mohammad, Abolfazl Halvaei Niasar, and Behzad Asaei. "Hybrid electric vehicles: An overview." 2015 International Conference on Connected Vehicles and Expo (ICCVE). IEEE, 2015.

32. Momoh, Omonowo D., and Michael O. Omoigui. "An overview of hybrid electric vehicle technology." 2009 IEEE vehicle power and propulsion conference. Ieee, 2009.

33. Wojciech, M,. Zdzislaw, J., Series Hybrid Electric Vehicle with 2-Stroke Internal Combustion Engine. CONAT 20042032. January 2004.

34. Simic, D., "Modeling, Simulation, and Evaluation of a Powertrain of a Hybrid Electric All-Terrain vehicle (ATV)", Conference paper DOI:10.13140/2,1,3791.8405, AIT Austrian Institute of Technology – January 2010.

35. Luj´ an JM, García A, Monsalve-Serrano J, Martínez-Boggio S. Effectiveness of hybrid powertrains to reduce the fuel consumption and Nox emissions of a Euro 6d-temp diesel engine under real-life driving conditions. Energy Convers Manag 2019;199:111987. https://doi.org/10.1016/j.enconman.2019.111987.

36. Ahire, Vaibhav, Mahesh Shewale, and Ali Razban. "A review of the state-of-the-art emission control strategies in modern diesel engines." Archives of Computational Methods in Engineering (2021): 1-19.

37. N Nichols RJ. The methanol story: a sustainable fuel for the future. J Sci Ind Res India 2003;62:97–105.

38. Specht M, Bandi A. The methanol cycle – sustainable supply of liquid fuels. Stuttgart, Germany: Centre for Solar Energy and Hydrogen Research (ZSW); 1999. Available from: ⟨www.zsw-bw.de⟩, January 2005.

39. Rauch R. Biomass gasification to produce synthesis gas for dual cells, liquid fuels and chemicals. Technology brief. IEA bioenergy agreement, Task 33: thermal gasification of biomass (2001–2003); 2002.

40. DOE (US Department of Energy). Assessment of costs and benefits of flexible and alternative fuel use in the US transportation sector. Technical report 5: costs of methanol production from biomass. Rebort no. DOE/PE-0097P. Washington, DC, USA: Office of Policy, Planning and Analysis, DOE; 1990.

41. Donnelly RG, Heywood JB, LoRusso J, O'Brien F, Reed TB. Methanol as an automotive fuel: a summary of research in the M. I. T. Energy Laboratory. Final report; 1976.

42. Gore, M., Nonavinakere Vinod, K., & Fang, T. (2023). Experimental Investigation of Gaseous Mixtures of Ethane, Methane, and Carbon Dioxide as an Alternative to Conventional Fuel in Spark Ignition Engines. Journal of Energy Resources Technology, 145(3), 032301.

43. Environmental Protection Agency. (n.d.). Global Greenhouse Gas Emissions Data. EPA. Retrieved March 17, 2022, from https://www.epa.gov/ghgemissions/global-greenhouse-gas-emissions-data.

44. de Persis, S., Foucher, F., Pillier, L., Osorio, V., & Gökalp, I. (2013). Effects of O2 enrichment and CO2 dilution on laminar methane flames. Energy, 55, 1055-1066.

45. Neal, L.M., Yusuf, S., Sofranko, J.A., Li, F., Oxidative dehydrogenation of ethane: a chemical looping approach. Energy Technology. 2016 Oct; 4(10):1200-8.

46. Neal, L.M., Haribal, V.P., Li, F., Intensified Ethylene Production via Chemical Looping through an Exergetically Efficient Redox Scheme. iScience. 2019 Sep 27; 19:894-904.

47. Brody, L., Neal, L., Haribal, V., & Li, F. (2021). Ethane to liquids via a chemical looping approach–Redox catalyst demonstration and process analysis. Chemical Engineering Journal, 417, 128886.

48. Baratta, M., Chiriches, S., Goel, P., & Misul, D. (2020). CFD modelling of natural gas combustion in IC engines under different EGR dilution and H2-doping conditions. Transportation Engineering, 2, 100018.

49. Nitta, Y., Yoo, D. H., Nishio, S., Ichikawa, Y., Hirata, K., & Yamasaki, Y. (2016, October). Evaluation of emissions characteristics by charging exhaust gas from lean burn gas engine into marine diesel engine. In Internal Combustion Engine Division Fall Technical Conference (Vol. 50503, p. V001T04A002). American Society of Mechanical Engineers.

50. Cho, H. M., & He, B. Q. (2009). Combustion and emission characteristics of a natural gas engine under different operating conditions. Environmental Engineering Research, 14(2), 95-101.

51. Shudo, T., Kitahara, S., & Ogawa, H. (2006). Influence of carbon dioxide on combustion in an HCCI engine with the ignition-control by hydrogen (No. 2006-01-3248). SAE Technical Paper.

52. Karim, G. A., & Wierzba, I. (1992). Methane-carbon dioxide mixtures as a fuel (No. 921557). SAE Technical Paper.

53. Rao, A., Wu, Z., Mehra, R. K., Duan, H., & Ma, F. (2021). Effect of hydrogen addition on combustion, performance and emission of stoichiometric compressed natural gas fueled internal combustion engine along with exhaust gas recirculation at low, half and high load conditions. Fuel, 304, 121358.

54. Mohr, J., Zdanowicz, A., Tryner, J., Gustafson, K., Venegas, J., Windom, B., ... & Marchese, A. (2019). Ignition, Flame Propagation, and End-Gas Autoignition Studies of Natural Gas/EGR Blends in a Rapid Compression Machine. (2019).

55. Holton, M. M., Gokulakrishnan, P., Klassen, M. S., Roby, R. J., & Jackson, G. S. (2010). Autoignition delay time measurements of methane, ethane, and propane pure fuels and methane-based fuel blends. Journal of Engineering for Gas Turbines and Power, 132(9).

56. Hashemi, H., Jacobsen, J.G., Rasmussen, C.T., Christensen, J.M., Glarborg, P., Gersen, S., van Essen, M., Levinsky, H.B., Klippenstein, S.J., High-pressure oxidation of ethane. Combustion and Flame, 182 (2017), pp. 150-166.

57. Yossefi, D., Ashcroft, S.J., Hacohen, J., Belmont, M.R., Thorpe, I., Combustion of methane and ethane with CO2 replacing N2 as a diluent. Volume 74, Issue 7, 1995, Pages 1061-1071, ISSN 0016-2361,

58. Liu, Y., Cheng, J., Zou, C., Lu, L., Jing, H., Ignition delay times of ethane under O2/CO2 atmosphere at different pressures by shock tube and simulation methods. Combustion and Flame. 2019 Jun 1; 204:380-90.

59. Hu E., Chen Y., Zhang Z., Li X., Cheng Y., Huang Z., Experimental study on ethane ignition delay times and evaluation of chemical kinetic models. Energy Fuels, 29 (2015), pp. 4557-4566.

60. Huang, J., Crookes, R.J., Assessment of simulated biogas as a fuel for the spark ignition engine, Fuel, Volume 77, Issue 15, 1998, Pages 1793-1801, ISSN 0016-2361,

61. Vinod, K. N., Gore, M., Lee, A., Neal, L., Li, F., & Fang, T. Combustion and flame analysis of byproduct fuel mixture with high CO2 dilution from the Cl-ODH process of

ethane to ethylene conversion. In 2020 Spring Technical Meeting of the Eastern States Section of the Combustion Institute, 2020.

62. Malenshek, M., & Olsen, D. B. (2009). Methane number testing of alternative gaseous fuels. Fuel, 88(4), 650-656.

63. Cho, H. M., & He, B. Q. (2009). Combustion and emission characteristics of a natural gas engine under different operating conditions. Environmental Engineering Research, 14(2), 95-101.

64. Shi, Y., Jia, Y., Pan, W., Huang, L., Yan, J., & Zheng, R. (2017). Potential evaluation on CO2-EGR in tight and low-permeability reservoirs. Natural Gas Industry B, 4(4), 311-318.

65. Liu, Y., Cheng, J., Zou, C., Lu, L., Jing, H., Ignition delay times of ethane under O2/CO2 atmosphere at different pressures by shock tube and simulation methods. Combustion and Flame. 2019 Jun 1; 204:380-90.

66. Li, H., Haugen, G., Ditaranto, M., Berstad, D., & Jordal, K. (2011). Impacts of exhaust gas recirculation (EGR) on the natural gas combined cycle integrated with chemical absorption CO2 capture technology. Energy Procedia, 4, 1411-1418.

67. Agarwal, Deepak, Shrawan Kumar Singh, and Avinash Kumar Agarwal. "Effect of Exhaust Gas Recirculation (EGR) on performance, emissions, deposits and durability of a constant speed compression ignition engine." Applied energy 88.8 (2011): 2900-2907.

68. Maiboom, Alain, Xavier Tauzia, and Jean-François Hétet. "Experimental study of various effects of exhaust gas recirculation (EGR) on combustion and emissions of an automotive direct injection diesel engine." Energy 33.1 (2008): 22-34.

69. Wei, Haiqiao, et al. "Gasoline engine exhaust gas recirculation–A review." Applied energy 99 (2012): 534-544.

70. Heywood, John B. Internal combustion engine fundamentals. McGraw-Hill 2nd edition., 2018. APA. Heywood, John B.

71. Kumar, J. Thirumala Sai, et al. "Effect of reformed EGR on the performance and emissions of a diesel engine: a numerical study." Alexandria Engineering Journal 57.2 (2018): 517-525.

72. Karnik, Amey Y., and Michael H. Shelby. "Effect of exhaust gas temperature limits on the peak power performance of a turbocharged gasoline engine." (2010): 112801.

73. Kee, Robert J., et al. "Measurement of exhaust gas temperatures in a high performance two-stroke engine." SAE transactions (1998): 2413-2423.

74. Cheng, Wai K., et al. "An overview of hydrocarbon emissions mechanisms in spark-ignition engines." (1993).

75. Stedman, Donald H. "Automobile carbon monoxide emission." Environmental Science & Technology 23.2 (1989): 147-149.

76. Ristovski, Z. D., et al. "Particle and carbon dioxide emissions from passenger vehicles operating on unleaded petrol and LPG fuel." Science of the Total Environment 345.1-3 (2005): 93-98.

77. Chaichan, Miqdam T., and Qahtan A. Abass. "Study of NOx emissions of SI engine fueled with different kinds of hydrocarbon fuels and hydrogen." Al-Khwarizmi Engineering Journal 6.2 (2010): 11-20.

78. Evans, Jimmie, et al. "2006 Mississippi Curriculum Framework: Secondary Small Engine Repair.(Program CIP: 47.0606-Small Engine Mechanic and Repairer)." Research and Curriculum Unit (2006).

79. M. Ehsani, Y. Gao, and A. Emadi, Modern Electric, Hybrid Electric and Fuel Cell Vehicles :Fundamentals, Theory and Design, 2nd edition. CRC Press, 2010.

80. Gebrehiwot, M., Van de Bossche, A., Range Extenders for Electric Vehicles. Department of Electrical Energy, Systems, & Automation.

81. D. H. Choi, S. J. Lee, B. H. Cho, and Y. G. Yoon, “Development of design tool for hybrid power systems of hybrid electric military combat vehicles,” Veh. Power Propuls. Conf. (VPPC), 2010 IEEE, pp. 1–5, 2010.

82. Gritli Y, Tani A, Rossi C, Casadei D. Assessment of current and voltage signature analysis for the diagnosis of rotor magnet demagnetization in five-phase AC permanent magnet generator drives. Math Comput Simul. 2019;158:91-106.

83. Plug-in electric vehicle charging: The Basics | US EPA. (2023, September 27). US EPA. https://www.epa.gov/greenvehicles/plug-electric-vehicle-charging-basics.

84. Bryden, Thomas S., et al. "Electric vehicle fast charging station usage and power requirements." Energy 152 (2018): 322-332.

85. De Almeida, Aníbal T., Fernando JTE Ferreira, and André Quintino. "Technical and economical considerations on super high-efficiency three-phase motors." 48th IEEE Industrial & Commercial Power Systems Conference. IEEE, 2012.

86. 1. Aoki, Kaoru, et al.: "Development an Integrated Motor Assist Hybrid System", JSAE No. 98-99 161.

87. Yamaguchi, Tetsuro: "CVT Control in the HONDA Hybrid 'IMA'", No. 9908 JSAE SYMPOSIUM, Latest Motive Power Transmission Technologies '99, p.37- 40.

88. C. F. Wang, M. J. Jin, J. X. Shen, and C. Yuan, “A permanent magnet integrated starter generator for electric vehicle onboard range extender application,” IEEE Trans. Magn., vol. 48, no. 4, pp. 1625–1628, 2012.

89. Abe, Shoei, and Masashi Murata. Development of IMA motor for 2006 civic hybrid. No. 2006-01-1505. SAE Technical Paper, 2006.

90. Aoki, Kaoru, et al.: "Development an Integrated Motor Assist Hybrid System", JSAE No. 98-99 161.

91. Yamaguchi, Tetsuro: "CVT Control in the HONDA Hybrid 'IMA'", No. 9908 JSAE SYMPOSIUM, Latest Motive Power Transmission Technologies '99, p.37- 40.

92. Heywood, J. B., & Sher, E. (1999). The Two-Stroke Cycle Engine: Its Development, Operation, and Design. Society of Automotive Engineers.

93. Blair, Gordon P. The basic design of two-stroke engines. SAE International, 1990.

94. Blair, Gordon. Design and simulation of two-stroke engines. SAE International, 1996.

95. Genibrel, J. L. (2011). The Complete YAMAHA KT100. Genibrel Publications.

96. Yamaha Sportsman KT100 Kart Racing Engine. (n.d.). GoKarts USA. https://gokartsusa.com/Yamaha-KT100-Sportsman-Engine.aspx.

97. Yamaha KT100 Engine Parts :: 2-Cycle Engine Parts :: Engines & Parts :: Comet Kart Sales. (n.d.). https://cometkartsales.com/Yamaha-KT100-Parts/.

98. Digital Rotary Torque Sensor, 0.1/5/300/1000 Nm to 10000 Nm. (n.d.). ATO.com. https://www.ato.com/rotary-torque-sensor-10000-

nm?affiliate=shopping&gad_source=1&gclid=Cj0KCQiA84CvBhCaARIsAMkAvkJfAr697nx4WlynG8AS6CwOwhXTuy5vdLJo22eZajF_kkbWIzX2VlEaAuSQEALw_wcB.

99. Department of Energy of the United States of America, http://www.doe.gov 9. National www. Renewable Energy Laboratory of the United States of America, http://www.nrel.gov.

100. Z. Rezvani, J. Jansson, J. Bodin. Advances in Consumer Electric Vehicle Adoption Research: A Review and Research Agenda, Volume 34,2015, Pages 122-136, ISSN 1361-9209. https://doi.org/10.1016/j.trd.2014.10.010.

101. G. Krishna. Understand and Identifying Barriers to Electric Vehicle Adoption Through Thematic Analysis. Volume 10, 2021. 100364. ISSN 2590-1982. https://doi.org/10.1016/j.trip.2021.100364.

102. O. Egbue, S. Long. Barriers to Widespread Adoption of Electric Vehicles: An Analysis of Consumer Attitudes and Perceptions, Energy Policy, Volume 48, 2012, Pages 717-729, ISSN 0301-4215, https://doi.org/10.1016/j.enpol.2012.06.009.

103. Eberle, Ulrich & Helmolt, Rittmar. (2010). Sustainable Transportation Based on Electric Vehicle Concepts: A Brief Overview. Energy & Environmental Science. 3. 689. 10.1039/C001674H.

104. Jena, R. (2020). An Empirical Case Study on Indian Consumers' Sentiment Towards Electric Vehicle: A Big Data Analytics Approach." Industrial Marketing Management 90 (2020): 605-616.

105. Tran, M.-K.; Bhatti, A.; Vrolyk, R.; Wong, D.; Panchal, S.; Fowler, M.; Fraser, R. A Review of Range Extenders in Battery Electric Vehicles: Current Progress and Future Perspectives. World Electr. Veh. J. 2021, 12, 54. https://doi.org/10.3390/ wevj12020054.

106. Husain, I. Electric and Hybrid Vehicles Design Fundamentals, 2nd ed.; CRC Press Taylor & Francis Group: Boca Raton, FL, USA, 2011.
107. Szybist, J.; Wagner, R.; Curran, S. Internal Combustion Engines for Hybrid Electric Configurations; National Transportation Research Center: Knoxville, TN, USA, 2017.
108. Heron, A.; Reinderknecht, F. Comparison of Range Extender Technologies for Battery Electric Vehicles. In Proceedings of the 2013 8th International Conference and Exhibition on Ecological Vehicles and Renewable Energies, Stuttgart, Germany, 27–30 March 2013.
109. Friedl, H.; Friedl, G.; Hubmann, C.; Sorger, H.; Teuschl, G.; Martin, C. Range Extender Technology for Electric Vehicles. In Proceedings of the 2018 5th International Conference on Electric Vehicular Technology, Surakarta, Indonesia, 30–31 October 2018.
110. Vortisch, Peter; Chlond, Bastian; Weiß, Christine; Mallig, Nicolai (June 2015). "Electric Vehicles with Range Extender as a Suitable Technology (EVREST)". Karlsruher Institut für Technologie. Retrieved 2015-05-18.
111. Borghi, M.; Mattarelli, E.; Muscoloni, J.; Rinaldini, C.A.; Savioli, T.; Zardin, B. Design and experimental development of a compact and efficient range extender engine. Appl. Energy 2017, 202, 507–526.
112. Chan, C.C, Chau, K.T. (2001). “Modern Electric Vehicle Technology”. Oxford University Press.
113. Seabaugh, C. (2022) Ford F-150 Lightning XLT's 300-mile battery costs nearly as much as one maverick pickup, MotorTrend. MotorTrend. Available at: https://www.motortrend.com/news/2022-ford-f-150-lightning-extended-range-battery-configurator/ (Accessed: March 7, 2023).

114. Sonawane, Utkarsha, and Nirendra Nath Mustafi. "Design and development of small engines for UAV applications." Advanced Combustion Techniques and Engine Technologies for the Automotive Sector (2020): 231-246.

115. Shah, Rajesh, Muqsit Khan, and Vikram Mittal. "Usage of 2-Stroke Engines for Hybrid Vehicles." SAE International Journal of Sustainable Transportation, Energy, Environment, & Policy 3.13-03-02-0011 (2022): 129-138.

116. Echekki, T, and Hessam M. "Principal component transport in turbulent combustion: A posteriori analysis." Combustion and Flame 162.5 (2015): 1919-1933.

117. Glassman, Irvin, Richard A. Yetter, and Nick G. Glumac. Combustion. Academic press, 2014.

118. Morandin, Mattia, Marco Ferrari, and Silverio Bolognani. "Power-train design and performance of a hybrid motorcycle prototype." IEEE Transactions on Industry Applications 51.3 (2014): 2216-2226.

119. Sheu, Kuen-Bao, and Tsung-Hua Hsu. "Design and implementation of a novel hybrid-electric-motorcycle transmission." Applied Energy 83.9 (2006): 959-974.

120. Cameron, K., “Two-Stroke Engines: Defining Their Purpose,” Cycle World, August 16, 2021, https://www. cycleworld.com/2015/04/06/two-stroke-motorcycle-enginesexplained-tech-talk-by-kevin-camero.

121. Mittal, V., “Design Parameters for Small Engines Based on Market Research,” SAE Technical Paper 2018-01-1717, 2018, https://doi.org/10.4271/2018-01-1717.

122. Kollman, R., Lestz, S., and Meyer, W., “Exhaust Emission Characteristics of a Small 2-Stroke Cycle Spark Ignition Engine,” SAE Technical Paper 730159, 1973, https://doi. org/10.4271/730159. 11.

123. Faiz, A. and Gautam, S., “Technical and Policy Options for Reducing Emissions from 2-Stroke Engine Vehicles in Asia,” International Journal of Vehicle Design 34, no. 1 (2004): 1-11.

124. Turner, J., Head, R., Chang, J., Engineer, N. et al., “2-Stroke Engine Options for Automotive Use: A Fundamental Comparison of Different Potential Scavenging Arrangements for Medium-Duty Truck Applications,” SAE Technical Paper 2019-01-0071, 2019, https://doi.org/10.4271/2019-01-0071.

125. Garthwaite, J., “The Two-Stroke Engine, Reconsidered,” MIT Technology Review, April 2, 2020, accessed August 24, 2021, https://www.technologyreview.com/2010/09/16/200401/thetwo-stroke-engine-reconsidered/?msclkid=f32b6111ab6e11ec bdf674a917622de5.

126. Duret, P., Venturi, S., and Dewangan, P., “Small Gasoline Direct Fuel Injection Two-Stroke Engines for Range Extender Applications,” in SIA Powertrain Conference, Versailles, France, 1-9, 2015.

127. Juda, Z. and Marek, W., “Series Hybrid Electric Vehicle with 2-Stroke Internal Combustion Engine,” Paper CONAT20042032, 2004.

128. Mattarelli, E., Rinaldini, C., and Baldini, P., “Modeling and Experimental Investigation of a 2-Stroke GDI Engine for Range Extender Applications,” SAE Technical Paper 2014-01-1672, 2014, https://doi.org/10.4271/2014-01-1672.

129. Kurata, M., Okubo, M., Yamada, Y., and Kitano, S., “Study on Robust Fuel Performance with Differing Fuel Types in a 2-Stroke CAI Combustion Engine,” SAE Technical Paper 2019-32-0573, 2020, https://doi.org/10.4271/2019-32-0573.

130. Trattner, A., Pertl, P., Schmidt, S.P., and Sato, T., “Novel Range Extender Concepts for 2025 with Regard to Small Engine Technologies,” SAE Int. J. Alt. Power. 1, no. 2 (2012, 2012): 566-583, https://doi.org/10.4271/2011-32- 0596.

131. Addepalli S. Krishna, J.M. Mallikarjuna, Davinder Kumar, Effect of engine parameters on in-cylinder flows in a two-stroke gasoline direct injection engine, Applied Energy, Volume 176, 2016, Pages 282-294, ISSN 0306-2619, https://doi.org/10.1016/j.apenergy.2016.05.067.

132. J. Javier López, Santiago Molina, Antonio García, Jorge Valero-Marco, Frédéric Justet, Analysis of the potential of a new automotive two-stroke gasoline engine able to operate in spark ignition and controlled autoignition combustion modes, Applied Thermal Engineering, Volume 126, 2017, Pages 834-847, ISSN 1359-4311, https://doi.org/10.1016/j.applthermaleng.2017.07.213.

133. Verhelst, S., Turner, J., Sileghem, L., Methanol as a Fuel for Internal Combustion Engines. Progress in Energy and Combustion Science, Vol. 70, p.g. 43-88. ISSN 0360-1285 https://doi.org/10.1016/j.pecs.2018.10.001.

134. Zhang, Z.; Wen, M.; Cui, Y.; Ming, Z.; Wang, T.; Zhang, C.; Ampah, J.D.; Jin, C.; Huang, H.; Liu, H. Effects of Methanol Application on Carbon Emissions and Pollutant Emissions Using a Passenger Vehicle. Processes 2022, 10, 525. https:// doi.org/10.3390/pr1003052.

135. Zhen, X., Yang, W. An Overview of Methanol as an Internal Combustion Engine Fuel. 7 November 2014. Received 26 March 2014. Renewable and Sustainable Energy Reviews.

136. Ebersole, G. D., Manning, F. S. Engine Performance and Exhaust Emissions: Methanol vs. Isooctane. SAE Transactions, Vol. 81, SECTION 3: Papers 720447–720743 (1972),

pp. 2076-2095,2108-2111. SAE International. https://www.jstor.org/stable/44722859. Accessed: 25-10-2023 17:46 +00:00.

137. Verhelst, S., Turner, J., Sileghem, L., Methanol as a Fuel for Internal Combustion Engines. Progress in Energy and Combustion Science, Vol. 70, p.g. 43-88. ISSN 0360-1285 https://doi.org/10.1016/j.pecs.2018.10.001.

138. Zhang, Z.; Wen, M.; Cui, Y.; Ming, Z.; Wang, T.; Zhang, C.; Ampah, J.D.; Jin, C.; Huang, H.; Liu, H. Effects of Methanol Application on Carbon Emissions and Pollutant Emissions Using a Passenger Vehicle. Processes 2022, 10, 525. https://doi.org/10.3390/pr1003052.

139. Gudden, A., Pishinger, S., Geiger, J., Heuser, B., Muther, M., An Experimental Study on Methanol as a fuel in Large Bore High Speed Engine Applications – Port Fuel Injected Spark Ignited Combustion. FUEL 303 (2021) 121292.

140. Menrad H, Bernhardt W, Decker G. Methanol vehicles of Volkswagen - a contribution to better air quality. SAE paper no. 881196; 1988.

141. McCall D, Lalk T, Davison R. et al. Performance and emissions characteristics of a spark ignition engine fueled with dissociated and steam-reformed methanol. SAE technical paper 852106; 1985.

142. Waterfront Shipping Company Limited. Methanol-fueled vessels mark one year of safe, reliable, and efficient operations. 2018.

143. Richards B. Methanol-fueled Caterpillar 3406 engine experience in on highway trucks. SAE Technical Paper 902160; 1990.

144. Bos, M. J. et al. (2020), “Wind power to methanol: Renewable methanol production using electricity, electrolysis of water and CO2 air capture”, Applied Energy, Vol. 264, p. 114672.

145. Chaplin, A. G. (2013), “Renewable methanol. An analysis of technological potentials in light of the EU biofuels policy objectives of greenhouse gas savings, security of supply and employment”, Master’s thesis, Sustainable Energy Planning and Management, Aalborg University.

146. Ellis, P. et al. (2019), “Renewable methanol synthesis using electrochemistry”, presentation at the 15th Biennial International Methanol Technology Operators Forum (IMTOF), London, 16-19 June.

147. Fuss, S. et al. (2018), “Negative emissions—Part 2: Costs, potentials and side effects”, Environmental Research Letters, Vol. 13, p. 063002.

148. Goeppert, A. et al. (2014), “Recycling of carbon dioxide to methanol and derived products – closing the loop”, Chem. Soc. Rev., Vol. 43, pp. 7995-8048.

149. Klein, T. (2020), Methanol: A Future-Proof Fuel, a primer prepared for the Methanol Institute, https://www. methanol.org/wp-content/uploads/2020/03/FutureFuel-Strategies-Methanol-Automotive-Fuel-Primer. pdf.

150. IRENA and IEA-ETSAP (2013), “Production of BioMethanol”, Technology Brief 108, IEA-ETSAP and IRENA.

151. Law, K. et al. (2013), “Methanol as a renewable energy resource”, white paper prepared for the Methanol Institute by TIAX LLC.

152. Mignard, D. et al. (2003), “Methanol synthesis from fluegas CO2 and renewable electricity: a feasibility study”, Int. J. Hydrog. Energ., Vol. 28, pp. 455-464.

153. Walbro Atomizer Carb - Buller Built Bully Clutches. (n.d.). Buller Built Bully Clutches.https://www.buller.net/index.php?app=ecom&ns=prodshow&ref=wlbatomizer&sid=uvhx8ksu0ls61463823un9e9ehtr86j1.

154. Rohrer, R. and Chehroudi, B., "Preliminary Heat Release Analysis in a Single-Cylinder Two-Stroke Production Engine," SAE Technical Paper 930431, 1993, https://doi.org/10.4271/930431.

155. Z. Rezvani, J. Jansson, J. Bodin. Advances in Consumer Electric Vehicle Adoption Research: A Review and Research Agenda, Volume 34,2015, Pages 122-136, ISSN 1361-9209. https://doi.org/10.1016/j.trd.2014.10.010.

156. Nonavinakere, K., Gore, M., Fang, T. Experimental Evaluation of Ammoina, Methane, and Gasoline Fuel Blends in Small Scale Spark Ignited Engines. Spring Technical Meeting Eastern States Section of the Combustion Institute.

157. Kobayashi, Hideaki, Hayakawa. A, Somarathne, and Ekenechukwu C. Okafor. Science and technology of ammonia combustion. Proc. Combust. Inst. 37, (2019): 109-133.

158. M.C. Chiong, C.T. Chong, H., Mashruk, Chong, Samiran, A. Valera-Medina, Advancements of combustion technologies in the ammonia-fuelled engines. Energy Conversion and Management, (2021) 244, 114460.

159. Reiter, J. Aaron, Song-Charng Kong. Combustion and emissions characteristics of compression-ignition engine using dual ammonia-diesel fuel. Fuel 90, no. 1 (2011) 87-97.

160. E. Brohi, Ammonia as fuel for internal combustion engines? (Master's thesis) (2014).

161. Yamaha Motorcycle Technology. (n.d.). YAMAHA MOTOR CO., LTD. https://global.yamaha-motor.com/business/mc/mc-tech/main-technology/ypvs.html.

162. Tan, Yee Hern, Horizon Gitano, and Ahmad Syazli Mohd Khalil. Development of a transfer port injection system for two-stroke engines. No. 2012-32-0115. SAE Technical Paper, 2012.

163. Winkler, Franz, et al. Characterization of different injection technologies for high performance two-stroke engines. No. 2016-32-0001. SAE Technical Paper, 2016.

164. Momoh, Omonowo D., and Michael O. Omoigui. "An overview of hybrid electric vehicle technology." 2009 IEEE vehicle power and propulsion conference. Ieee, 2009.

165. Juda, Z., “Simulation of Energy Conversion in Advanced Automotive Vehicles”, SAE Paper 2001-01-3341, Automotive & Transportation Technology Congress and Exhibition, Barcelona – October 1-3, 2001, ATTCE 2001 Proceedings volume 5, ISBN 0-7680-0864-6.

APPENDICES

Appendix A

A-1: KT-100 Heat Transfer Analysis

The following is a preliminary analysis of the heat transfer expected from the KT-100 during operation. This analysis was performed to estimate the total heating capacity needed during experimentation. Because the engine was air cooled, a large fraction of the engine cooling took place via natural convection. However, the blower was used to ensure that the engine did not overheat. It should be noted that methanol operation required less cooling. Methanol has a much higher cooling effect due to the high latent heat of vaporization. Further, it should be noted that the final prototype of this work is envisioned to remain air cooled. Although less efficient, air cooling permits the system to function without a radiator and save weight. If the generator were to be used in a UAV application where loading is expected to be high, air from the rotors could be directed over the engine. In addition, if the generator were to be used in a powersport application, the natural convection cooling effects would be enhanced by forced convection from the generator moving through the air.

MAE 895 | HT-101 Heat Transfer | Matt Gore | 2/3/22

Average heat transfer rate = $\dot{m}_f Q_{LHV}(1-\eta_f)$

↳ $SFC = \dot{m}_f / P \rightarrow \dot{m}_f = SFC(P)$

Let BSFC ≅ $\underline{425}$ (g/kw-h) ≈ $\underline{19.3\%}$ efficient $\quad Q_{LHV} = 12.89$ kwh/kg

→ $\dot{m}_f = (425\ g/kw\text{-}h)(11\ kw) \rightarrow 4675\ g/hr \rightarrow$ Table heat →

$\bar{Q} = (.4675\ kg/hr)(12.89\ kwh/kg)(1-.193)$

↳ $\boxed{\bar{Q} = 48.63\ kw}$ ← must remove ≈ 49 kw of heat

- Modify heat transfer equation to calculate airflow (Honeywell)

↳ $\dot{Q} = \dot{m} c_p \Delta T \rightarrow \bar{Q} = c_p(\dot{m}_{air})(\rho_{air})\Delta T \rightarrow CFM = \bar{Q}/c_p \rho \Delta T$

- let $\Delta T \cong 250°F$ (120°C $\quad \rho \cong 1.1\ kg/m^3 \quad c_p = .017 \frac{kw\text{-}m}{kg\ C}$

$$\dot{m}_{air} = \frac{49\ kw}{\left(.017 \frac{kw\text{-}min}{kg\ C}\right)\left(1.1\ kg/m^3\right)(120°C)} \qquad \frac{kw}{\frac{kw\text{-}(min)}{kg\ C}\left(kg/m^3\right)(C)}$$

$= 21.6713\ m^3/min \qquad \frac{1\ ft^3/min}{.0283\ m^3/min} \cong 765.2628$

- P.E. Reference Holbrook recommends selecting a fan ≈ 1.3-2x the CFM requirement

$= 765.2628 \frac{(1.3+2)}{2} = 1262.694\ CFM$

$\boxed{\therefore \text{ Fan needs to be approx } \leq 1250\ CFM}$

A-2: KT-100 Port Map, Ignition Timing, Tuned Exhaust [95]

As mentioned throughout this work, the engine porting of the KT100 heavily influenced the performance. The porting map with this particular engine comes from the factory to facilitate high RPM operation. To improve the discussion of the porting, a port map has been included in this appendix. The ignition timing was further modified to optimize the engine for methanol. A copy of the ignition timing parameters is also included.

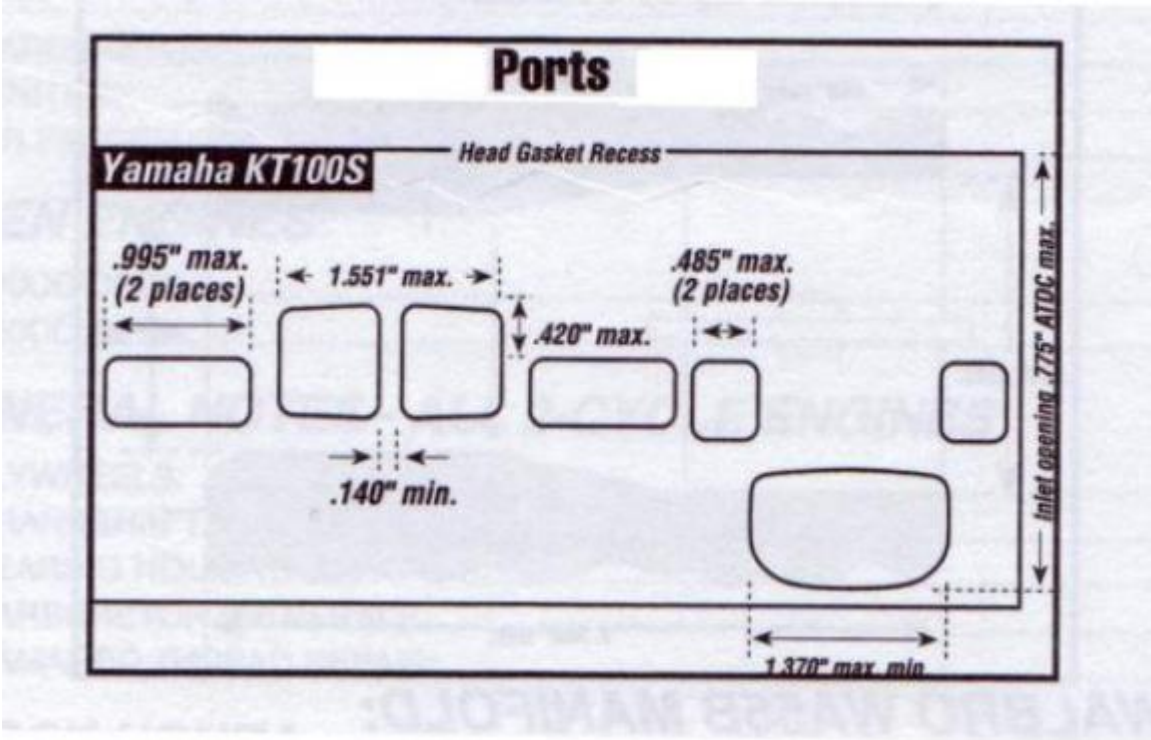

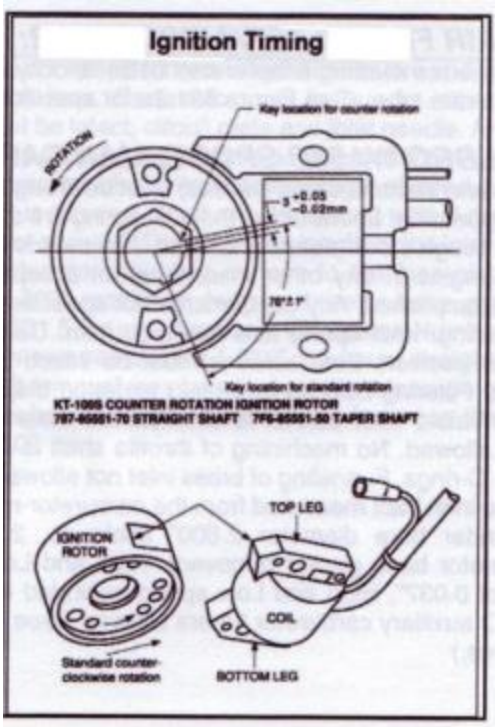

A-3: Post Experiment Methanol Evaluation

After the methanol experiments were conducted, the engine was disassembled and inspected to gauge the mechanical health in an objective manner. Due to the qualitative the nature of this analysis it was not included in the body of the dissertation. However, the author feels like a qualitative analysis of this nature should be performed. Below is a collage of images taken after the engine was disassembled.

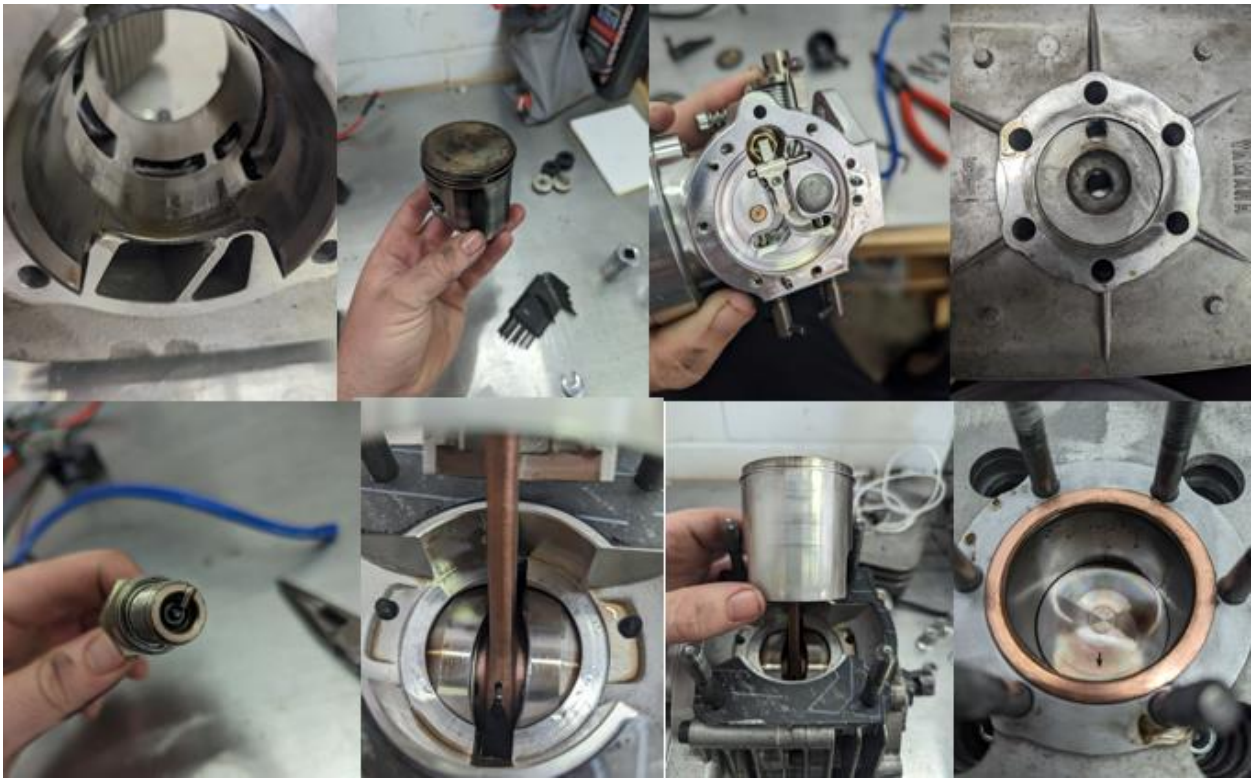

A-4: Pulley Ratios

During the tuning phase the variety of pulley ratios was explored. These ratios who created from a combination of the pulleys that were available. Below is a list of available ratio combinations that were considered.

			at engine 9500 rpm		at engine 7500 rpm		at engine 4500 rpm			
new sproket	ratio	percent difference	new rotor rpm	new torque	new rotor rpm	new torque	new rotor rpm	new torque		old ratio
28.00	2.00	0.14	4750.00	14.00	3750.00	12.00	2250.00	10.00	3000	1744.186
30.00	2.14	0.20	4433.33	15.00	3500.00	12.86	2100.00	10.71	4000	2325.581
32.00	2.29	0.25	4156.25	16.00	3281.25	13.71	1968.75	11.43	5000	2906.977
36.00	2.57	0.33	3694.44	18.00	2916.67	15.43	1750.00	12.86	6000	3488.372
40.00	2.86	0.40	3325.00	20.00	2625.00	17.14	1575.00	14.29	7000	4069.767
48.00	3.43	0.50	2770.83	24.00	2187.50	20.57	1312.50	17.14	8000	4651.163
									9000	5232.558

A-5: Image of testing

The following is an image of the testing during testing. This image is included to demonstrate the hardware, including the cooling fan starter motor and load plates.


OPEN
DieHard